

國立交通大學

機械工程學系

博士論文

可變壓縮比渦卷式壓縮機之研究

Research on Scroll Compressors with Variable Compression Ratio

研究生：劉陽光

指導教授：洪景華 教授

中華民國九十九年六月

可變壓縮比渦卷式壓縮機之研究

Research on Scroll Compressors with Variable Compression Ratio

研究生: 劉陽光

Student: Yangguang Liu

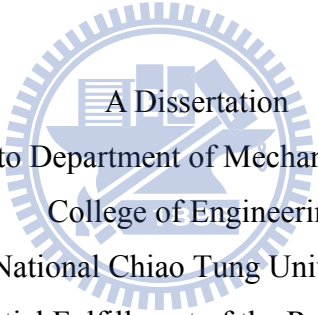
指導教授: 洪景華

Advisor: Chinghua Hung

國立交通大學

機械工程學系

博士論文



A Dissertation
Submitted to Department of Mechanical Engineering
College of Engineering
National Chiao Tung University
in partial Fulfillment of the Requirements
for the Degree of
Doctor of Philosophy
in
Mechanical Engineering
June 2010
Hsinchu, Taiwan, Republic of China

中華民國九十九年六月

可變壓縮比渦卷式壓縮機之研究

研究生：劉陽光

指導教授：洪景華

國立交通大學機械工程學系博士班

摘要

對高效能與可變負載之冷凍空調系統而言，為因應其變動負載之需求，搭配變頻馬達之可變壓縮比渦卷式壓縮機已成為目前發展之主流。本研究第一步先探討渦卷之旁通機構，此為裝於固定渦卷背端之閥機構，用於防止當負載變動時因為渦卷幾何線形之固定容積比限制而在壓縮腔內產生之過壓縮；且其亦有避免冷媒剛進入壓縮腔時因過熱度不足而造成的液阻卻。將此步驟發展之旁通機構數學模型整合於一渦卷式壓縮機模擬軟體中，並針對高壓與低壓外殼之壓縮機架構分別進行模擬分析。結果發現不論在何種負載下，設置之旁通孔皆能有效地排除過壓縮與液阻卻。而配合開發中的渦卷式壓縮機也藉由實驗結果驗證此機構在不同負載條件下，能有效地提升壓縮機之效率。

另一方面，針對變動負載之設計需求，也整合最佳化流程於上述渦卷壓縮機模擬軟體中，以輔助產品開發時之參數最佳化設計。並對降低摩擦功之軸承尺寸最佳化問題加以研究，藉最佳化之流程而獲得在考量強度與液動壓潤滑限制條件下，軸承尺寸的最佳參數組合，以作為產品開發時之設計依據。

此外，針對提高渦卷對之壓縮比(亦即提高線形之容積比)以匹配更寬廣的負載需求方面，本研究也發展可變基圓半徑圓漸開線之渦卷線形的數學模型，並以此發展一種中心較厚且由內向外厚度漸薄之圓漸開線渦卷渦片，其強度與剛性於高溫與高壓負載條件下極具優勢。同時也驗證了圓弧與直線此兩種用於傳統渦卷對以修整中心干涉並達到完美嚙合的數學模型，也可應用於此可變基圓半徑圓漸開線之渦卷線形上，進而達成嚙合修正，同時亦可提高渦卷對之壓縮比。

Research on Scroll Compressors with Variable Compression Ratio

Student: Yangguang Liu

Advisor: Dr. Chinghua Hung

Department of Mechanical Engineering
National Chiao Tung University

ABSTRACT

A scroll-type compressor (STC) with variable compression ratio using a variable-speed motor has become a major trend in recent years because of the requirements for variable capacities in high efficient refrigeration and air-conditioning systems.

This study first develops a bypass valves mechanism which is disposed to the backside of a fixed scroll of STC. The over-compression resulted from the mismatch between the intrinsic volume ratio (the designed compression ratio) in STC and the variable operating pressure ratio (variable capacity) can be prevented by using this mechanism. In addition, this mechanism can also avoid the liquid slug while the refrigerant flows into the chamber of STC without enough superheat for fully vaporized.

The mathematical model for the bypass valves has been constructed and integrated into a STC simulation computer package, and the high and low side structures of STC are also simulated respectively. Simulation results find that the subtle disposition of bypass valves can prevent the over-compression and liquid slug problems regardless various operating conditions. One practical STC product, with bypass valves built in it, has also validated the effect through the actual STC efficiency experiments.

In addition, an optimization module had been combined into the simulation package for aiding the design of STC with variable capacities and speeds. One application regarding reducing frictional losses in bearing components of STC is demonstrated and discussed in this dissertation. By using the numerical optimization procedure, the optimum parametric combinations in bearings can be found with considerations of hydrodynamic lubrication and strength constraints. It is expected that this procedure can become the base in developing STC

product design.

In order to raise the compression ratio for the scroll pair (i.e. to raise the intrinsic volume ratio) to match even wider loading conditions, a new geometric model of the scroll profiles constructed from an involute of circle with variable radii has been built. One kind of these profiles with greater wrap thickness at the center and decreasing thickness from the inside outwards can provide better strength and rigidity.

Finally, this study also demonstrates that the arc and line modifications, used in the conventional scroll profile, can be also applied to this new scroll profile. The two most important purposes, avoiding interference at the center of the scroll pair and boosting the intrinsic volume ratio to match the specified operating conditions, are both achieved by properly choosing one of these two modifications according to design requirements.



誌謝

在交大已經待了七年，經歷兩千五百多個日子終於能畢業了。當然首先感謝的就是引領我踏入交大的碩士班恩師曾錦煥老師。督促學業之外，老師改變了自信心不足和單線思考的我，激發我對研究的興趣和對知識的渴求，使我在面對問題時能更多面向地思考，進而提出豐富的創意與手段來解決它。在曾老師辭世後的那段日子，博一剛入學的我，更想過是否要放棄學業而進入職場。在這裡深深感謝博士班恩師洪景華老師，辛苦地延續指導我的工作，不斷地給我鼓勵和鞭策。除了幫助我提升在專業領域的學養和知識外，更針對進行博士研究所應具備的精神和態度傾囊相授。在這我想向老師致上我最深的感謝，謝謝老師。此外，我也特別感謝張鈺炯學長在這段期間教導我這個晚輩，傳授在產品設計、系統測試等專業知識，以及科技結合人文與時間管理等觀念。謝謝學長。

感謝我的口試委員，蔡忠杓老師、宋震國老師、陳俊勳老師、陳申岳老師以及林聰穎老師。謝謝老師們對學生論文的建議和教導，讓學生能進一步改進論文，提升到更好的層次。謝謝實驗室的各位師兄弟姐妹對我的照顧和幫助，也感謝齒輪實驗室的成員們這幾年與我同在一間研究室中互相砥礪和提攜。同時也特別感謝工研院能環所的先進們，不管是待人接物和研究工作上，對我的指導和照顧，使我獲益良多。

謝謝我的父母和家人對我的支持讓我能完成這個目標，在我面對挫折和徬徨失據時成為我的依靠，謝謝你們。最後也謝謝我的愛人，在博士班這段期間始終沒有出現，讓我能專心一致地完成研究。

感謝我所愛以及愛我的人，謝謝大家。

LIST OF CONTENTS

| | |
|--|------|
| 摘要 | i |
| ABSTRACT | ii |
| 誌謝 | iv |
| LIST OF CONTENTS..... | v |
| LIST OF TABLES | viii |
| LIST OF FIGURES..... | ix |
| NOMENCLATURE..... | xi |
| CHAPTER 1 INTRODUCTION..... | 1 |
| 1.1 Scroll-type compressor (STC)..... | 1 |
| 1.2 Simulation program for STC..... | 4 |
| 1.3 Variable speed and compression ratio | 5 |
| 1.4 Design optimization for variable compression ratio | 6 |
| 1.5 Scroll profiles based on an involute of circle with variable radii | 6 |
| 1.6 Dissertation Scope | 7 |
| CHAPTER 2 STC SIMULATION MODEL AND PROCESS | 8 |
| 2.1 Developments in mathematical models of STC | 8 |
| 2.1.1 Geometry of scroll profiles..... | 8 |
| 2.1.2 Thermodynamics in the scroll pair | 9 |
| 2.1.3 Dynamics of components and bearing models..... | 9 |
| 2.2 Geometrical model of STC | 10 |
| 2.2.1 Scroll profile design by involute of circle with a fixed radius | 10 |
| 2.2.2 Derivation of volume and its ratio of the scroll chambers | 12 |
| 2.3 Thermodynamic model | 13 |
| 2.3.1 Refrigerant property | 13 |
| 2.3.2 Suction and discharge superheating calculations | 14 |
| 2.3.3 Compression and discharge process..... | 16 |
| 2.3.4 Leakage flows..... | 16 |
| 2.4 Dynamics in mechanical components and mechanisms in STC | 18 |
| 2.4.1 Dynamic forces and moments | 18 |
| 2.4.2 Counterweight analysis | 20 |
| 2.5 Frictional losses in mechanical components | 21 |
| 2.5.1 Thrust bearing..... | 21 |

| | |
|---|-----------|
| 2.5.2 Journal bearings..... | 24 |
| 2.6 Simulation process in the STC computer model..... | 24 |
| 2.6.1 Simulation process..... | 25 |
| 2.6.2 Output results..... | 26 |
| 2.7 Summarization of the STC simulation model | 28 |
| CHAPTER 3 MATHEMATICAL MODEL OF BYPASS VALVES | 29 |
| 3.1 Developing history regarding bypass valves | 29 |
| 3.2 Geometry of bypass holes | 31 |
| 3.2.1 Geometry of bypass holes | 31 |
| 3.2.2 Uncovered area of the bypass holes | 34 |
| 3.2.3 Corresponding chambers to bypass holes..... | 34 |
| 3.3 Bypass valve model | 34 |
| 3.4 Simulation model..... | 35 |
| 3.5 Remarks | 37 |
| CHAPTER 4 SIMULATION FOR BYPASS VALVES IN STC..... | 38 |
| 4.1 Simulations with low-side structure | 38 |
| 4.1.1 Geometric observation..... | 38 |
| 4.1.2 Simulation results during working cycle..... | 38 |
| 4.1.3 Simulation results of two different arrangements..... | 41 |
| 4.2 Simulations with high-side structure | 45 |
| 4.2.1 Effect of bypass valves behavior | 47 |
| 4.2.2 Effect of bypass valves in thermodynamics | 50 |
| 4.3 Verification of bypass mechanism | 51 |
| 4.3.1 Experimental apparatus | 51 |
| 4.3.2 Verification of bypass action | 55 |
| 4.4 Remarks | 55 |
| CHAPTER 5 OPTIMIZATION PROCEDURE APPLIED IN STC MODEL | 56 |
| 5.1 Researches about optimum design of STC | 56 |
| 5.2 Verification of simulation results and experiments | 56 |
| 5.3 Optimization solver | 60 |
| 5.3.1 Formulation of optimization problem | 61 |
| 5.3.2 Optimization procedure | 61 |
| 5.4 Case study: optimization in reducing frictional losses | 62 |
| 5.4.1 Selection of objective function and design variables | 62 |

| | |
|---|-----------|
| 5.4.2 Selection of constraint conditions..... | 63 |
| 5.5 Case study: optimum results and discussions | 64 |
| 5.5.1 Selection of testing conditions..... | 64 |
| 5.5.2 Optimum results | 64 |
| 5.5.3 Discussions | 67 |
| 5.6 Remarks | 68 |
| CHAPTER 6 INVESTIGATION ON INVOLUTE OF CIRCLE WITH VARIABLE RADII IN A STC..... | 69 |
| 6.1 Various studies for scroll profiles | 69 |
| 6.2 Geometric model of the scroll profile constructed from an involute of circle with variable radii | 70 |
| 6.2.1 Theorem of planar orbiting mechanisms | 70 |
| 6.2.2 Conceptual illustration and formulations | 71 |
| 6.3 Application for different k values and volume calculations..... | 75 |
| 6.3.1 Different k values | 75 |
| 6.3.2 Volume calculations..... | 79 |
| 6.4 Parametric study and discussion..... | 80 |
| 6.4.1 Fixed suction volume, volume ratio and housing size..... | 80 |
| 6.4.2 Fixed suction volume, volume ratio and wrap height | 83 |
| 6.5 Remarks | 84 |
| CHAPTER 7 PERFECTLY MESHING MODIFICATION FOR INVOLUTE OF CIRCLE WITH VARIABLE RADII..... | 85 |
| 7.1 Introduction of modifications at the center of the scroll pair | 85 |
| 7.2 Arc modification of involutes of circle with variable radii..... | 85 |
| 7.2.1 Formulation | 86 |
| 7.2.2 Discussion..... | 87 |
| 7.3 Line modification of involutes of circle with variable radii | 89 |
| 7.3.1 Formulation | 89 |
| 7.3.2 Discussion..... | 90 |
| 7.4 Remarks | 91 |
| CHAPTER 8 CONCLUSIONS AND FUTURE WORKS | 93 |
| 8.1 Conclusions | 93 |
| 8.2 Future works | 95 |
| REFERENCES | 97 |

LIST OF TABLES

| | |
|--|----|
| Table. 4-1 Parameters of the STC..... | 39 |
| Table. 4-2 Parameters of bypass hole..... | 39 |
| Table. 4-3 Parameters of bypass hole: Case (A)..... | 42 |
| Table. 4-4 Parameters of bypass hole: Case (B)..... | 43 |
| Table. 4-5 Parameters of bypass hole: Case (C)..... | 44 |
| Table. 4-6 Parameters of the STC..... | 46 |
| Table. 4-7 STC operating conditions..... | 46 |
| Table. 4-8 Comparisons of sim. & exp. results of \dot{m} , η_v & η_c | 55 |
| Table. 5-1 Parameters and operating conditions of the STC..... | 58 |
| Table. 5-2 Specifications of calorimeter for measuring STC performance..... | 59 |
| Table. 5-3 Comparison of sim. & exp. results in different conditions..... | 59 |
| Table. 5-4 Bounds of design variables and constraints..... | 62 |
| Table. 5-5 Optimized results with design variables..... | 65 |
| Table. 6-1 Combinations of design parameters and related results..... | 80 |
| Table. 6-2 ODP/GWP values to several refrigerants..... | 82 |
| Table. 6-3 Combinations of design parameters and related results..... | 83 |

LIST OF FIGURES

| | |
|---|----|
| Fig. 1-1 A complete cycle of STC: suction→compression→discharge | 2 |
| Fig. 1-2 A schematic of a STC..... | 3 |
| Fig. 2-1 Parametric definition for the involute of circle..... | 10 |
| Fig. 2-2 Inner and outer Profiles of fixed scroll | 12 |
| Fig. 2-3 Illustration of “Refprop7” linking to STC simulation package | 14 |
| Fig. 2-4 Low-side and High side structure of STC [1]..... | 15 |
| Fig. 2-5 Illustration of end-side leakage..... | 17 |
| Fig. 2-6 Illustration of flank leakage | 17 |
| Fig. 2-7 Dynamic forces of the orbiting scroll | 19 |
| Fig. 2-8 Dynamic balance of the driving shaft..... | 20 |
| Fig. 2-9 Schematic of the three journal bearings and the thrust bearing..... | 21 |
| Fig. 2-10 Parameters of the thrust bearing | 22 |
| Fig. 2-11 Nominal height of oil-film | 23 |
| Fig. 2-12 Motor torque-efficiency-power for specified speed | 24 |
| Fig. 2-13 Flowchart of the simulation process in STC package..... | 25 |
| Fig. 2-14 Flowchart of thermodynamics with leakage model in STC package | 26 |
| Fig. 3-1 Bypass holes during one orbiting scroll [41]..... | 30 |
| Fig. 3-2 Speed, volume vs. pressure ratio & bypass design [42] | 31 |
| Fig. 3-3 Scheme of bypass holes (a) range of positions (b) relations from fixed scroll (c) relations from orbiting scroll..... | 33 |
| Fig. 3-4 Uncovered areas of the orbiting scroll and the bypass hole..... | 35 |
| Fig. 3-5 The flowchart of the STC simulation process..... | 36 |
| Fig. 3-6 The flowchart of leakage and bypass model in STC | 37 |
| Fig. 4-1 Position of bypass holes..... | 39 |
| Fig. 4-2 Uncovered interval of bypass holes | 40 |
| Fig. 4-3 Working cycle | 40 |
| Fig. 4-4 Working cycle at different condition..... | 40 |
| Fig. 4-5 Position of bypass holes: Case (A) | 42 |
| Fig. 4-6 Position of bypass holes: Case (B) | 43 |
| Fig. 4-7 Position of bypass holes: Case (C) | 44 |
| Fig. 4-8 Working cycle at different cases | 45 |

| | |
|--|----|
| Fig. 4-9 The scheme of the STC and bypass holes on fixed scroll..... | 46 |
| Fig. 4-10 Change of the uncovered area of bypass holes | 48 |
| Fig. 4-11 Uncovered area of bypass holes in (a) chamber 2 and chamber 3 (b) chamber 2' and chamber 3' | 49 |
| Fig. 4-12 Prediction of performance of \dot{m}, η_v, η_c | 50 |
| Fig. 4-13 Prediction of pressure variation with and without bypass valves (a) chamber 2, 3 (b) chamber 2', 3' | 52 |
| Fig. 4-14 CO ₂ test rig..... | 53 |
| Fig. 4-15 Working procedure of CO ₂ test rig | 54 |
| Fig. 5-1 Frictional losses in (a) Condition A (b) Condition B (c) maximum loading in Condition A | 60 |
| Fig. 5-2 Flow chart of the optimization procedure..... | 63 |
| Fig. 5-3 Iteration history (a) Objective function (b) Constraints 1–4 (c) Constraints 5–8 | 66 |
| Fig. 5-4 Frictional losses in all testing conditions..... | 68 |
| Fig. 6-1 Illustration: theorem of planar orbiting mechanisms..... | 71 |
| Fig. 6-2 Sketch map and parametric definitions of an involute of circle with variable radii..... | 72 |
| Fig. 6-3 Parametric relations of the scroll profiles constructed from an involute of circle with variable radii..... | 74 |
| Fig. 6-4 Sketch map of the scroll profiles for different k values | 78 |
| Fig. 6-5 Structure of orbiting scroll ($k=1, \alpha=50^\circ$ and $\delta_0 = -0.05\text{mm}$)..... | 78 |
| Fig. 6-6 Scroll profiles from A0 to A4 | 82 |
| Fig. 6-7 Reduction ratio in A1 to A4 and A1' to A4', A0 as standard..... | 84 |
| Fig. 7-1 Parametric definitions of the arc modification | 87 |
| Fig. 7-2 Comparison of different β values to the scroll profile with arc modification | 88 |
| Fig. 7-3 Parametric definitions of the line modification | 90 |
| Fig. 7-4 (a) Comparison of different Δr values ($\beta=105^\circ (21\pi/36 \text{ rad})$) (b) Comparison of different β values ($\Delta r=0.5 \text{ mm}$)..... | 92 |

NOMENCLATURE

| | |
|----------------------|--|
| a | radius of base circle (mm) |
| a_0 | initial radius of base circle (mm) |
| A | area |
| A_{By} | uncovered cross section area |
| A_{dis} | equal flow area |
| A_i, A_o | enclosed area by involutes |
| A_{in}, A_{ou} | leakage area from clearances |
| C, C_{valve} | coefficient |
| C_0, C_1 | contact points |
| C_{in}, C_{ou} | joint points |
| C_b | clearance of journal bearing (mm) |
| CC_1 | convergence criterion |
| d | distance |
| d, d' | distance used in arc and line modification (mm) |
| $d_{tu,s}, d_{tu,d}$ | tube diameter |
| D | diameter (mm) |
| D_b | diameter of journal bearing (mm) |
| D_m | minimum endplate diameter of the orbiting scroll (mm) |
| $D_{i,th}, D_{o,th}$ | inner and outer diameter of thrust bearing (mm) |
| F | force (N) |
| F_b | force from journal bearing (N) |
| f | flow friction factor |
| g | gravity |
| h | height (m) |
| h_{in}, h_{ou} | inlet and outlet enthalpies (kJ/kg) |
| $h_{tu,s}, h_{tu,d}$ | coefficient of heat convection ($W m^{-2} K^{-1}$) |
| H, H_0 | oil-film clearance (mm); nominal oil-film clearance (mm) |
| L_b | length of journal bearing (mm) |
| $L_{tu,d}$ | length of the tube |
| L_i | length of the inner involute |
| L_o | length of the outer involute |
| li | distance between inner involute and bypass hole center |
| lo | distance between outer involute and bypass hole center |
| \dot{m} | mass flow rate (kg/s) |
| m | mass (kg) |
| m_{slo} | slope |
| m_{ob} | mass of orbiting scroll (kg) |
| M | moment ($N \cdot m$) |
| N | turn number of scrolls |
| n | polytropic index |
| p, P | pressure (MPa); power (W) |
| P_b | frictional loss from journal bearing (W) |
| P_{th} | frictional loss from thrust bearing (W) |
| Pr | Prandtl number |
| p_t | pitch of scroll |
| Q | heat transefer quantity(kW) |
| Q_c | cooling capacity (kW) |

| | |
|-------------|---|
| R, R' | radius of the modified arcs (mm) |
| Ra_L | Rayleigh number, $Ra_L = (g\beta\Delta TL^3 / \alpha\nu) !$ |
| Re | Renolds number |
| r | radius of circular bypass hole (m) |
| r_{eq} | equivalent radius (m) |
| r_{ob} | orbiting radius (m) |
| T | temperature (K) |
| t, t_h | time (s); thickness (mm) |
| U | surface velocity ($m \cdot s^{-1}$) |
| V | volume (mm^3) |
| V_{dis} | discharge volume |
| Vol_r | volume ratio |
| V_{suc} | suction volume |
| x, y | coordinate |
| R, Θ | cylindrical coordinate |

Greek letters

| | |
|----------------------|---|
| α | initial angle of involute |
| α_{lp} | tilting angle (rad) |
| β | modified angle between the outer and inner involute curve ($^\circ$, rad) |
| β_{el} | directional turning angle (rad) |
| γ | derivative angle (rad) |
| σ | derivative angle (rad) |
| Δr | modified distance (mm) |
| δ | clearance (m) |
| δ_0 | corrected increment (mm) |
| ϕ | involute angle of scroll |
| ϕ_e, ϕ_{dis} | ended involute angle (rad); corresponding involute angle at discharge (rad) |
| ϕ_r | roll angle (or called ended angel) of scroll pair |
| θ | orbiting angle of scroll(rad) |
| θ_e | modified angle to specified end involute angle (rad) |
| θ_{dis} | orbiting angle at discharge (rad) |
| ψ | independent angle parameter (rad) |
| Φ | phase difference (rad) |
| λ | coefficient of heat conductivity ($W m^{-1} K^{-1}$) |
| ρ | radius of curvature (mm) |
| ρ^* | density (kg/m^3) |
| ω | angular velocity ($rad \cdot s^{-1}$) |
| ε | eccentricity ratio |
| μ | viscosity ($Pa \cdot s$) |
| η_c, η_v | compressor efficiency, volumetric efficiency |
| Π_f, Π_m | coordinate planes |

Subscripts

| | |
|----|-----------------|
| ax | axial direction |
| A | adiabatic |

| | |
|------------|---|
| b | base circle |
| back | back-side |
| b,cr | crank journal bearing |
| b,low | lower journal bearing |
| b,upp | upper journal bearing |
| C | compressor |
| c | center position |
| cur | current |
| c,ersh | centrifugal direction of crank shaft |
| c,lcw | centrifugal direction of lower counterweight |
| c,ob | centrifugal direction of orbiting scroll |
| c,ucw | centrifugal direction of upper counterweight |
| dis | discharge |
| dw | downstream |
| e | end-side |
| f | flank |
| f,in | inner involute of fixed scroll |
| f,ou | outer involute of fixed scroll |
| f,b , f,th | friction of the journal and thrust bearing |
| g | gas |
| i, j, k | index number |
| in | inner |
| l | leakage |
| l,b | bypass leakage |
| l,cur | current leakage |
| l,e | end side leakage |
| l,f | flank leakage |
| l,pre | previous leakage |
| Me | mechanical |
| motor | motor |
| m,in | inner involute of orbiting scroll |
| m,ou | outer involute of orbiting scroll |
| ou | outer |
| o_a | corresponding involute angle for bypass hole |
| o_By | bypass hole coordinate to outer involute |
| o_l | lower limit of the outer involute angle for bypass hole |
| o_u | upper limit of the outer involute angle for bypass hole |
| r | radial direction |
| R | refrigeration |
| suc | suction |
| scr | locus of the turning moment |
| suc,h | superheat |
| t | tangent coordinate |
| tu | tube |
| up | upstream |
| V | volumetric |
| vg | average |
| θ | tangential direction |
| ,b | bearing |



CHAPTER 1 INTRODUCTION

1.1 Scroll-type compressor (STC)

Scroll-type compressor (STC), as one kind of positive displacement pumps, has been developing vigorously since 1980s. With commercial, domestic and automotive applications such as refrigeration, air-conditioning and heat-pump, STC has been regarded as a suitable substitute to other type of rotary compressors because of its higher efficiency, lower noise and fewer numbers of components. In virtue of these characteristics, the STC becomes the research objective in this dissertation.

One orbiting motion, as the most important motion in STC, is composed of the two key components, fixed scroll and orbiting scroll. Both these two scrolls have a circular end-plate and a protrusion extended from one surface of it with spiral profile or so called “scroll”. Before proceeding with this motion, the orbiting scroll must be rotated first by 180 degrees (π rad) relative to the stationary fixed scroll. After that, the orbiting scroll, with a crank mechanism driving it, orbits with a constant radius around a designate point on the fixed scroll and at the same time, an anti-rotation coupling (ex. Oldham ring) is assembled to it for preventing the self-rotation arising from the orbiting scroll. The spiral protrusions of both scrolls can be meshed with each other by this orbiting motion and several crescent and enclosed chambers are generated thereon. These chambers, accompanying with moving inward from the periphery to the center, make their volumes decrease gradually, and vice versa. Hence the scroll pair can be used as compressors, expanders and pumps by virtue of its direction of the orbiting motion.

Figure 1.1 shows a complete cycle of the STC. The scroll pair inhales the gas at the periphery into the chambers and compresses it progressively toward the center with gradually smaller chambers and after reaching the discharger step, it is exhausted through the discharge port of the fixed scroll out of the scroll pair. Because of its simultaneous compression and discharge movement in several continuous chambers and without suction or discharge valves, the gas pulsation and flow losses can be reduced for smoother flow pattern. Therefore the STC is operated at lower torque variation, lower noise and vibration levels and easier to start and restart. Besides, the lower flow losses indicate the higher volume efficiency and the smoother operation means the better reliability of STC.

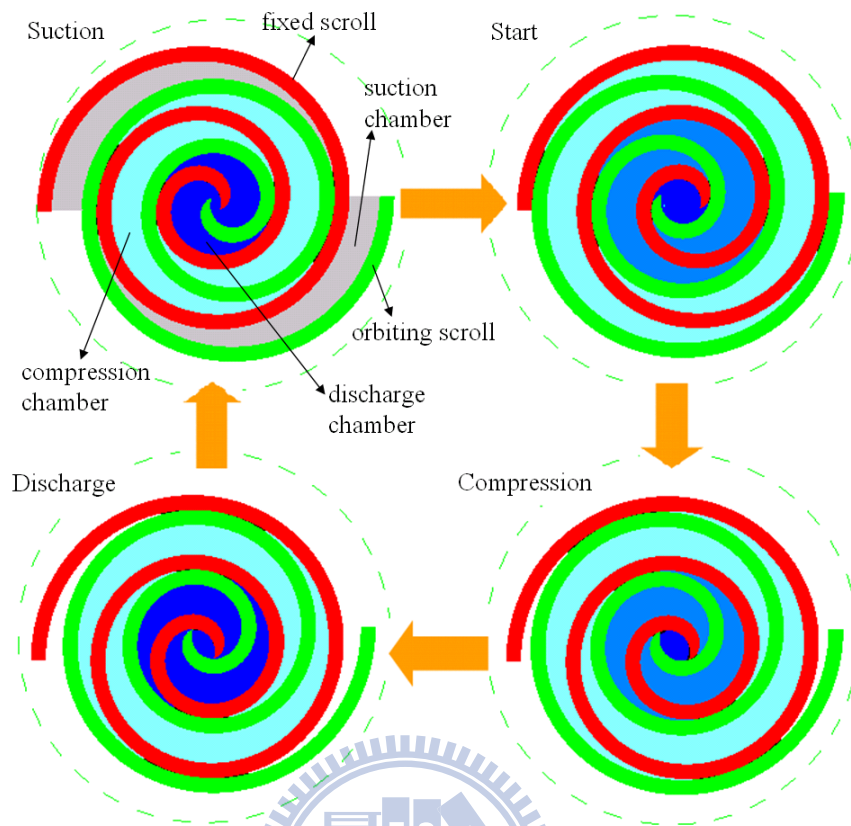


Fig. 1-1 A complete cycle of STC: suction→compression→discharge

The key components for a STC includes a orbiting scroll, a fixed scroll, an Oldham ring, a frame structure, a shaft with eccentric crank, a motor and several counterweight parts, bearing components and compliment mechanisms as shown in Fig1.2. Generally speaking, a STC is more durable than other rotary type compressors because of having fewer parts.

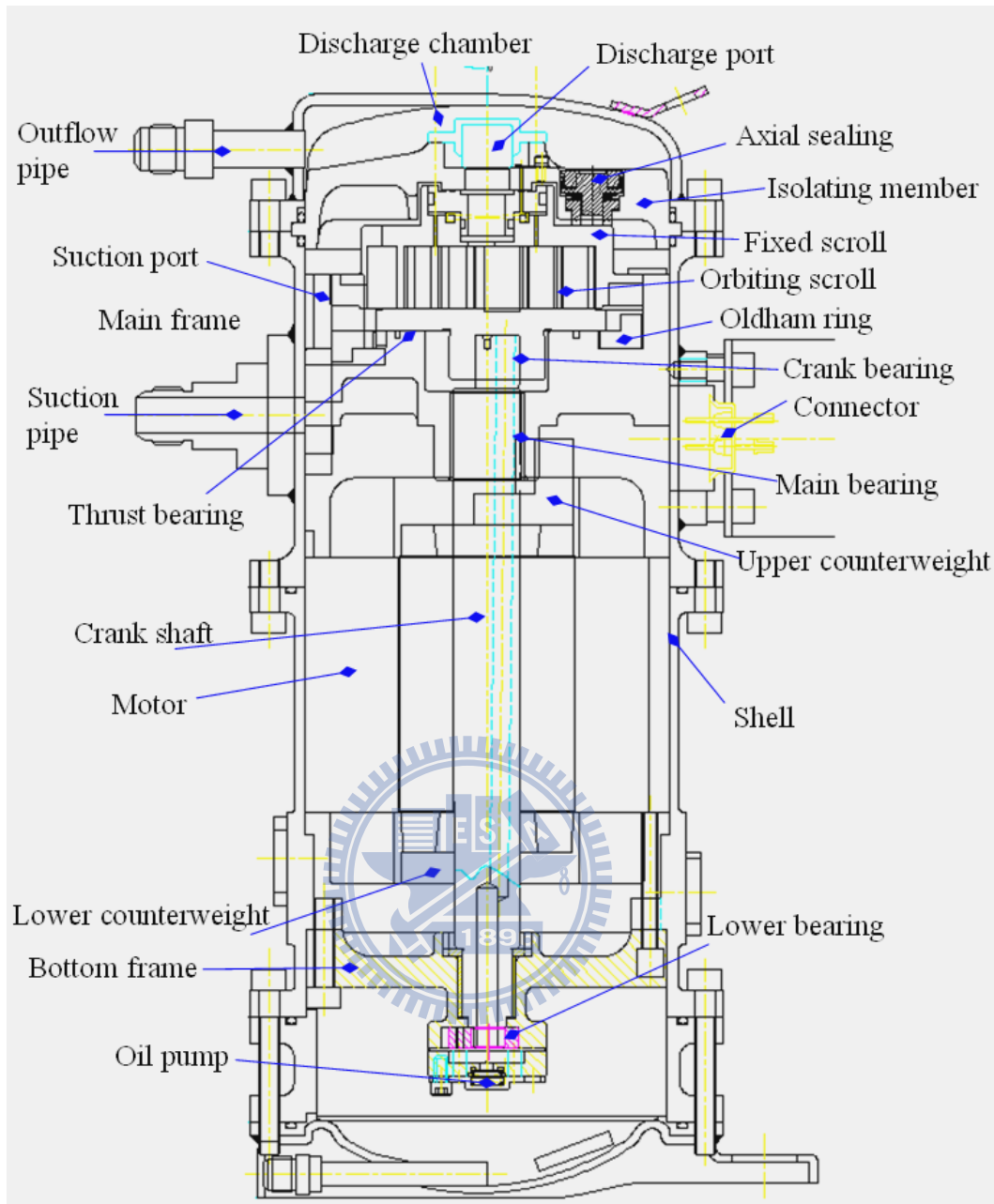


Fig. 1-2 A schematic of a STC

Though the idea of scroll machine was originated since 1905 and has been evaluated for many benefits, it did not be commercialized before 1970's due to the need of precise manufacturing and assembly technique and the accompanied requirements of keeping the low cost for their key components, such as orbiting and fixed scrolls, Oldham ring and crankshaft. Besides, the sealing mechanism for reducing leakage between the contact regions to promote higher efficiency is also a critical topic. These two issues have been solved since 1975 from lots of disclosed patents and literatures. The mass production of STC products, including resident, commercial and automobile air-conditioning and refrigeration fields, were launched

since 1980. Several well-known companies commercialized STC products, like Sanden Corp., Hitachi Ltd., Trans Corp., and so on (Chang [1]). Among them, Copeland Corp., by means of its innovative technology, has made their STCs with high efficiency, easy fabrication and low cost and this company dominated the STC development for occupying over 50% share of total STC markets (7 millions units per year).

With regard to developing STC, many particular designs have been disclosed from patents and research papers. However, except a few experiments and simulation results presented in them to verify their claimed merits, most literatures possessed just a few descriptions to their functions that they claimed without any proof of feasibility. Therefore, a simulation model based on the mathematical foundation must be constructed to analyze the effects regarding those design improvements. This procedure not merely provides useful estimations analyzing from the simulation results, but also reduces the times and cost expending on the experiments and tests.

Owing to various design concepts of mechanisms applied to the STC, the general mathematical models about those new and innovative designs must be constructed and the simulation process be programmed, and the analysis to the simulation results be executed to fully evaluate the benefits and defects through those designs.

1.2 Simulation program for STC

One STC simulation program, as a developing tool, is essential to be constructed for estimating various design concepts and assisting engineers in advancing the development of STC. By extending the previous developed one constructed by ITRI, a STC simulation program has been developed for more powerful functions. Up to now, the program has contained 5 main modules as follows; the user interface with I/O handling, the geometrical model with scroll profiles and related mechanisms, the thermodynamics model for compression and discharge in chambers, the dynamics and bearing models dealing with loadings coming from thermodynamic results, and the optimization model for deriving optimum parametric combinations. In addition, several individual mathematical models with regard to mechanism design used in STC have also been constructed to assess their values towards STC. Details of this STC simulation program, including the formulations, procedures, functions and limitations, will be revealed throughout this dissertation.

1.3 Variable speed and compression ratio

Traditionally, the STC, in consideration of simplifying complicated layout and saving cost, is designed to operate at constant speed by using single or multiple phases AC (alternating current) inductive motor. It means that the STC can suit to a specified operating condition or thermal loading (cooling or heating capacity) with constant-speed operation. That is to say, the STC running at one design point has advantageous performance. But deviated from this specific operating condition, other ones with which a STC is faced, will result in various thermal loadings owing to varied environmental temperatures. Hence the STC must be turned off and on to match different thermal loadings, but these switching on/off actions do result in unnecessary power consumption and bring about loud noise and vibration to the pipes and the frame of STC. Therefore, it is incapable of guaranteeing that the STC has high efficiency when running away from the specific design point.

With global warming effect and increasing environmental consciousness, development in STC with higher efficiency and more power saving has been considered. Due to this, a STC that can operate at variable pressure ratio (compression ratio) and speed and can produce optimum efficiency at different operating conditions has been studied in recent years. For variable speeds purpose, several innovative designs of motors have been put in use with STC for providing wider range in operating speed with superior motor efficiency, for example, the 3 phases AC induction motor (Sarma [2] and Engelmann *et al.* [3]) and PMSM synchronous motor (Engelmann *et al.* [3] and Igata *et al.* [4]).

The pressure ratio, on the other hand, is defined as the ratio of the saturated condenser pressure to the saturated evaporator pressure ($p_{\text{dis}}/p_{\text{suc}}$) and is decided for ambient operating conditions. In general, volume ratio is fixed after the geometrical parameters of the scroll pair in STC have been decided. Due to the intrinsic limitation of fixed volume ratio and separated compression chambers in the STC, when the pressure ratio does not match with the volume ratio of the STC, two cases, over-compression and under-compression, will happen (Schein [5]). For under-compression, the repetitive compression in the final chamber or back flow from discharge chamber unavoidably will occur in different designs of STC. For over-compression, the STC will compress the gas to its design point regardless of the high pressure in chambers and extra power is consumed.

Under-compression could not be prevented except by designing a STC with low volume ratio while narrowing the range of operating conditions and eventually reducing the thermal

capacity. Nevertheless, over-compression could be reduced by using bypass valves added to the fixed scroll. Application of bypass valves can change fixed volume ratio to match up with varied operating conditions. Therefore, STC with variable compression ratio can be designed and produced with superior efficiency. In view of this, the mathematical model of bypass valves has been constructed in this study and comparison with experiment, important discussions to the simulation results of STC program were also investigated.

1.4 Design optimization for variable compression ratio

After constructing of a parametric computer model to the STC, one interesting issue is how engineers or designers use it to aid the design process about STC. Due to a great number of parameters defined in the STC model can be selected as design variables and many important simulations results be provided as constraint conditions and cost function, many engineering experiences in STC fields must be introduced into the optimization procedure for finding not only the optimum, but also the possible and reasonable combination of parameters used in designing STC.

This study has developed an optimization module, including the user interface, the procedure flow and input/output formatted files, for this STC design package and the solver “MOST” (Tseng [6]) has been integrated into it as the calculation kernel. After that, one case riveted on reduction of the frictional losses for bearing components in STC and investigation of relevant effects, was analyzed for demonstrating the optimization procedure.

1.5 Scroll profiles based on an involute of circle with variable radii

Based on using an involute of circle with a fixed radius as scroll profiles, numerous technical researches were proposed for advancing the performance of STC. However, the intrinsic volume ratio to this type of scroll profile is constrained because of the considerations on the strength and stiffness to the scroll wrap, the rigidity and difficulty to the cutting tool, and the housing size to the space and disposition. This means that the volume ratio in STC can just be lifted to a limited extent by using the scroll profile based on involute of circle with a fixed radius.

Though the volume ratio in STC can be improved by modifying the center portion of the scroll pair, the severer loading could be confronted because of the higher pressure difference generated on the center portion scroll wrap between the adjacent chambers. On the other hand,

the higher volume ratio means the higher pressure conditions for the needed operating temperature with which the STC must confront. Due to this, developing a scroll pair in a STC with better rigidity and strength to endure these high pressure conditions has become an issue.

In this study, a complete geometrical model of the scroll curves constructed from an involute of circle with variable radii will be formulated and proved by utilizing the theorem of planar orbiting mechanisms to overcome the mentioned difficulties. After that, several case studies will be implemented and discussed to distinguish the values of this type of scroll profiles. Furthermore, two types of perfectly meshing modifications, arc and line shapes to the center portion of this new scroll profile will also be developed.

1.6 Dissertation Scope

The content of this dissertation are outlined as below. Chapter 1 briefly introduces the STC simulation computer package, bypass mechanism for variable compression ratio and variable speed consideration, the numerical optimization module and the geometrical model of the scroll profiles based on an involute of circle with variable radii. In Chapter 2, the complete structure about the STC simulation package has been depicted. Several important literatures will be reviewed firstly, and mathematical models such as geometry, thermodynamics and mechanism dynamics, will be built up, based on those ones.

Chapter 3 investigates the bypass mechanism used in STC products. Then the mathematical model will be constructed and integrated into the developed STC package. The simulation results of the bypass mechanism regarding different STC structures, described in Chapter 4, are connected to energy saving and liquid-slug protection. The verification for these results is executed by one test platform constructed for an actual STC product using CO₂ as refrigerant.

Development of an optimization module for design of STC products is introduced in Chapter 5. It includes the user interface and the optimum solver. One case on reduction of the frictional losses for bearing components will be studied to estimate the benefits by means of the optimization procedure.

Chapter 6 constructs a mathematical model about the scroll profiles based on an involute of circle with variable radii. Its values will be illustrated. In Chapter 7, two kinds of modification regarding the center portion of the scroll profiles created by an involute of circle with variable radii will be provided. Several case studies will exhibit their uses, defects, and constraints. Finally, conclusions and future works are summarized in Chapter 8.

CHAPTER 2 STC SIMULATION MODEL AND PROCESS

Before proceeding with designing the STC products, it goes without saying that a STC simulation process with several important mathematical models must be constructed firstly and integrated into a computer program. The whole models include geometry of the scroll, thermodynamics with refrigerant in compression and discharge processes, leakage through clearances, back pressure mechanism, superheat of suction pipe, and dynamic balance of the mechanical components.

2.1 Developments in mathematical models of STC

Numerous literatures about the mathematical model of STC were published since 1980's. Among them, Morishta *et al.* [7, 8] constructed one analytical model for a STC. This included the geometry of scroll profile, the thermodynamics during compression and discharge process and the dynamics of related mechanical components used in STC. Based on this primitive model, a great many technical researches have been issued for the respective mathematical models or concerning the integral process during the two decades.

2.1.1 Geometry of scroll profiles

With regard to the scroll pair (which mean the fixed and orbiting scroll), many papers and patents have been proposed to refine them in order to improve the STC's performance. In the theoretic study, Lee and Wu [9] proved that several theorems related to planar orbiting mechanisms can be used to design a scroll pair. In addition, the planar curves expressed by the intrinsic equation (Gravesen and Henrisken [10]) have also been developed, to derive the closed analytical expression about several types of scroll profiles (Bukac [11] and Qiang [12]).

By way of using differential geometry, many curve profiles, in addition to the conventional involute of circle with a fixed radius, have been used to create the scroll pair and investigate its application continuously. These includes the archimedes spirals (Gagne and Nieter [13]) and segmental arcs (Mahfouz *et al.* [14], Liu and Liu [15]). Moreover, Wang et al. [16] provided a modified mathematical model for the discrepant angle to the profiles of

involute.

On the other hand, several methods and modifications for reaching the perfectly meshing engagement at the center of the scroll pair and avoiding the mutual interference have been exhibited (Terauchi and Hiraga [17], Hirano and Hagimoto [18] and Lee and Wu [19]). It is expected that these modifications can improve the STC efficiency and durability. Furthermore, Li *et al.* [20] compared different curves which were used to generate the scroll wrap profiles in a STC, and discussed their advantages and defects.

2.1.2 Thermodynamics in the scroll pair

By referring the rotatory compressor, Yanagisawa *et al.* [21, 22] estimated the suction heating and leakage losses. Extending their methods and on the basis of polytropic process, Morishita *et al.* [7, 8], Nieter and Gagne [23] and Morimoto *et al.* [24] derived their respectively analytical model for STC. By referring to the above references, Chen *et al.* [25, 26], using the mass and energy conservation equations with the 1st law of thermodynamics, developed a detailed mathematical model of STC with consideration of scroll geometry, compression and discharge process and two kinds of leakage between the adjacent chambers. Several important indices about thermal efficiency were also derived under different operating conditions. Moreover, Schein and Radermacher [5] not only disclosed the simulation results of their STC computer model, but explained the causes of under-compression and over-compression which may happened during the compression stage of STC.

2.1.3 Dynamics of components and bearing models

In addition to the scroll pair, the most important one in STC is the coupling mechanism which is used to prevent the orbiting scroll from revolving on its own axis. The dynamic model of the orbiting scroll coupled with the Oldham-ring [7] can handle this mechanism. In additions, the dynamic forces and moments which generated from the gas pressure in chambers and the inertial effect of components (such as counterweight parts and some eccentric components) were also derived and solved to obtain the needed supporting forces of the bearings through the STC mathematical model disclosed by Morishita *et al.* [7, 8].

In machine design for STC, the journal and thrust bearings must be used for supporting the lateral and axial loadings since their inexpensive cost as compared with the ball or roller bearings. In light of this, Kulkari [27, 28] and Sato *et al.* [29] have developed the thrust bearing models with hydrodynamic lubrication theory. For journal bearing, the numerical model utilizing mobility method for journal bearings (Booker [30–32] and Geonka [33]) has

been provided and this study will refer these well-developed models for calculating the frictional losses and predicting some important indices.

2.2 Geometrical model of STC

Most STC products take the involute of circle with a fixed radius for the profiles of scroll wrap because of its inexpensively manufacturing cost. Hence the mathematical formulations of it must be introduced at first.

2.2.1 Scroll profile design by involute of circle with a fixed radius

An involute of circle with a fixed radius and the area enveloped by it is shown in Fig. 2-1. Let the involute angle ϕ be one variable and the involute can be expressed in Cartesian coordinate system as below:

$$\begin{cases} x = a[\cos \phi + (\phi) \sin \phi] \\ y = a[\sin \phi - (\phi) \cos \phi] \end{cases} \quad (2.1)$$

where a represents the radius of base circle.

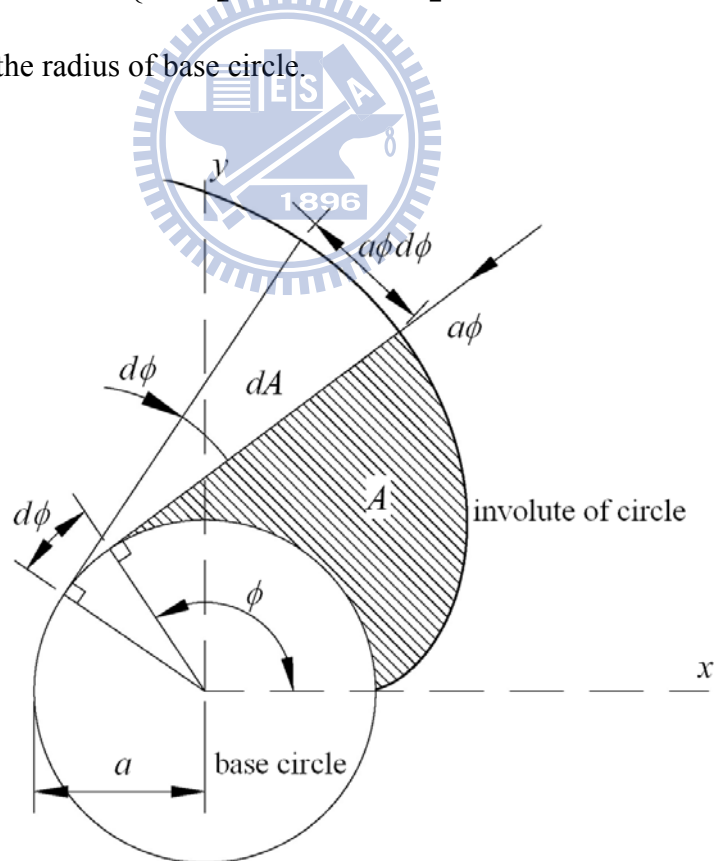


Fig. 2-1 Parametric definition for the involute of circle

If adding or subtracting an increment α (also called initial angle) to equation (2.1), the

outer and inner involute profiles of a fixed scroll can be written as

$$\begin{cases} x_{f,ou} = a [\cos \phi + (\phi - \alpha) \sin \phi] \\ y_{f,ou} = a [\sin \phi - (\phi - \alpha) \cos \phi] \end{cases} \quad (2.2)$$

$$\begin{cases} x_{f,in} = a [\cos \phi + (\phi + \alpha) \sin \phi] \\ y_{f,in} = a [\sin \phi - (\phi + \alpha) \cos \phi] \end{cases} \quad (2.3)$$

By using the equations (2.2) and (2.3) with consideration of coordinate transformation, the orbiting scroll also can be generated as below:

$$\begin{cases} x_{m,ou} = -x_{f,ou} - r_{ob} \cos(\theta + \theta_e) \\ y_{m,ou} = -y_{f,ou} + r_{ob} \sin(\theta + \theta_e) \end{cases} \quad (2.4)$$

$$\begin{cases} x_{m,in} = -x_{f,in} - r_{ob} \cos(\theta + \theta_e) \\ y_{m,in} = -y_{f,in} + r_{ob} \sin(\theta + \theta_e) \end{cases} \quad (2.5)$$

Some important parameters used above and in this geometrical model are defined firstly as follows:

$$\begin{cases} a: \text{radius of base circle} \\ a = \frac{p_t}{2\pi} \end{cases} ; \begin{cases} \alpha: \text{initial angle of involute} \\ \alpha = \frac{t_h}{2r_b} \end{cases} ; \begin{cases} r_{ob}: \text{orbiting radius} \\ r_{ob} = \frac{p_t}{2} - t_h \end{cases} \quad (2.6)$$

$$\begin{cases} N: \text{number of chambers} \\ N = \text{Int}\left(\frac{\phi_e - \phi_{dis}}{2\pi}\right) + 1 \end{cases}$$

where ϕ_{dis} the discharged involute angle decided by cutting condition

$$\begin{cases} \theta_e: \text{modified angle to specified end involute angle} \\ \theta_e = 2\pi \cdot (N + 1/4) - \phi_e \end{cases}$$

$$\begin{cases} \theta_{dis}: \text{discharged orbiting angle at one revolution} \\ \theta_{dis} = (\phi_e - \phi_{dis}) - 2\pi \cdot (N - 1) \end{cases}$$

Figure 2-2 shows the fixed and orbiting scrolls when they are just ready to proceed with compression process.

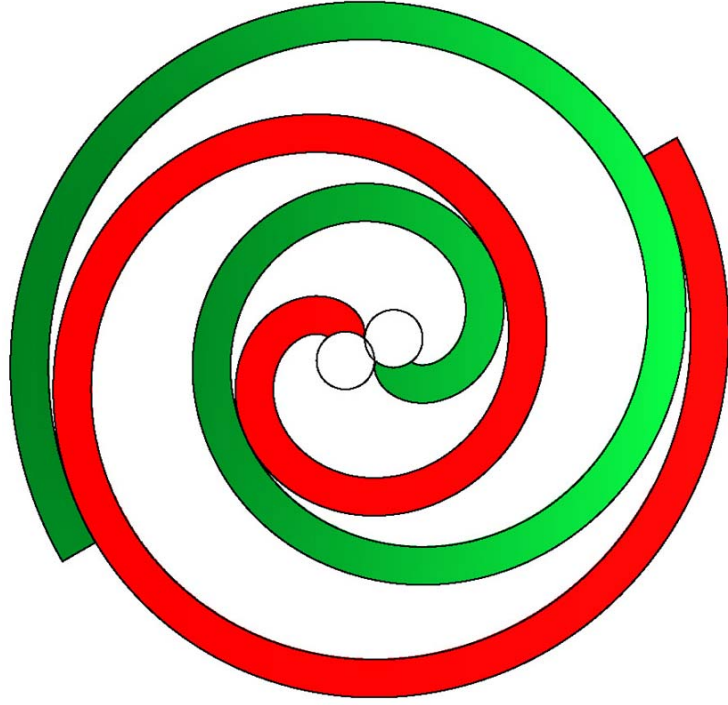


Fig. 2-2 Inner and outer Profiles of fixed scroll

2.2.2 Derivation of volume and its ratio of the scroll chambers

Referring to Fig. 2-1 again, the enclosed chamber's area can be formed from the inner involute on one scroll wrap and the outer involute on another one, those areas can be derived by integrating the minute area dS along with the involute angle ϕ , hence the enclosed areas created by the inner involute is

$$\begin{aligned}
 A_i &= \int_{\phi-\alpha-\pi}^{\phi-\alpha} \left[\frac{1}{2}(a\phi)^2 d\phi - \frac{1}{2}(a(\phi-2\pi))^2 d\phi \right] \\
 &= \int_{\phi-\alpha-\pi}^{\phi-\alpha} [2\pi a^2(\phi-\pi)] d\phi \\
 &= \pi^2 a^2 [2(\phi-\alpha) - 3\pi]
 \end{aligned} \tag{2.7}$$

Similarly, the areas by the outer involute is

$$\begin{aligned}
 A_o &= \int_{\phi-3\pi}^{\phi-\pi} \left[\frac{1}{2}(a(\phi+\alpha))^2 d\phi - \frac{1}{2}(a(\phi-\alpha))^2 d\phi \right] \\
 &= \int_{\phi-3\pi}^{\phi-\pi} 2a^2 \alpha \phi d\phi \\
 &= 4\pi^2 a^2 \alpha (\phi-2\pi)
 \end{aligned} \tag{2.8}$$

Assume the scroll warp have symmetric chambers, therefore, the enclosed areas can be expressed as follows

$$\begin{aligned}
A &= 2(A_i - A_o) = 2\pi a(2\phi - 3\pi)(\pi a - 2\alpha a) \\
&= p_t \left(\frac{p_t}{2} - t_h \right) (2\phi - 3\pi)
\end{aligned} \tag{2.9}$$

Nevertheless, another method using differential geometry to derived the enclosed chamber areas can also be adopted and expressed as below

$$\begin{aligned}
A &= \frac{1}{2} \int_{\phi-2\pi}^{\phi} \left| x_{m,in} \cdot \frac{d(y_{m,in})}{d\phi} - y_{m,in} \cdot \frac{d(x_{m,in})}{d\phi} \right| d\phi \\
&\quad - \frac{1}{2} \int_{\phi-2\pi}^{\phi} \left| x_{f,ou} \cdot \frac{d(y_{f,ou})}{d\phi} - y_{f,ou} \cdot \frac{d(x_{f,ou})}{d\phi} \right| d\phi
\end{aligned} \tag{2.10}$$

Multiplying equation (2.9) by the wrap height h , the chamber volume can be derived as

$$V(\phi) = h \cdot A = hp_t \left(\frac{p_t}{2} - t_h \right) (2\phi - 3\pi) \tag{2.11}$$

If we decide the ended involute angle ϕ_e and ϕ_{dis} as the involute angle while the meshing is at the discharge step, the volume ratio can be expressed as

$$Vol_r = \frac{2\phi_e - 3\pi}{2\phi_{dis} - 3\pi} \tag{2.12}$$

The details to the fundamental formulas applied in modifying the discharge angle ϕ_{dis} to the involute angle with constant radius for raising the volume ratio and preventing interference can refer to the papers derived by Morishita *et al.* [7, 8], and Nieter and Gagne [23].

2.3 Thermodynamic model

The thermodynamics including suction/discharge superheat, the compression and discharge with variations in pressure and temperature are considered. In addition, the leakage clearances of the scroll pair, including the end-side and flank leakage, are dynamically and linearly linked to pressure ratio and back-pressure (Chen *et al.* [25]), and those linear functions are expressed in this model. Also, several important indices related to thermodynamics will also be formulated in the following paragraph.

2.3.1 Refrigerant property

The ‘‘Refprop7’’ published by NIST [34], as a powerful tool, is used in this model to obtain lots of data for most known refrigerants. The STC simulation package integrates it by

linking the dynamic link libraries (.dll) to acquire the related properties which will be used for calculation during the compression and discharge processes. The linking procedure can refer to Fig. 2-3.

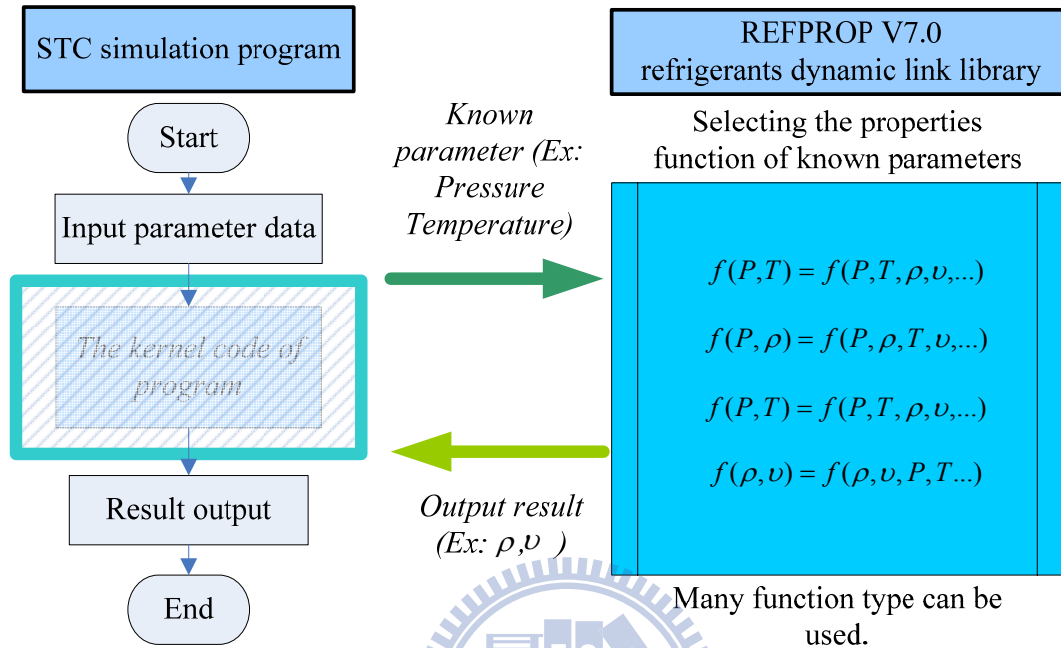


Fig. 2-3 Illustration of “Refprop7” linking to STC simulation package

2.3.2 Suction and discharge superheating calculations

In general, the STC can be divided into two structures—high and low-side structures. The low-side structure means the chamber above the fixed scroll is at discharge pressure, but the other regions in the housing are at suction pressure. The high-side structure is at discharge pressure in the whole housing except the suction and compression chambers. The main benefits and drawbacks of those two structures are summarized as follows:

Low-side:

Benefits:

- (1) Simple motor/load application and radial compliance.
- (2) Large housing chamber used as suction muffler and good overturning moment control.

Drawbacks:

- (1) Complex thrust bearing design, axial compliance mechanism and small discharge muffler volume.
- (2) Difficulties in designing and machining intermediate pressure holes and more suction gas

heating.

- (3) Exact scroll set machining and fine finishes are need for minimal leak paths.

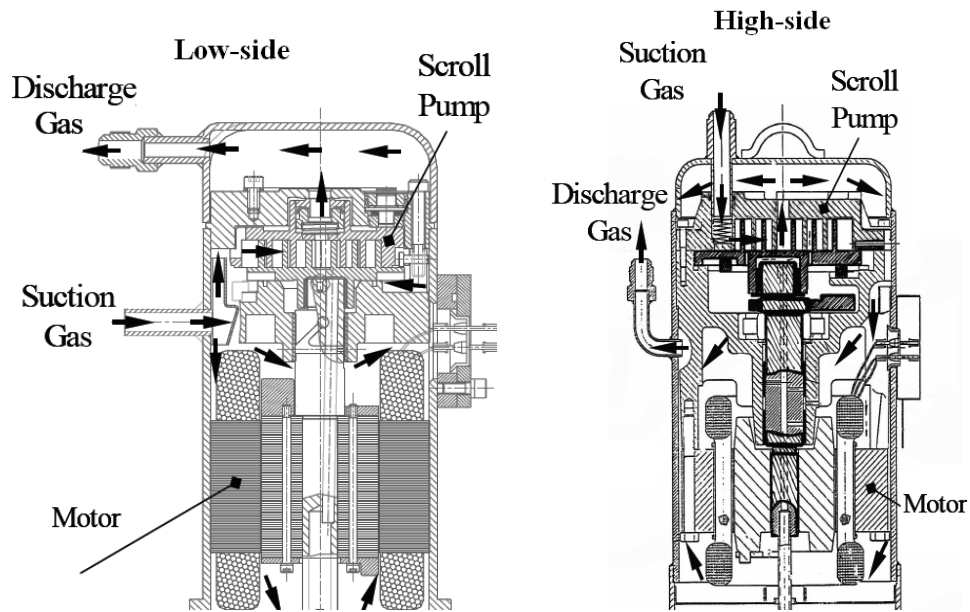


Fig. 2-4 Low-side and High side structure of STC [1]

High-side:

Benefits:

- (1) Simple pressure control and no intermediate pressure holes can avoid leakage.
- (2) Simple machining, minimal suction superheat and large housing chamber used as discharge muffler.
- (3) Simple radial and axial compliance mechanism, and no problem involved passing large quantities of oil through the scroll set.
- (4) Oil can help control overturning moment and provide to seal leak paths.

Drawbacks:

- (1) Small suction muffling and hardness in motor/load application.
- (2) Severer housing design to conform the ultimate rest requirements.

Owing to the different structure of the two STC, their heat transfer coefficients for the pipe at suction (for low side structure and high side structure) and discharge (for high side structure) can be expressed by two experienced formulas—the Gnielinski relationship (Winandy *et al.* [35]) and Squire-Eckert prediction (Fukuta *et al.* [36])—which expressed as

$$h_{tu,s} = \frac{\lambda}{d_{tu,s}} \cdot \frac{(f/8)(Re-1000)Pr}{1+12.7\sqrt{f/8}(Pr^{2/3}-1)} \quad (2.13)$$

$$h_{w,d} = 0.678 \frac{\lambda}{L} \cdot Ra_L^{0.25} \left(\frac{Pr}{0.952 + Pr} \right)^{0.25} \quad (2.14)$$

Then the suction and discharge superheat can be evaluated.

2.3.3 Compression and discharge process

This simulation model provides two ways for users to calculate the compression and discharge processes. Several assumptions must be employed in the model for simplicity, such as neglecting the turbulent flow of refrigerant and oil effects inside the chambers. Those are stated as below:

1. Refrigerant in working chambers is homogeneous.
2. Gravitational, kinetic energy variations are neglected.
3. Oil effects are neglected.
4. Chambers of the scroll pairs are symmetric.

(1): The mass conservation of refrigerant in chambers (control volume) with polytropic process consideration. These can be described as

$$\begin{cases} \dot{m} = \dot{m}_{in} - \dot{m}_{ou} \\ p_{cur} = p_{suc} \left(\frac{\rho_{cur}^*}{\rho_{suc}^*} \right)^n \end{cases} \quad (2.15)$$

where n can be measure by laboratory experiment (DeBlois and Stoeffler [37]).

(2): The mass conservation of refrigerant in chambers (control volume) with the simplified first law of thermodynamics, which can be expressed as

$$\begin{cases} \dot{m} = \dot{m}_{in} - \dot{m}_{ou} \\ \frac{dT_g}{d\theta} = \frac{1}{m_g c_{vg}} \left[T_g \left(\frac{\partial p_g}{\partial T_g} \right)_v \left(\frac{dV_g}{d\theta} - \frac{1}{\rho_g^*} \left(\frac{dm_{g,in}}{d\theta} - \frac{dm_{g,ou}}{d\theta} \right) \right) \right. \\ \left. + \sum \frac{dm_{g,in}}{d\theta} (h_{g,in} - h_g) + \frac{dQ}{d\theta} \right] \end{cases} \quad (2.16)$$

2.3.4 Leakage flows

Generally speaking, there are two kinds of leakage paths—end-side and flank leakage—existed in a STC. Fig. 2-5 and 2-6 show the illustration about these two paths and the leakage mass flow can be shown as follow:

$$\dot{m}_1 = \dot{m}_{1,e} + \dot{m}_{1,f} \quad (2.17)$$

Where $\dot{m}_{1,e}$ and $\dot{m}_{1,f}$ are end-side and flank leakage mass flow rate.

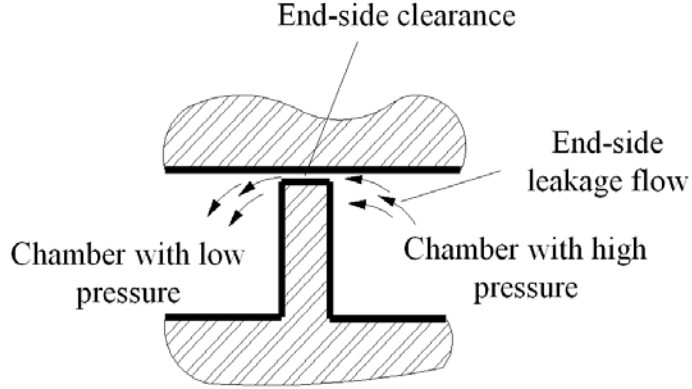


Fig. 2-5 Illustration of end-side leakage

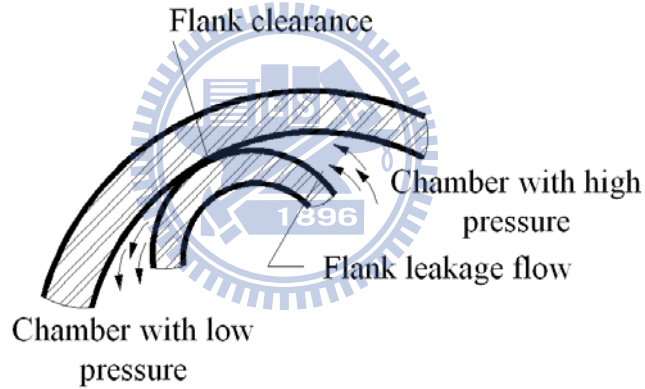


Fig. 2-6 Illustration of flank leakage

Gap sizes of the two kinds of leakage are both dynamically related to the operating pressure, pressure ratio and back-pressure mechanisms acted on scroll pairs. These three ones are dependent on various design structures of STC (such as low side and high side structures). The end-side gap δ_e , in meters, can be derived as below:

$$\delta_e = \left[1.02 \cdot \left(\frac{p_{dis} - p_{back}}{p_{suc}} \right) - 0.45 \right] \cdot 10^{-6} \quad (2.18)$$

The end-side flow areas can be calculated [25] as:

$$\begin{aligned} A_{in} &= \delta_e \int_{\phi_k}^{\phi_{k+1}} L_o d\phi \\ A_{out} &= \delta_e \int_{\phi_k}^{\phi_{k+1}} L_i d\phi \end{aligned} \quad (2.19)$$

where ϕ_{k+1} and ϕ_k are the involute angles of the conjugate end points for the scroll pair.

For end-side leakage, one-dimensional isentropic compressible flow in a nozzle is used as

$$\begin{aligned} \dot{m}_{l,e} &= C \cdot A \left\{ p_{up} \cdot \rho_{up}^* \cdot \frac{2n}{n-1} \left[\left(\frac{p_{dw}}{p_{up}} \right)^{\frac{2}{n}} - \left(\frac{p_{dw}}{p_{up}} \right)^{\frac{n+1}{n}} \right] \right\}^{0.5}; \text{ when } \left(\frac{p_{dw}}{p_{up}} \right) \geq \left(\frac{2}{n+1} \right)^{\frac{n}{n-1}}, \\ \dot{m}_{l,e} &= C \cdot A \left[p_{up} \cdot \rho_{up}^* \cdot n \cdot \left(\frac{2}{n+1} \right)^{\frac{n+1}{n-1}} \right]^{0.5}; \text{ when } \left(\frac{p_{dw}}{p_{up}} \right) < \left(\frac{2}{n+1} \right)^{\frac{n}{n-1}} \end{aligned} \quad (2.20)$$

where A is A_{in} or A_{out} for inflowing or outflowing conditions. Similarly, the flank gap is expressed in meters as follow:

$$\delta_f = \left[-6 \cdot \left(\frac{p_{dis} - p_{back}}{p_{suc}} \right) + 20 \right] \cdot 10^{-6} \quad (2.21)$$

The flank flow area is

$$A_f = h \delta_f \quad (2.22)$$

For $\dot{m}_{l,f}$, equation (2.20) also be used with $A = A_f$. Thus the total leakage mass flow rate can be calculated.

2.4 Dynamics in mechanical components and mechanisms in STC

2.4.1 Dynamic forces and moments

The dynamic model of the orbiting scroll coupled with the Oldham ring (Morishita *et al.* [7]) is adopted in this study. Several dynamic forces caused by gas pressure in chambers and acted on the orbiting scroll are considered. Those forces are classified as tangential, radial and axial ones. As shown in Fig. 2-7, the tangential force (F_θ) and radial force (F_r) can be expressed as follows:

$$F_\theta = \sum_{i=1}^N F_{\theta i} = \sum_{i=1}^N r_b \cdot h \cdot (2\phi - \pi) \cdot (p_i - p_{i+1}) \quad (2.23)$$

$$F_r = \sum_{i=1}^N F_{r i} = \sum_{i=1}^N 2 \cdot r_b \cdot h \cdot (p_i - p_{i+1}) \quad (2.24)$$

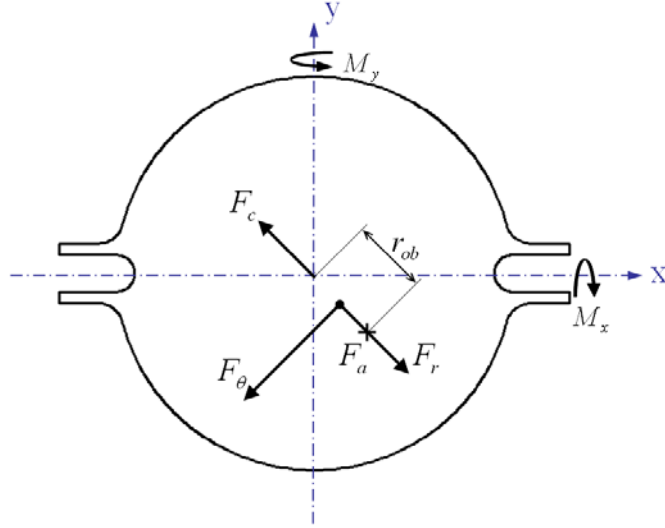


Fig. 2-7 Dynamic forces of the orbiting scroll

In axial direction, the back pressure mechanism is used to reduce the axial load and the resultant axial force is

$$F_{ax} = \sum_{i=1}^N p_i \cdot A_i - F_{back} + m_{ob} \cdot g \quad (2.25)$$

where A_i represented the chamber area derived by Morishita *et al.* [8]. Moreover, by neglecting the inertial force with constant speed consideration, the centrifugal force of the orbiting scroll is

$$F_{c,ob} = m_{ob} \cdot r_{ob} \cdot \left(\frac{d\theta}{dt} \right)^2 \quad (2.26)$$

The force and moment equations of the orbiting scroll coupled with Oldham ring are used to derive the bearing force of the crank journal bearing ($F_{b,cr}$) set up on the crank shaft [7]. Furthermore, by assuming the resultant axial force (F_{ax}) and turning moment (M) must be balanced by reaction components resulted from the thrust surface [7], the turning moment M and the directional turning angle β of the orbiting scroll can be shown as follows:

$$\begin{cases} M_x = F_{ax} \cdot (y_{scr} - r_{ob} \sin \theta) \\ M_y = F_{ax} \cdot (x_{scr} + r_{ob} \cos \theta) \end{cases}$$

$$M = \sqrt{M_x^2 + M_y^2} \quad (2.27)$$

$$\beta_{el} = \tan^{-1} \left(\frac{M_y}{M_x} \right)$$

where (x_{scr}, y_{scr}) represents the locus of the turning moment on the thrust surface.

2.4.2 Counterweight analysis

Another important part is the counterweight analysis. Fig. 2-8 is the force diagram in x-direction, the crank bearing force ($F_{b,cr}$) and the centrifugal forces from the crank shaft ($F_{c,cr}$), the upper and lower counterweights ($F_{c,ucw}$ & $F_{c,lcw}$) are considered. The upper and lower journal bearings are used to support the driving shaft. By assuming the center of the upper journal bearing as the pivot, the two bearing forces can be derived as follows

$$\begin{cases} F_{bx,low} \cdot z_{bx,low} = F_{bx,cr} \cdot z_{bx,cr} + F_{cx,cr} \cdot z_{cx,cr} + F_{cx,ucw} \cdot z_{cx,ucw} - F_{cx,lcw} \cdot z_{cx,lcw} \\ F_{by,low} \cdot z_{by,low} = F_{by,cr} \cdot z_{by,cr} + F_{cy,cr} \cdot z_{cy,cr} + F_{cy,ucw} \cdot z_{cy,ucw} - F_{cy,lcw} \cdot z_{cy,lcw} \\ F_{bx,upp} + F_{cx,ucw} = F_{bx,cr} + F_{cx,cr} + F_{bx,low} + F_{cx,lcw} \\ F_{by,low} + F_{cy,ucw} = F_{by,cr} + F_{cy,cr} + F_{by,low} + F_{cy,lcw} \end{cases} \quad (2.28)$$

$$F_{b,low} = \sqrt{F_{bx,low}^2 + F_{by,low}^2} ; F_{b,upp} = \sqrt{F_{bx,upp}^2 + F_{by,upp}^2}$$

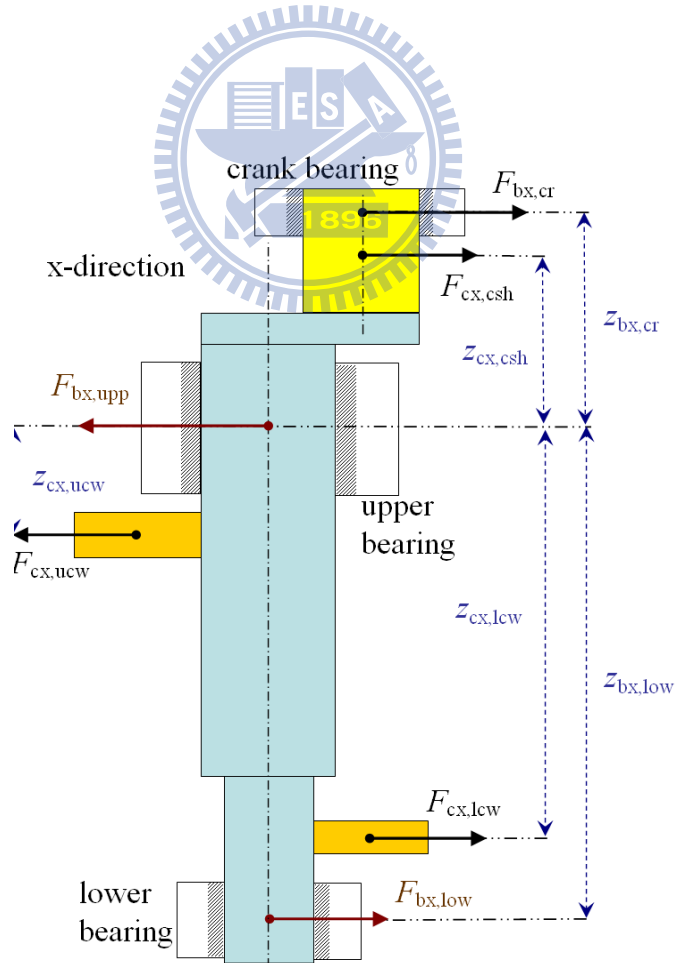


Fig. 2-8 Dynamic balance of the driving shaft

2.5 Frictional losses in mechanical components

In addition to the compression power consumed during STC operation, other main expenses are the frictional losses from the mechanical components. Those losses are mainly caused from the thrust surface (as thrust bearing) and the three journal bearings. In addition, by assuming the frictional losses around the other mechanical components (such as Oldham ring) is negligibly small compared with the bearing losses (Ishii *et al.* [38]), the frictional coefficient of the other mechanical components is set as 0.013 [38] to calculate the friction force and losses in this study.

2.5.1 Thrust bearing

As shown in Fig. 2-9, the thrust bearing is used to support against the resultant axial force F_{ax} and turning moment M . Several models have been investigated in literatures (Kulkarni [27, 28], Sato *et al.* [29], Akei *et al.* [39] and Oku *et al.* [40]). Among those, one rigid-body wobbling model [27, 28, 39] with hydrodynamic lubrication theory is adopted in this developed STC model. The definitions of relevant parameters are showed in Fig. 2-10.

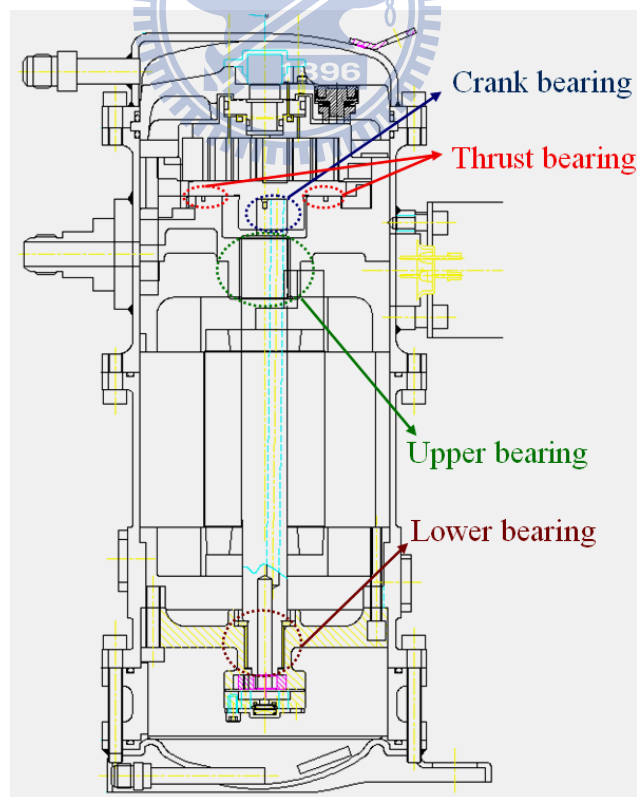


Fig. 2-9 Schematic of the three journal bearings and the thrust bearing

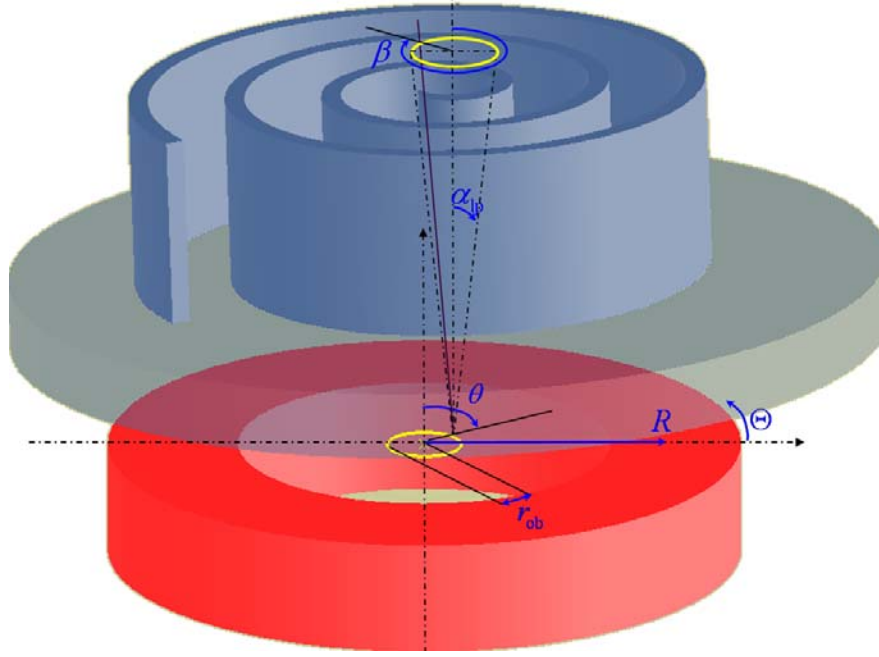


Fig. 2-10 Parameters of the thrust bearing

By assuming sufficient circulation of lubricant through the thrust bearing and the steady temperature, the Reynolds equation, including the wedge and squeeze terms for generating the pressures on the circular thrust surface, can be expressed in cylindrical coordinates as:

$$\begin{aligned} & \frac{1}{R} \frac{\partial}{\partial R} \left(RH^3 \frac{\partial p}{\partial R} \right) + \frac{1}{R^2} \frac{\partial}{\partial \Theta} \left(H^3 \frac{\partial p}{\partial \Theta} \right) \\ & = 6\mu \left(\frac{1}{R} \frac{\partial}{\partial R} (RHU_R) + \frac{1}{R} \frac{\partial}{\partial \Theta} (HU_\Theta) + 2 \frac{\partial H}{\partial t} \right) \end{aligned} \quad (2.29)$$

The oil-film clearance H between the tilting orbiting scroll and thrust surface is

$$H = H_0 - \tan \alpha_{lp} (R \sin(\Theta + \beta) - r_{ob} \cos(\theta - \beta)) \quad (2.30)$$

where H_0 is the nominal oil-film clearance (shown in Fig. 2-11), α_{lp} is the tilting angle and β_{el} is the directional tilting angle. The surface velocities and velocity derivatives of the orbiting scroll can be simplified as:

$$\begin{aligned} U &= r_{ob} \cdot \omega, \\ \begin{cases} U_R = U \cos(\Theta + \theta), & \frac{\partial U_R}{\partial R} = 0 \\ U_\Theta = -U \sin(\Theta + \theta), & \frac{\partial U_\Theta}{\partial \Theta} = -U \cos(\Theta + \theta) \end{cases} \end{aligned} \quad (2.31)$$

The following assumptions simplify the squeezing effect:

$$\dot{H}_0 = 0, \quad \dot{\alpha} = 0, \quad \dot{\beta} = \dot{\theta} = \omega \quad \text{and} \quad \frac{\partial H}{\partial t} = \frac{\partial H}{\partial \Theta} \omega \quad (2.32)$$

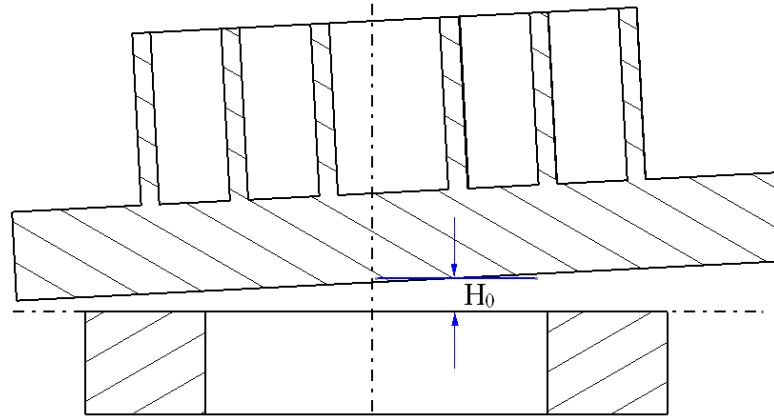


Fig. 2-11 Nominal height of oil-film

The average Reynolds equation (2.29) is approximated by the finite difference operators and the successive over-relaxation (SOR) method is used as solution approach and the suction pressure is set as the boundary condition of the thrust surface. Once the pressure distribution is known, the force and moment from the lubrication oil can be integrated as

$$F'_{ax} = \int_0^{2\pi} \int_{R_i}^{R_o} p \cdot R dR d\Theta \quad (2.33)$$

$$M'_x = \int_0^{2\pi} \int_{R_i}^{R_o} p \cdot R \sin \Theta \cdot R dR d\Theta, \quad M'_y = \int_0^{2\pi} \int_{R_i}^{R_o} p \cdot R \cos \Theta \cdot R dR d\Theta \quad (2.34)$$

$$M' = \sqrt{M'^2_x + M'^2_y} \quad \text{and} \quad \beta_{el}' = \tan^{-1} \left(\frac{M'_y}{M'_x} \right)$$

By equating the force and moment in equations (2.25), (2.33) and (2.27), (2.34), there are two simultaneous equations with two unknowns H_0 and α_{lp} , and the Newton-Raphson method is used to solve the equations. Then the friction force $F_{f,th}$ and the frictional losses P_{th} are derived as below:

$$F_{f,th} = \int_0^{2\pi} \int_{R_i}^{R_o} \mu \frac{R^2 \omega}{H} dR d\Theta, \quad (2.35)$$

$$P_{th} = F_{f,th} \cdot U$$

Finally the average frictional losses of thrust bearing can be calculated.

2.5.2 Journal bearings

For journal bearing, selection of the inside diameter D_b , the clearance C_b and the length L_b can decide its frictional characteristics. In order to estimate the frictional losses, the numerical model utilizing mobility method for journal bearings [32, 33] is used and the frictional force becomes

$$F_{fb} = \frac{F_b C_b \varepsilon}{D_b} \sin \Phi + \frac{2\pi\mu\omega L_b}{C_b (1-\varepsilon^2)^{0.5}} \left(\frac{D_b}{2}\right)^2 \quad (2.36)$$

where ε is the eccentricity ratio and Φ is the phase difference from eccentric and load direction. The frictional loss P_b is

$$P_b = F_{fb} \cdot \frac{D_b}{2} \cdot \omega \quad (2.37)$$

Then the average frictional loss of the journal bearings can be calculated.

2.6 Simulation process in the STC computer model

The complete simulation model for STC is programmed by C++ Builder combined with “Refprop7”. The inputs include scroll geometry, related mechanisms, operating conditions and motor Torque-Efficiency-Power curves (as shown in Fig. 2-12) from dynamometer test for specified speed used in this dissertation.

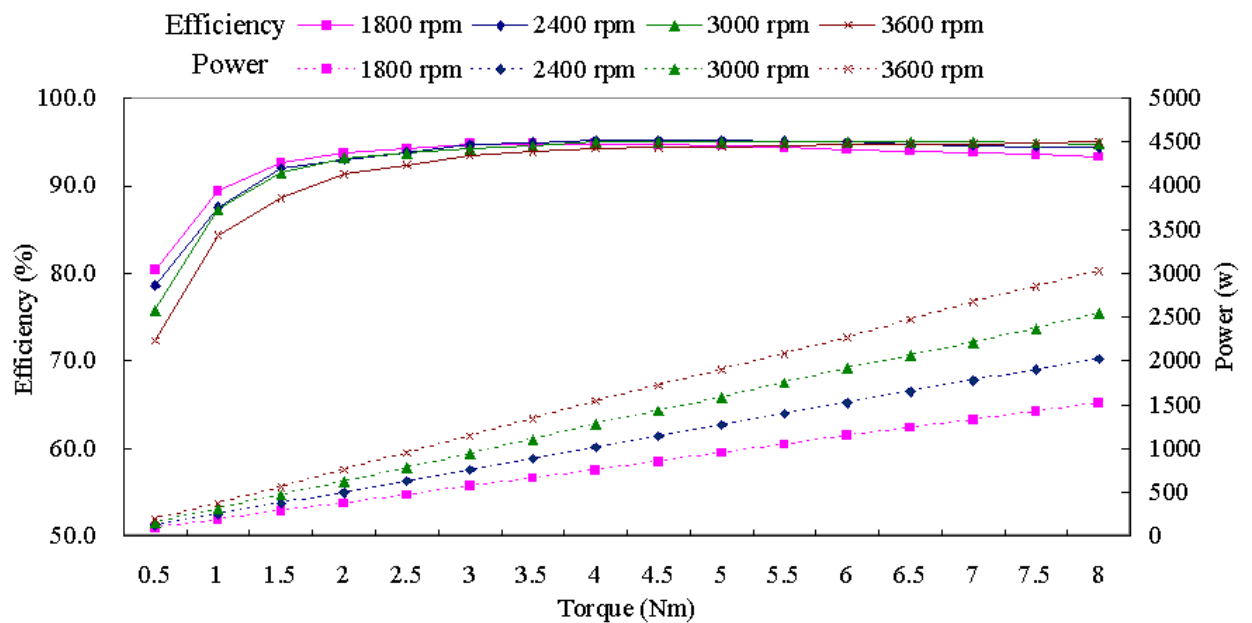


Fig. 2-12 Motor torque-efficiency-power for specified speed

2.6.1 Simulation process

The flowchart of the package is shown in Figure 2-13. The geometry and thermodynamic models are solved with numerical iterations. After that, the dynamics and frictional losses of bearings are also calculated with the previous models iteratively and finally, the output results can be obtained.

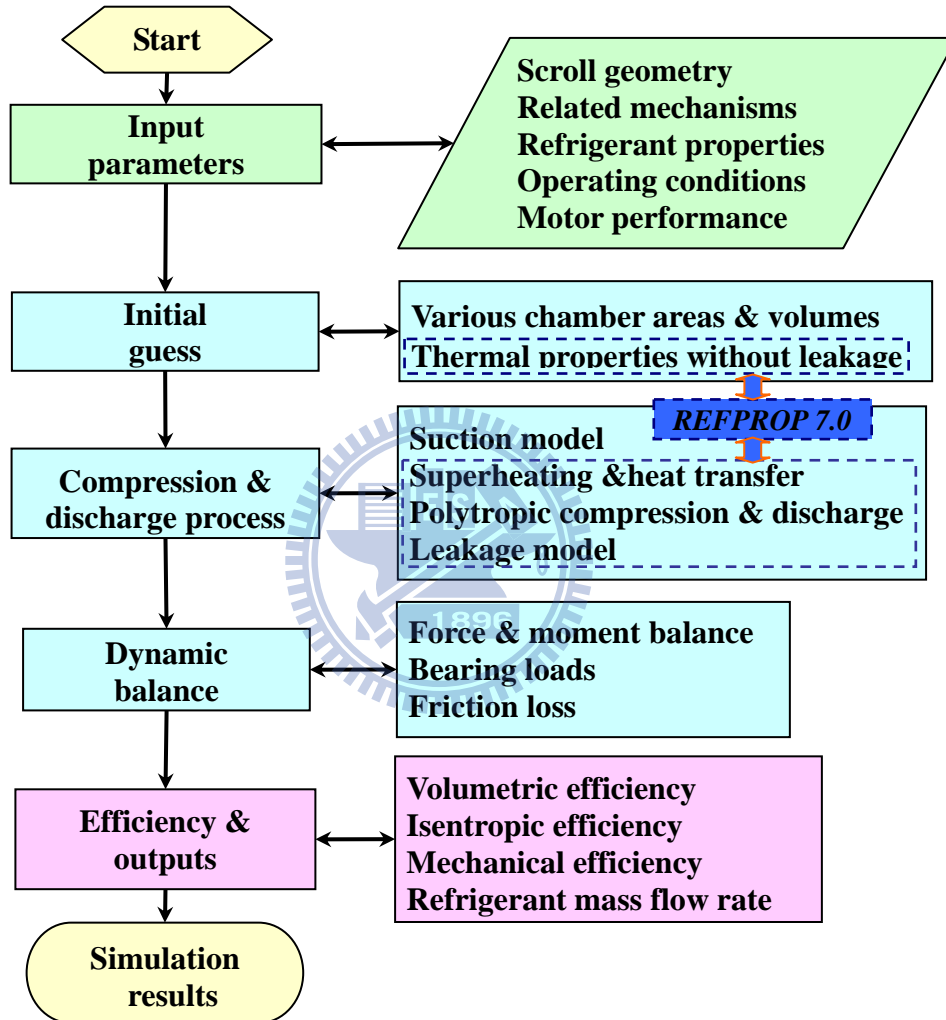


Fig. 2-13 Flowchart of the simulation process in STC package

Among the process, the leakage model is included in the polytropic compression and discharge process (or the energy conservation with compression and discharge process) and then is solved with the 4th Runge-Kutta method (as shown in Fig. 2-14). The 4th R-K method is the solution with convergent criterion as follow:

$$\frac{|\dot{m}_{1,pre} - \dot{m}_{1,cur}|}{\dot{m}_{1,cur}} < CC_1 \quad (2.38)$$

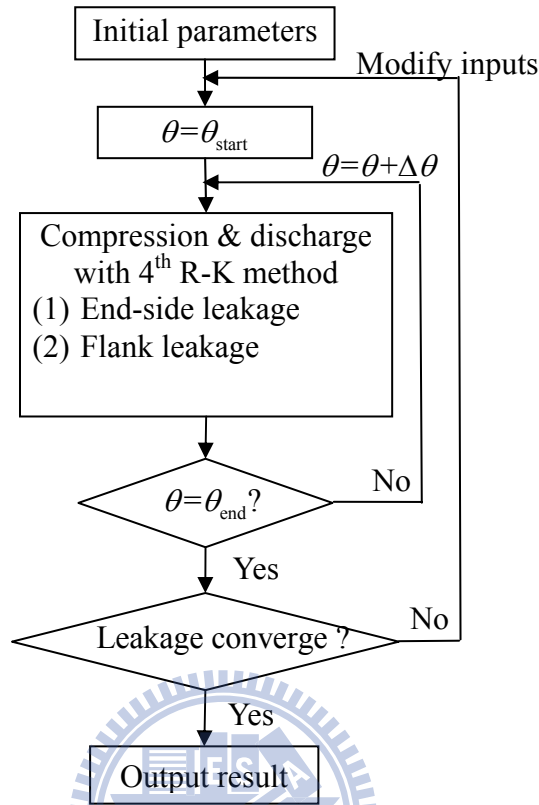


Fig. 2-14 Flowchart of thermodynamics with leakage model in STC package

2.6.2 Output results

After carrying on the above-mentioned simulation process, various performance indices as output data can be obtained. These basic but important outputs used in this dissertation are expressed as follows:

➤ Volumetric efficiency:

$$\eta_V = \frac{\dot{m}_{\text{suc,h}} - \dot{m}_l}{\dot{m}_{\text{suc}}} \quad (2.39)$$

➤ Mass flow rate:

$$\dot{m} = \eta_V \cdot \omega_{\text{motor}} \cdot \rho_{\text{suc}} \cdot V_{\text{suc}} \quad (2.40)$$

where ω is the specified operating speed, ρ_{suc} is the density of the suction refrigerant and V_{suc} represents the designated suction volume of the scroll pair in STC.

➤ Cooling capacity:

$$\dot{Q}_C = \dot{m} \cdot (h_{in} - h_{out}) \quad (2.41)$$

where h_{in} and h_{out} represent the enthalpies of refrigerant at evaporator inlet and outlet respectively.

➤ Adiabatic power:

$$P_{adiabatic} = \eta_V \left\{ \left(\frac{n}{n-1} \right) \cdot P_{suc} \cdot V_{suc} \left[\left(\frac{P_{dis}}{P_{suc}} \right)^{(n-1)/n} - 1 \right] \cdot \omega_{motor} \right\} \quad (2.42)$$

➤ Compression power:

$$P_{compression} = F_\theta \cdot r_{ob} \cdot \omega_{motor} = T_\theta \cdot \omega_{motor} \quad (2.43)$$

➤ Adiabatic compression efficiency:

$$\eta_A = \frac{P_{adiabatic}}{P_{compression}} \quad (2.44)$$

➤ Frictional losses:

$$P_{frictional\ loss} = P_{thrust\ bearing} + P_{journal\ bearings} + P_{other\ mechanisms} \quad (2.45)$$

where $P_{other\ mechanisms}$ are the power resulted from other mechanisms in STC, such as oldham coupling.

➤ Mechanical efficiency:

$$\eta_{Me} = \frac{P_{compression}}{P_{compression} + P_{frictional\ loss}} \quad (2.46)$$

➤ Motor power:

$$P_{motor} = \frac{(P_{compression} + P_{frictional\ loss})}{\eta_{motor}} \quad (2.47)$$

where η_{motor} is the motor efficiency at the specified speed and torque requirement (as shown in Fig. 2-12).

➤ Compressor efficiency:

$$\begin{aligned} \eta_C = \eta_A \cdot \eta_{Me} \cdot \eta_{motor} &= \left(\frac{P_{adiabatic}}{P_{compression}} \right) \cdot \left(\frac{P_{compression}}{P_{compression} + P_{frictional\ loss}} \right) \cdot \left(\frac{P_{compression} + P_{frictional\ loss}}{P_{motor}} \right) \\ &= \frac{P_{adiabatic}}{P_{motor}} \end{aligned} \quad (2.48)$$

➤ COP_R (coefficient of performance to the refrigeration on electrical power input):

$$COP_R = \frac{\dot{Q}_c}{P_{\text{motor}}} \quad (2.49)$$

2.7 Summarization of the STC simulation model

A complete mathematical model regarding the STC has been illustrated in this chapter, and a parametric computer package has been constructed by virtue of the model. The simulation process for the package includes the geometry of scroll pair, the thermodynamics in chambers of STC, the dynamics about the related mechanisms and the frictional calculation of bearing models. After executing the process, many important indices as output data can be derived. These outputs turn into a design foundation for STC and assist in various analyses further.



CHAPTER 3 MATHEMATICAL MODEL OF BYPASS

VALVES

A general bypass valves model, based on computation geometry, will be reviewed at first and completely constructed in this chapter. This model will be integrated into the above-mentioned STC package (exhibited in Chapter 2).

3.1 Developing history regarding bypass valves

The STC of variable pressure ratio was developed in recent years due to higher efficiency and power-saving considerations. The pressure ratio is defined as the ratio of the saturated condenser pressure to the saturated evaporator pressure ($p_{\text{dis}}/p_{\text{suc}}$), and is decided by operating conditions of temperature. In general, volume ratio of a STC is fixed after the geometric parameters regarding the scroll pair in it have been decided. When the pressure ratio does not match with the volume ratio of the STC, two cases, over-compression and under-compression, will happen [5].

For under-compression, the repetitive compression in the final (or called the central) chamber or back flow from discharge chamber will occur in different designs of STC. For over-compression, the STC will compress the gas to its design point regardless of the high pressure in chambers and extra work is consumed. Under-compression could not be avoided except by designing a STC with a lower volume ratio while narrowing the range of operating conditions it performs. Nevertheless, over-compression could be reduced by using bypass valves added to the fixed scroll.

Discussions regarding bypass valves of STC are seldom seen in papers but have been presented in several patents. Murayama *et al.* [41] designed two groups of bypass holes (Fig. 3-1) for each compression chamber with valves operated by pressure differences to prevent over-compression. Fuji *et al.* [42] use a plurality of symmetrical bypass holes (Fig. 3-2) to avoid over-compression caused by the open delay of the bypass valves. A STC with a back pressure mechanism for axial seal and bypass valves for over-compression is also exposed (Tsubono *et al.* [43]). In addition, a study using bypass mechanism and optimization of the volume ratio in STC was presented to improve efficiency by 10 to 20 % under the conditions of both low speed and low pressure ratio (Morimoto *et al.* [24]). Even so, the examples above

merely illustrated the design of bypass valves with abbreviated drawings and brief statements.

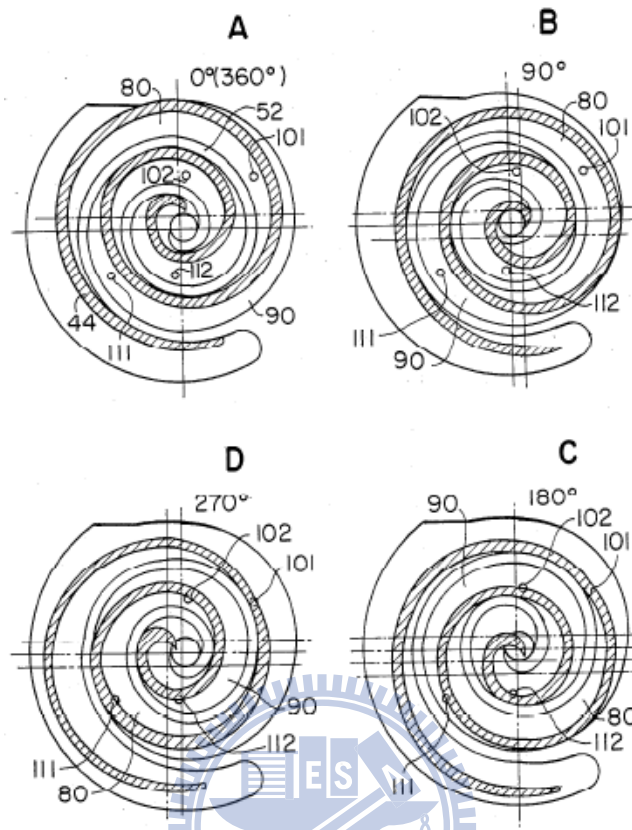


Fig. 3-1 Bypass holes during one orbiting scroll [41]

From literatures above, some summaries of technical breakthrough can be described as:

1. Decision of bypass holes' locations: Deciding suitable locations of bypass hole for lifting uncovered areas and extending uncovered interval as long as possible during one orbiting cycle are the main issues.
2. Numbers of bypass holes: The optimum numbers of bypass holes for air conditioning and refrigeration, depending on loading or operating conditions, are two and four ones.
3. Design of bypass valves: The appropriate design of bypass valves can avoid redundant power and back flow which caused from open and close delay effects.

Even so, those literatures merely illustrated the design of bypass valves with abbreviated drawings and brief statements. They do not disclose the detailed mathematical models of the bypass valve, such as the selection of the position of bypass holes, valve models, and the bypass behavior during the compression and discharge process. Hence this chapter will built up a general bypass valves model and integrates it into the already developed STC package.

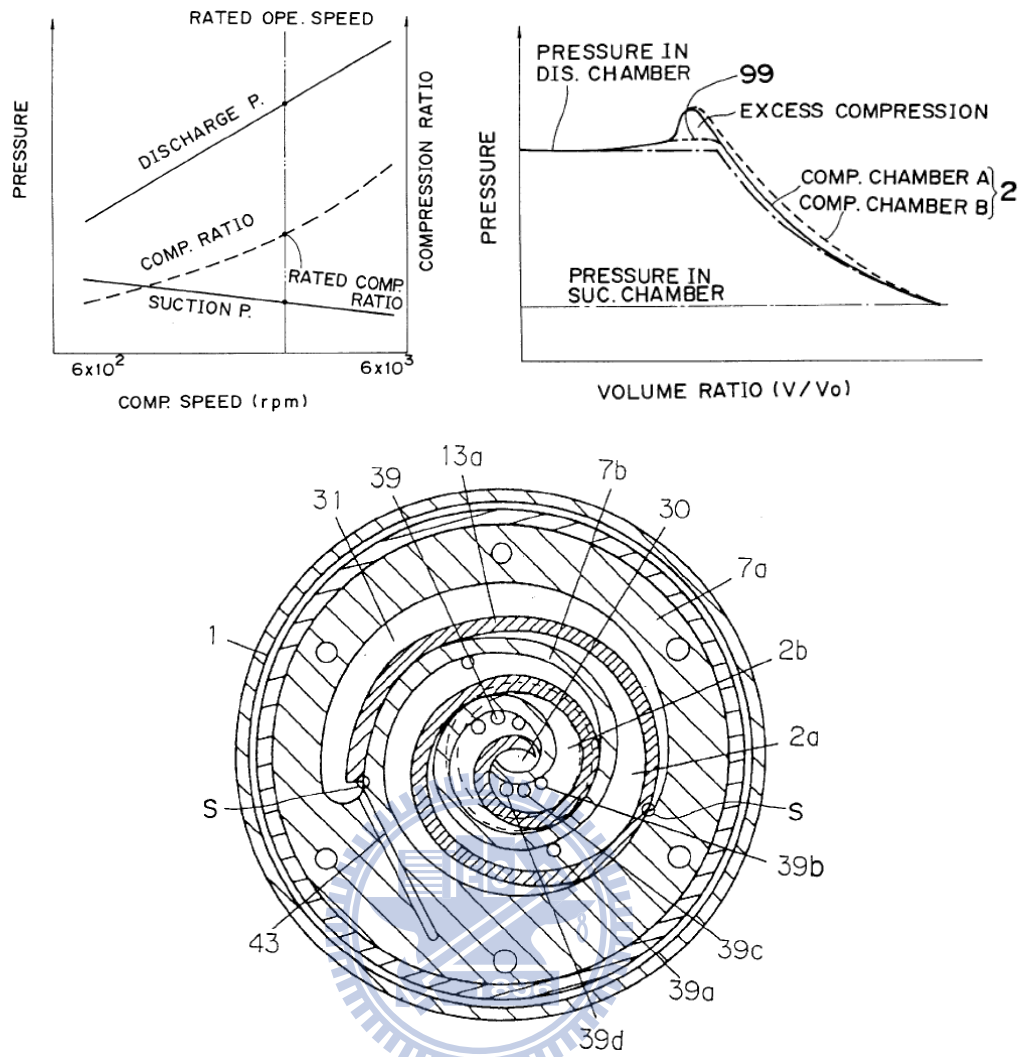


Fig. 3-2 Speed, volume vs. pressure ratio & bypass design [42]

3.2 Geometry of bypass holes

The scroll pairs were divided into several symmetrical chambers initially as shown in Fig. 3-3(a). The relation of bypass holes between fixed scroll and orbiting scroll during the orbiting operation can be derived by using coordinates transformation.

3.2.1 Geometry of bypass holes

First, the range of one bypass hole's position (Fig. 3-3(a)) with outer profile (equation (2.2)) on the fixed scroll is considered as follows:

$$\begin{aligned}
& \phi_{o_u} \geq \phi_{o_a} \geq \phi_{o_l} , \\
& \text{when } \phi_{o_u} > 2\pi, \begin{cases} \phi_{o_u} = \phi_r - \pi - (N-i)2\pi : i=1,2,\dots,N \\ \phi_{o_l} = \phi_{o_u} - 2\pi \end{cases} \\
& \text{when } \phi_{o_u} \leq 2\pi, \begin{cases} \phi_{o_u} = \phi_r - \pi - (N-i)2\pi : i=1,2,\dots,N \\ \phi_{o_l} = 0 \end{cases}
\end{aligned} \tag{3.1}$$

After the involute angle ϕ_{o_a} is defined, the other two parameters, r and d , shown in Fig. 3-3 (b), as constraints must be satisfied as follows:

$$\begin{cases} 0 \leq r \leq \frac{t_h}{2} \\ r \leq d \leq p_t - t_h - r \end{cases} \tag{3.2}$$

It is important to provide reasonable values to assure the simulated results are physically meaningful.

Secondly, by observing Fig. 3-3(b), the center of the bypass hole can be derived accordingly. Let the slope m_{slo} be:

$$\begin{cases} x_t = r_b \cos \phi_{o_a} \\ y_t = r_b \sin \phi_{o_a} \\ m_{slo} = \frac{(y_{o_a} - y_t)}{(x_{o_a} - x_t)} \end{cases} \tag{3.3}$$

The center of the bypass hole at the fixed scroll is:

$$\begin{cases} x_{o_By} = x_{o_a} + d \cos(\tan^{-1} m_{slo}) \\ y_{o_By} = y_{o_a} + d \sin(\tan^{-1} m_{slo}) \end{cases} \tag{3.4}$$

Then the line equation from the tangential of basic circle of the fixed scroll to the center of bypass hole was derived as:

$$y = m_{slo} (x - x_{o_By}) + y_{o_By} \tag{3.5}$$

The equations of the inner profile of the orbiting scroll and equation (3.5) are considered simultaneously as:

$$\begin{cases} y = m_{slo} (x - x_{o_By}) + y_{o_By} , \\ \begin{cases} x = -r_b [\cos \phi + (\phi - \alpha) \sin \phi] + r_{ob} \cos \theta \\ y = -r_b [\sin \phi - (\phi - \alpha) \cos \phi] - r_{ob} \sin \theta \end{cases} \end{cases} \tag{3.6}$$

Newton-Raphson method is used to solve these numerically and the corresponding involute angle ϕ on orbiting scroll can be obtained eventually.

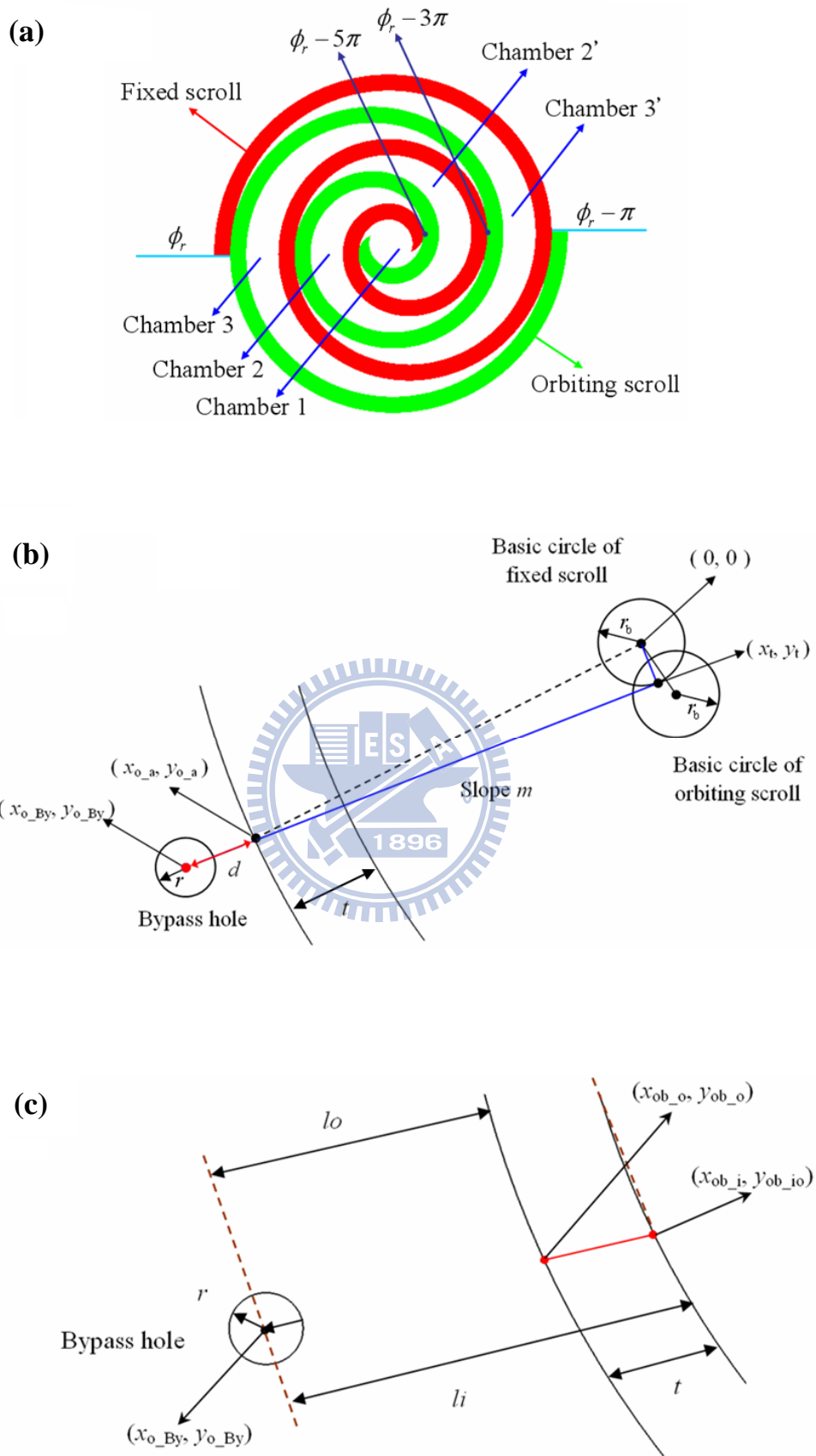


Fig. 3-3 Scheme of bypass holes (a) range of positions (b) relations from fixed scroll (c) relations from orbiting scroll

3.2.2 Uncovered area of the bypass holes

While ϕ is determined, the relations between the center of the bypass hole and orbiting scroll profile can be defined as Fig. 3-3(c). Therefore, two parameters lo and li are derived as:

$$\begin{aligned} lo &= \sqrt{(x_{o_By} - x_{ob_o})^2 + (y_{o_By} - y_{ob_o})^2}, \\ li &= \sqrt{(x_{o_By} - x_{ob_i})^2 + (y_{o_By} - y_{ob_i})^2} \end{aligned} \quad (3.7)$$

These two parameters can be used to define the uncovered area of the bypass hole.

If $lo < li$ holds, four possible calculations exist:

(A): As Condition (A) in Fig. 3-4, if $li \geq t + r$, then the uncovered area is

$$A_{By} = \pi r^2 \quad (3.8)$$

(B): As Condition (B) in Fig. 3-4, if $li \geq t$ and $li < t + r$, then

$$A_{By} = \left\{ \pi - \tan^{-1} \left[\frac{(r^2 - lo^2)^{0.5}}{lo} \right] \right\} r^2 + lo(r^2 - lo^2)^{0.5} \quad (3.9)$$

(C): As Condition (C) in Fig. 3-4, if $li \geq t - r$ and $li < t$, then

$$A_{By} = r^2 \tan^{-1} \left[\frac{(r^2 - lo^2)^{0.5}}{lo} \right] - lo(r^2 - lo^2)^{0.5} \quad (3.10)$$

(D): As Condition (D) in Fig. 3-4, if $li \leq t - r$, then $A_{By} = 0$.

If $lo > li$, those calculations still hold if the definition of the two parameters are interchanged. Aside from the uncovered area of the bypass holes to the outer profile of the orbiting scroll, the calculation to the inner profile proceeds similarly.

3.2.3 Corresponding chambers to bypass holes

Due to the motion of the orbiting scroll, the bypass holes may span to different chambers during a cycle. Determination of corresponding chambers to bypass holes must be performed. Observing the variations of the uncovered area of the bypass holes at current and previous steps during a cycle is a way to settle it.

3.3 Bypass valve model

An one-dimensional valve was used for simplicity (Chen, *et al.* [25]) and the dynamics of the bypass valve was neglected. If the pressure in the compression chamber surpasses p_{dis} , the valve opens and the distance raised is determined with static forces balance relation:

$$y = \pi r_{eq}^2 (p - p_{dis}) \frac{1}{C_{valve}} \quad (3.11)$$

where r_{eq} is the equivalent radius for the uncovered area as follows:

$$r_{eq} = \left(\frac{A_{By}}{\pi} \right)^{0.5} \quad (3.12)$$

Then the equivalent flow area is calculated by

$$A_{eq} = 2\pi r_{eq} y \quad (3.13)$$

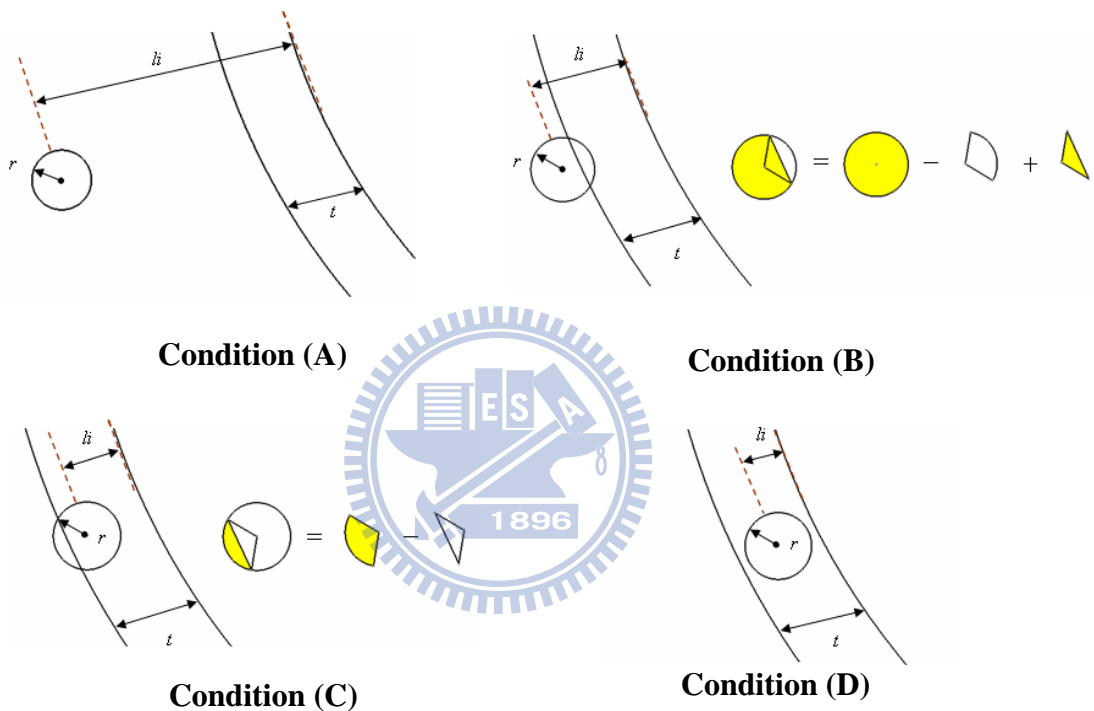


Fig. 3-4 Uncovered areas of the orbiting scroll and the bypass hole

3.4 Simulation model

By integrating the bypass model into the developed STC package (exhibited in Chapter 2), several important efficiencies and performance indices can be predicted. The inputs and outputs of the models and simulation process are described as below:

Inputs:

- (1) Scroll geometry: including the fixed and orbiting parameters.
- (2) Other mechanisms: containing Oldham ring, shaft and bearing parameters.
- (3) Bypass valves: bypass holes geometry and valves parameters.

- (4) System inputs: the refrigerant type and the operating conditions.
- (5) Motor inputs: Motor efficiency can be acquired from the dynamometer test.

Outputs:

The output results, such as η_v , η_c and \dot{m}_s , can refer to the illustration in Sec.2.6.2.

Simulation process:

The flowchart of the regarding the STC simulation package is shown in Fig. 3-5. The leakage and bypass model is included in the process and solved with numerical iterations. The flowchart of the leakage and bypass model is shown in Fig. 3-6. At the beginning, the initial calculations about the volumes, area of the chambers and flow area of the bypass holes and the thermodynamic properties inside the chambers without leakage are predicted at each step. After that, the polytropic compression and discharge processes proceeds. When the pressure in the chamber is greater than the pressure of the discharge chamber (p_{dis}), the bypass action occurs. Then the bypass flow can be calculated (by using equation (2.20) but replacing A with A_{eq} and 4th R-K method) as leakage flow in the model.

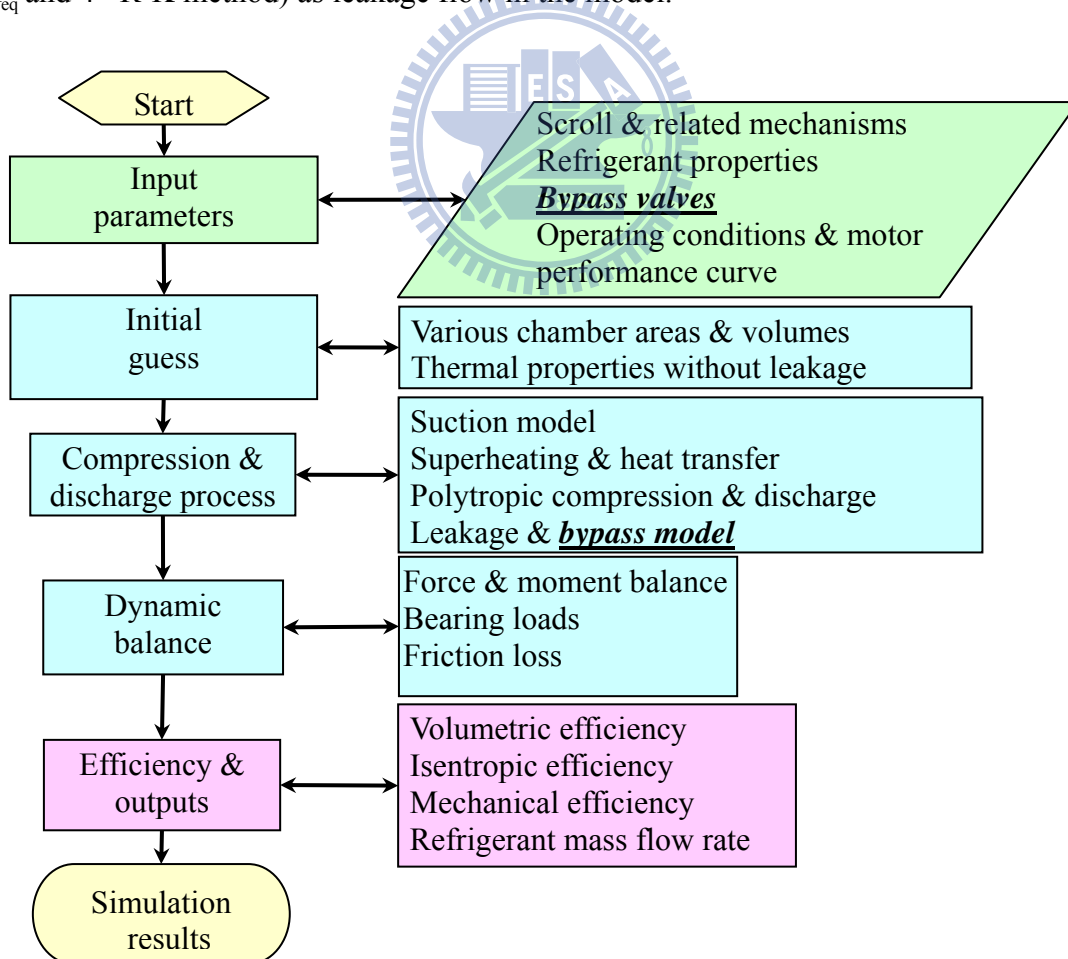


Fig. 3-5 The flowchart of the STC simulation process

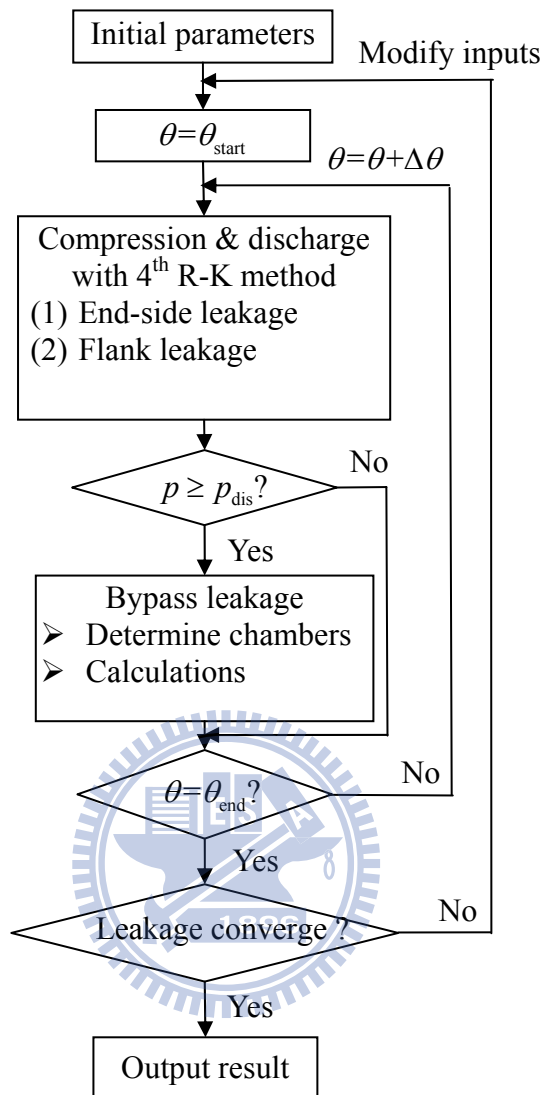


Fig. 3-6 The flowchart of leakage and bypass model in STC

3.5 Remarks

A parametric model for the bypass valves has been formulated in this chapter. It includes of determining the position and calculating the open areas and intervals of the bypass holes. This model also has been integrated into the simulation process of the STC computer package (developed in Chapter 2). In the next chapter, several simulated cases will be implemented for analyzing its value. Furthermore, one actual STC product with bypass valves will be used to verify the predicted results through the compressor performance test.

CHAPTER 4 SIMULATION FOR BYPASS VALVES IN STC

Two kinds of developed STC products, low-side and high-side structures, are cases to be studied respectively in this chapter. Through the simulation results, the effects of bypass mechanism in the STC are investigated. Furthermore, the reliability and accuracy of this model will be verified by the experimental test platform for an actual STC product.

4.1 Simulations with low-side structure

A STC product using R-22 as refrigerant with volume ratio 2.71 is analyzed initially and some major geometric parameters are given in Table. 4-1. One pair of symmetric bypass holes are located in the fixed scroll. The related parameters are shown in Table. 4-2 and Fig. 4-1 shows the position of the bypass holes.

4.1.1 Geometric observation

The uncovered interval is a range that the bypass holes are not be covered by wrap of the orbiting scroll. Due to the symmetry of bypass holes, the uncovered areas of bypass holes have the similar trend during the orbiting cycle as Fig. 4-2 shows. However, the uncovered interval does not represent the acting interval because of possible disagreement with the bypass condition ($P_{ch} > P_{dis}$) during the compression process. Therefore, different geometrical designs could produce different design requirements for the bypass holes. From the geometrical point of view, the major consideration is to design bypass holes which have longer uncovered intervals during an orbiting cycle.

4.1.2 Simulation results during working cycle

Figure 4-3 shows the working cycle about pressure v.s. crank angle of the STC with and without bypass mechanism at evaporating temperature $T_{evp} = 4.4$ °C and condensing temperature $T_{con} = 37.8$ °C, the pressure ratio in this condition is 2.63. It can be seen that the acting interval (100°) is shorter than the uncovered interval (300°), the pair of bypass holes can suit this operating condition. The compression efficiency η_C can be improved by 5.2% and a few rise on volumetric efficiency η_V (2.2%). The results show that the extra work can be reduced to avoid over-compression but the effect is limited because of this testing condition with high compression ratio and speed.

Figure 4-4 shows the same arrangement in STC with the same speed but different

operating condition, 2.23 in pressure ratio. The acting interval is extended (from 100° to 145°) and the position of bypass holes still match up the design requirement at this operating condition ($< 300^\circ$), and η_C can be lifted by 9.1%. Generally speaking, the η_C can be advanced by 2% to 10% for different operating conditions. Therefore, bypass mechanism used in STC is necessary regarding lower compression-ratio conditions for higher efficiency consideration.

Table. 4-1 Parameters of the STC

| Parameters | Unit | Value |
|---|------|-------|
| Base circle radius (r_b) | mm | 2.06 |
| Thickness of the scroll (t) | mm | 2.71 |
| Involute angle of the scroll (ϕ) | deg | 1100 |
| Height of the scroll (h) | mm | 22 |

Table. 4-2 Parameters of bypass hole

| Parameters | Unit | Value |
|--|------|-------|
| Involute angle of bypass hole 1 (ϕ_1) | deg | 340 |
| Diameter of bypass hole 1 (D_{m1}) | mm | 0.75 |
| Distance of bypass hole 1 (d_1) | mm | 1.2 |
| Involute angle of bypass hole 1' ($\phi_{1'}$) | deg | 520 |
| Diameter of bypass hole 1' ($D_{m1'}$) | mm | 0.75 |
| Distance of bypass hole 1' ($d_{1'}$) | mm | 1.2 |

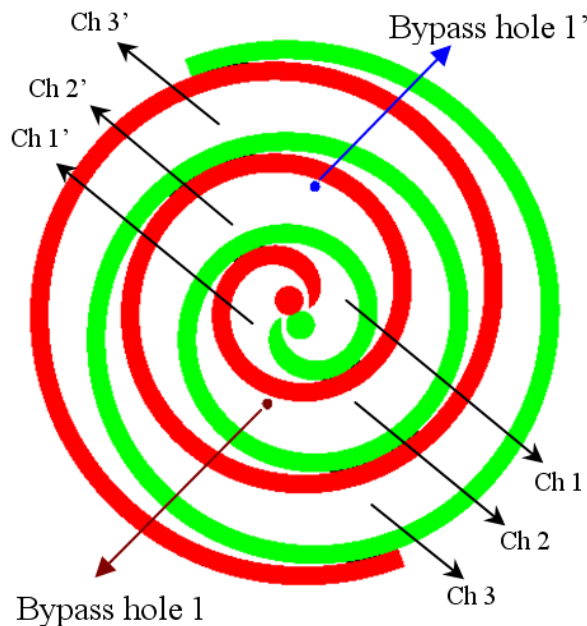


Fig. 4-1 Position of bypass holes

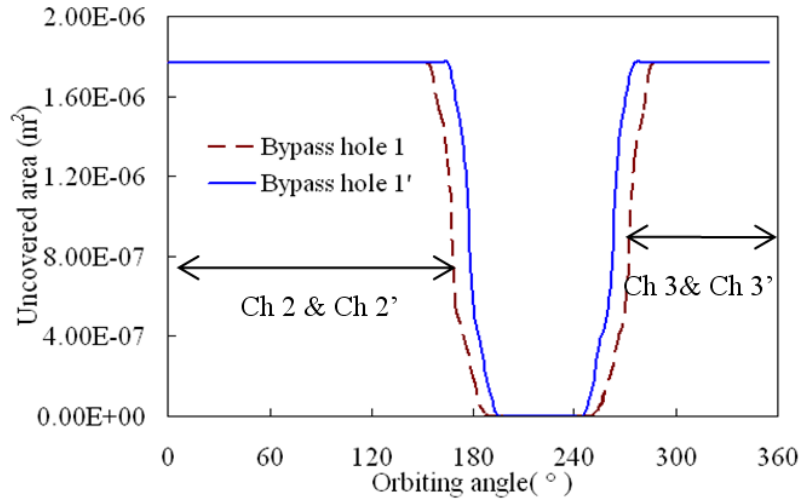


Fig. 4-2 Uncovered interval of bypass holes

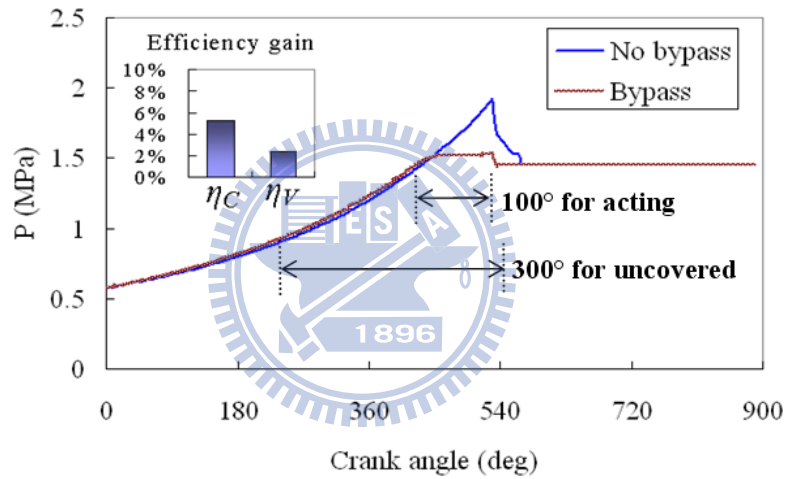


Fig. 4-3 Working cycle

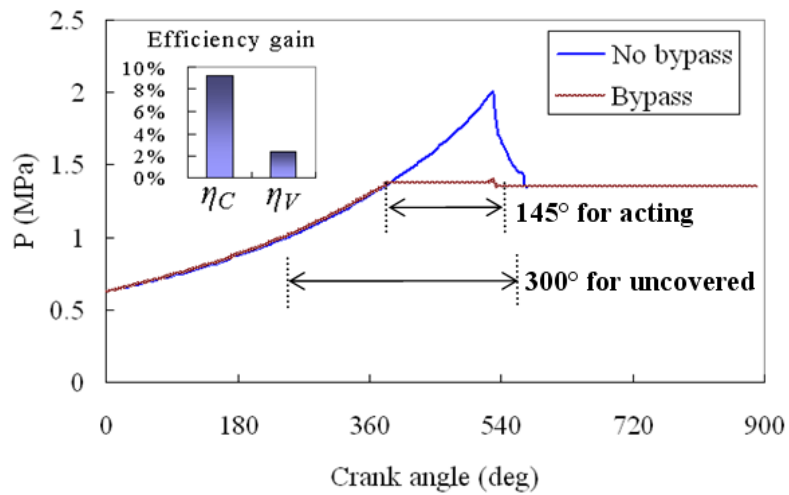


Fig. 4-4 Working cycle at different condition

4.1.3 Simulation results of two different arrangements

From the previous discussion, it can be seen that one pair of bypass holes which are shown in Fig. 4-1, have shorter uncovered interval (300°) than the working cycle. After that, three cases with different arrangements of two pairs of bypass holes have been investigated as below:

Case (A):

The same STC but with 2 pairs of bypass holes is analyzed firstly. For the case (A), the second pair of bypass holes are added (as shown in Fig. 4-5) but the first ones remained the same position as Fig. 4-1. Table. 4-1 depicts the parameters and the corresponding illustrations of uncovered interval of the three cases are shown in Fig. 4-8. It can be seen that the uncovered interval can be extended from 300° to 425° , however, the covered interval still exist at the beginning stage (0° to 130°) of the working cycle. Hence, two pairs of bypass holes can span the working interval but need more delicate arrangement to conform the design requirement.

Case (B):

Different locations about the second pair of bypass holes are presented in Fig. 4-6 and the related parameters are shown in Table. 4-4. From Fig. 4-8, the simulation results present that the uncovered interval is extended to the beginning stage ($0^\circ \sim 190^\circ$ and $255^\circ \sim 550^\circ$) but a covered interval, which is about 65° ($190^\circ \sim 255^\circ$), appears at the middle stage during the working cycle, can lead potential to arise over-compression. So the arrangement of these two pairs of bypass holes in case B is still unsatisfied.

Case (C):

Another arrangement of bypass holes is shown in Case (C) and the parameters and diagram are shown in Table. 4-5 and Fig. 4-7. From Fig. 4-8, it can be found that the uncovered interval, which is extended to 550° , can completely uncover bypass holes at every compression chamber throughout the whole working cycle. The result depict the arrangements of bypass holes in the STC with different operating conditions can bypass over-compressed refrigerant arbitrarily from any compression chambers.

Table. 4-3 Parameters of bypass hole: Case (A)

| Parameters | Unit | Value |
|--|------|-------|
| Involute angle of bypass hole 1 (ϕ_1) | deg | 340 |
| Diameter of bypass hole 1 (D_{m1}) | mm | 0.75 |
| Distance of bypass hole 1 (d_1) | mm | 1.2 |
| Involute angle of bypass hole 1' ($\phi_{1'}$) | deg | 520 |
| Diameter of bypass hole 1' ($D_{m1'}$) | mm | 0.75 |
| Distance of bypass hole 1' ($d_{1'}$) | mm | 1.2 |
| Involute angle of bypass hole 2 (ϕ_2) | deg | 460 |
| Diameter of bypass hole 2 (D_{m2}) | mm | 0.75 |
| Distance of bypass hole 2 (d_2) | mm | 1.2 |
| Involute angle of bypass hole 2' ($\phi_{2'}$) | deg | 640 |
| Diameter of bypass hole 2' ($D_{m2'}$) | mm | 0.75 |
| Distance of bypass hole 2' ($d_{2'}$) | mm | 1.2 |

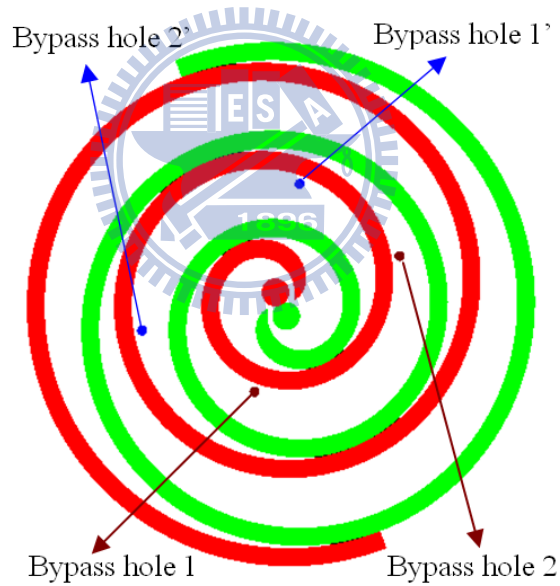


Fig. 4-5 Position of bypass holes: Case (A)

Table. 4-4 Parameters of bypass hole: Case (B)

| Parameters | Unit | Value |
|--|------|-------|
| Involute angle of bypass hole 1 (ϕ_1) | deg | 340 |
| Diameter of bypass hole 1 (D_{m1}) | mm | 0.75 |
| Distance of bypass hole 1 (d_1) | mm | 1.2 |
| Involute angle of bypass hole 1' ($\phi_{1'}$) | deg | 520 |
| Diameter of bypass hole 1' ($D_{m1'}$) | mm | 0.75 |
| Distance of bypass hole 1' ($d_{1'}$) | mm | 1.2 |
| Involute angle of bypass hole 2 (ϕ_2) | deg | 700 |
| Diameter of bypass hole 2 (D_{m2}) | mm | 0.75 |
| Distance of bypass hole 2 (d_2) | mm | 1.2 |
| Involute angle of bypass hole 2' ($\phi_{2'}$) | deg | 880 |
| Diameter of bypass hole 2' ($D_{m2'}$) | mm | 0.75 |
| Distance of bypass hole 2' ($d_{2'}$) | mm | 1.2 |

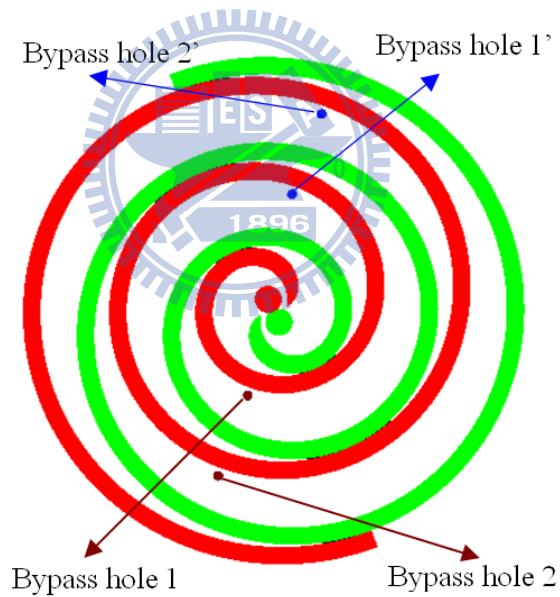


Fig. 4-6 Position of bypass holes: Case (B)

Table. 4-5 Parameters of bypass hole: Case (C)

| Parameters | Unit | Value |
|--|------|-------|
| Involute angle of bypass hole 1 (ϕ_1) | deg | 340 |
| Diameter of bypass hole 1 (D_{m1}) | mm | 0.75 |
| Distance of bypass hole 1 (d_1) | mm | 1.2 |
| Involute angle of bypass hole 1' ($\phi_{1'}$) | deg | 520 |
| Diameter of bypass hole 1' ($D_{m1'}$) | mm | 0.75 |
| Distance of bypass hole 1' ($d_{1'}$) | mm | 1.2 |
| Involute angle of bypass hole 2 (ϕ_2) | deg | 620 |
| Diameter of bypass hole 2 (D_{m2}) | mm | 0.75 |
| Distance of bypass hole 2 (d_2) | mm | 1.2 |
| Involute angle of bypass hole 2' ($\phi_{2'}$) | deg | 800 |
| Diameter of bypass hole 2' ($D_{m2'}$) | mm | 0.75 |
| Distance of bypass hole 2' ($d_{2'}$) | mm | 1.2 |

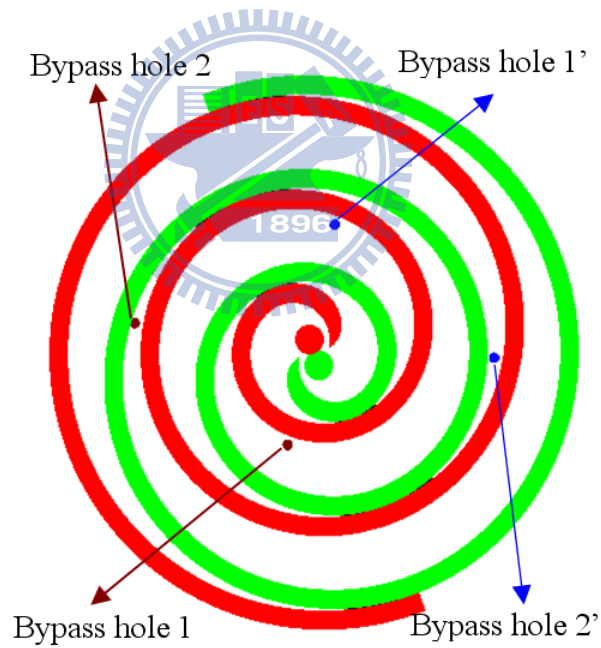


Fig. 4-7 Position of bypass holes: Case (C)

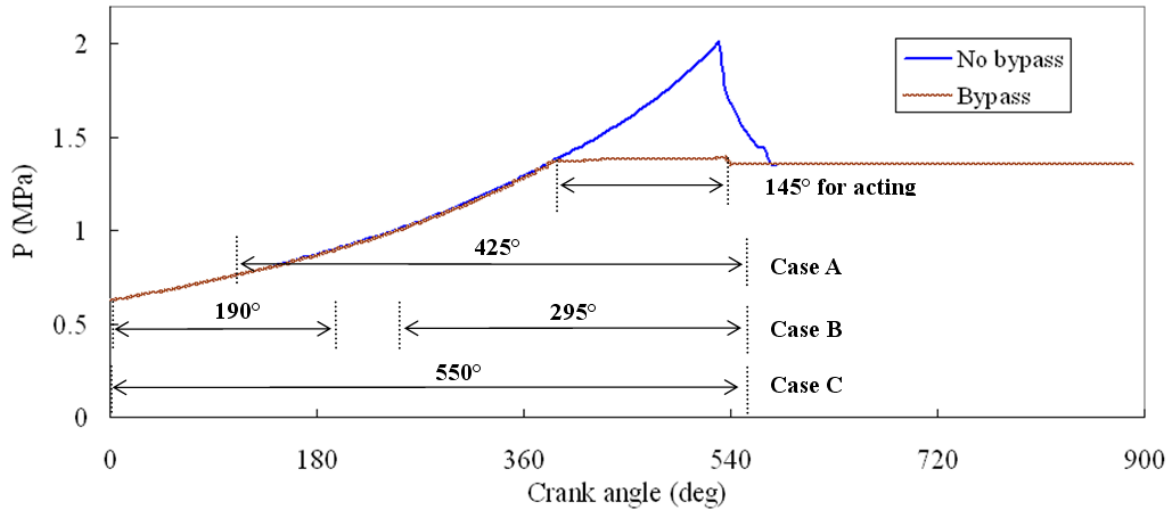


Fig. 4-8 Working cycle at different cases

Besides, liquid slug is another problem that must be considered (Wang *et al.* [44]). The liquid refrigerant is sucked into compression chambers of the STC during the suction stage due to not enough superheat. In general, a tiny amount of liquid refrigerant in chambers can be accepted. However, when too much liquid refrigerant is sucked into chambers, which means abnormal rise of pressure in chambers will take place and cause STC fatal damage. In order to prevent this phenomenon, the STC must have passages to conduct the abrupt high-pressure refrigerant. Hence, bypass mechanism with suitable design can be the way to settle it. The arrangement in case (C), besides avoiding over-compression, the liquid slug can be prevented because of completely uncovered interval throughout the working cycle.

4.2 Simulations with high-side structure

A high-side CO₂ STC product is simulated secondly. The design of the bypass holes is shown in Fig. 4-9. The geometric parameters of the scroll pairs and bypass holes are displayed in Table. 4-6. It can be seen that bypass hole 1 and bypass hole 2 are related to the outer involute and bypass hole 1' and bypass hole 2' to the inner involute. Five operating conditions for the simulation are used and the details are shown in Table. 4-7.

Table. 4-6 Parameters of the STC

| Parameters | Unit | Value |
|---|--------|-------|
| Basic circle radius (r_b) | mm | 1.91 |
| Thickness of the scroll (t) | mm | 3 |
| Roll angle of the scroll (ϕ_e) | degree | 990 |
| Height of the scroll (h) | mm | 4.27 |
| Involute angle of bypass hole 1 (ϕ_{o_a}) | degree | 234 |
| Radius of bypass hole 1 (r) | mm | 0.73 |
| Distance of bypass hole 1 (d) | mm | 1.21 |
| Involute angle of bypass hole 1' (ϕ_{o_a}) | degree | 402 |
| Radius of bypass hole 1' (r) | mm | 0.73 |
| Distance of bypass hole 1' (d) | mm | 1.34 |
| Involute angle of bypass hole 2 (ϕ_{o_a}) | degree | 407 |
| Radius of bypass hole 2 (r) | mm | 0.73 |
| Distance of bypass hole 2 (d) | mm | 0.92 |
| Involute angle of bypass hole 2' (ϕ_{o_a}) | degree | 770 |
| Radius of bypass hole 2' (r) | mm | 0.73 |
| Distance of bypass hole 2' (d) | mm | 1.57 |

Table. 4-7 STC operating conditions

| Refrigerant | CO ₂ | | |
|-------------|------------------------|--------------------------|------------------------|
| | Suction pressure (MPa) | Discharge pressure (MPa) | Motor revolution (RPM) |
| Condition 1 | 3.67 | 10.44 | 2400 |
| Condition 2 | 4.37 | 10.59 | 2892 |
| Condition 3 | 3.25 | 11.19 | 3180 |
| Condition 4 | 2.82 | 10.79 | 4200 |
| Condition 5 | 4.5 | 11.06 | 2892 |

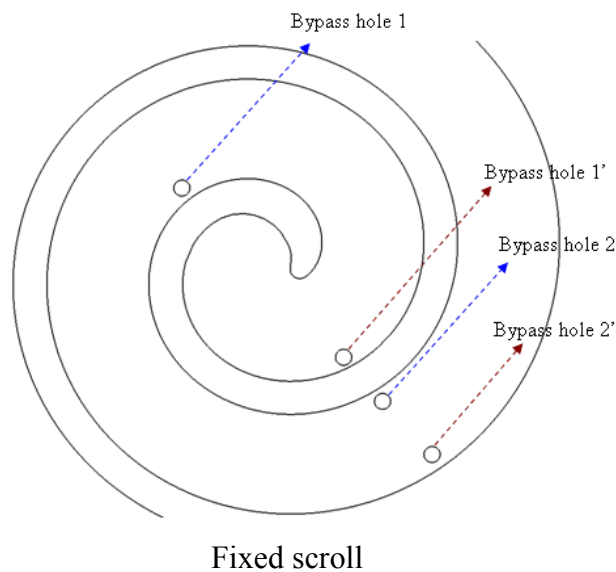


Fig. 4-9 The scheme of the STC and bypass holes on fixed scroll

4.2.1 Effect of bypass valves behavior

Bypass hole 1 and 2

Figure 4-10 shows the change of uncovered area of the four bypass holes. It can be seen that the bypass hole 1 initially opened in chamber 2 and is covered by the orbiting scroll from 180° to 256° . Afterward, it opens in chamber 3 up to the end of the orbiting cycle. The bypass hole 2 is uncovered in chamber 2 from 0° to 20° , and is covered up to 66° . Then it appeared again in chamber 3 and remains there toward the end of the cycle. Figure 4-11(a) illuminated that the two bypass holes may take effect in chamber 2 only from 720° to 797° (discharge angle) during the whole orbiting cycle, and after that, chamber 2 reaches the discharge stage. Similarly, chamber 3 also has a stage from 360° to 426° where the bypass holes were closed.

For chamber 2, the discharge angle of the scroll pairs must be considered. Since after the discharge angle, chamber 2 will communicate with chamber 1 and proceed to the discharge process. Therefore, if the discharge angle is appropriate, chamber 2 can avoid over-compression completely during the orbiting cycle. The discharge angle, 797° , is inside the useful acting interval of the bypass hole 1 (0° to 180°), so the design is good for chamber 2.

For chamber 3, discharge angle does not interfere with bypass action, hence it merely needs to design bypass holes that can appear during the orbiting cycle. However, Fig. 4-11(a) shows that there are no bypass holes that open in chamber 3 from 360° to 426° . Though the interval is not very long, it may exist possibility to cause over-compression in chamber 3. Besides, chamber 3 inhales refrigerant from the suction chamber. If too much liquid refrigerant flows into chamber 3, it could arise liquid slugging because of no bypass during the interval. It implies that the design of bypass holes in chamber 3 must be improved further.

Bypass hole 1' and 2'

Returning to Fig. 4-10 again, bypass hole 1' is initially open in chamber 2' and closed after 194° . At 260° , it is opened again in chamber 3'. A similar trend occurs to bypass hole 2', which is opened initially in chamber 3' and closed at 180° . After 260° , the hole is uncovered again in the next chamber (suction chamber).

As shown in Fig. 4-11(b), chamber 2' also can retain no over-compression during the cycle. For chamber 3', it can be seen that from 540° to 620° , bypass holes are covered, and if the refrigerant in chamber 3' is over-compressed, there is no passage to bypass it. The design of bypass holes in chamber 3' may cause serious effects because generally speaking, over-compression occurs at the middle or later interval in outer chambers and at the early

interval in inner chambers during a cycle. Hence, the possibility of over-compression in chamber 3' may occur during $540^\circ \sim 620^\circ$ because of the lack of bypass effect.

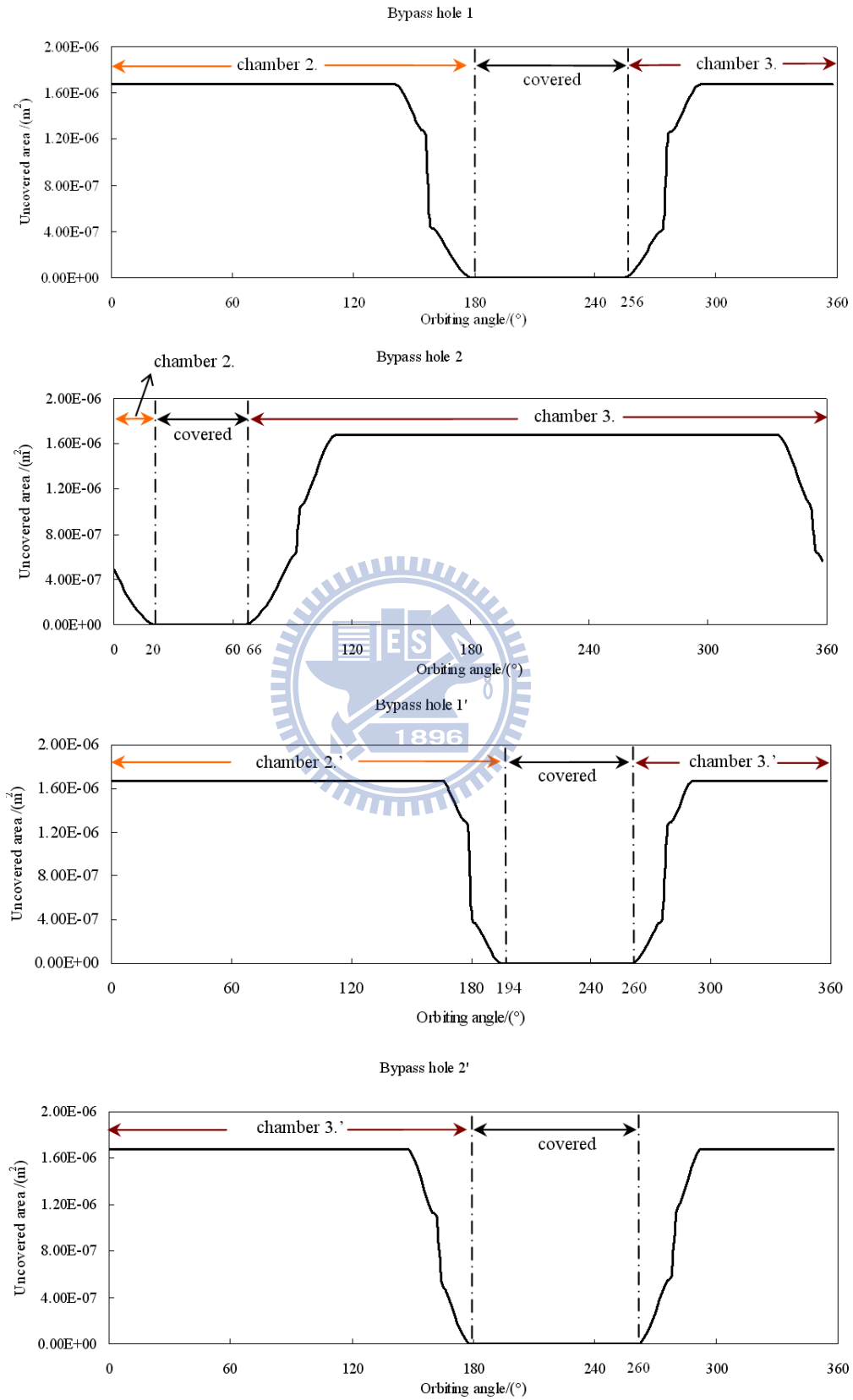


Fig. 4-10 Change of the uncovered area of bypass holes

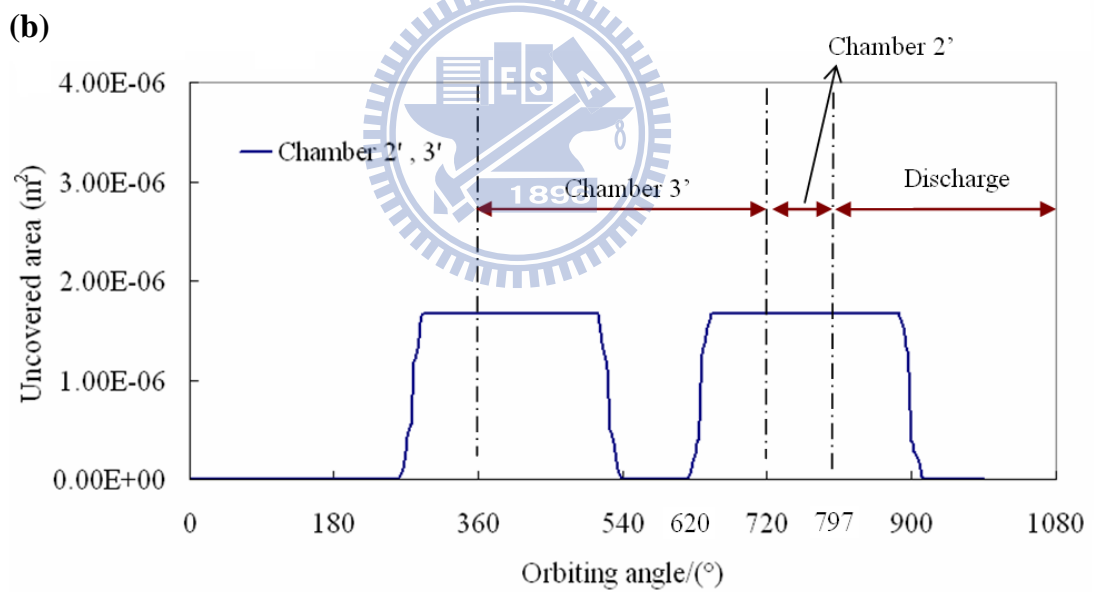
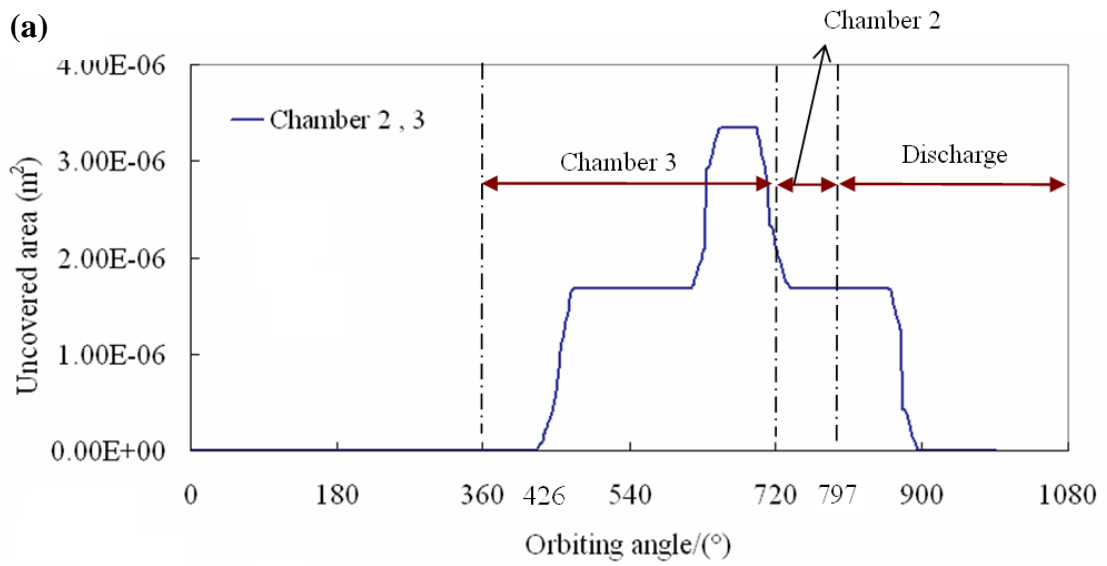


Fig. 4-11 Uncovered area of bypass holes in (a) chamber 2 and chamber 3 (b) chamber 2' and chamber 3'

4.2.2 Effect of bypass valves in thermodynamics

Effects with and without bypass action

Five conditions originated from JRAIA (Japan Refrigeration and Air Conditioning Industry Association) JRA4050:2005 were simulated with and without bypass action. Figure 4-12 shows the compared simulation results in mass flow rate (\dot{m}), volumetric efficiency (η_v) and compressor efficiency (η_c) of the STC with and without bypass action. It can be seen that \dot{m} and η_v have hardly been influenced by bypass action but η_c , which is related to the power consumption of the compression process, changes fiercely and depends on various operating conditions.

Improvement for bypass action in η_c at conditions 2 and 5 are almost 10% and 6% at condition 1, which implies the importance of the bypass action, even though at condition 3 and 4, a lesser improvement of 2.5% was found. The observations above explain the necessity of designing bypass valves in varied pressure ratio STC for more efficient and power-saving purposes.

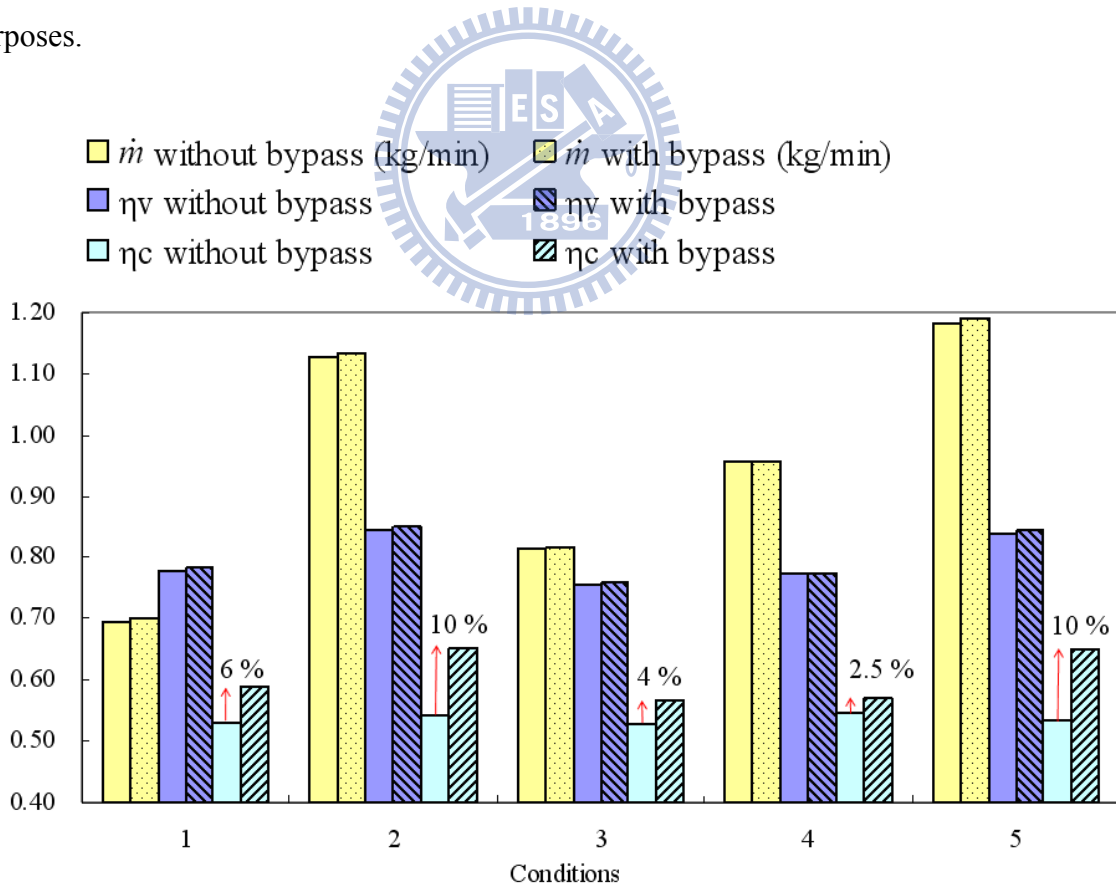


Fig. 4-12 Prediction of performance of \dot{m} , η_v , η_c

Variation of pressure inside the compression chambers

Take notice of Fig. 4-9 and Fig. 4-2 again. Chamber 3 and 3' are symmetrical with the same volume and the same change rate of volume during an orbiting cycle. The same conditions hold for chamber 2 and 2'. If bypass holes are designed inappropriately, they could produce pressure differences between the symmetrical chambers if bypass action occurs. Though the amount is small, the difference could affect the dynamic balance of scroll pairs and other mechanical components in STC (Yamada *et al.* [45]). For this reason, the design of bypass holes should make bypass action occurs at the same interval as far as possible in symmetrical chambers during a cycle and uncovered areas should close to equal.

Figure 4-13 presents the simulation results of the pressure variations inside the compression chambers with and without bypass action. Through Fig. 4-11 and Fig. 4-13, it can be seen that the design of the four bypass holes can completely prevent over-compression during the orbiting cycle under these five conditions. The pressure discrepancies between chamber 2, 3 (Fig. 4-13(a)) and chamber 2', 3' (Fig. 4-13(b)) during the cycle are small, so the influence to dynamic balance can be neglected. However, the explanation can not guarantee other operating conditions, because for chamber 3, bypass holes do not open during 360° to 426° (Sec 4.3.1) and for chamber 3' do not open during 540° to 620° (Sec 4.3.1) of the orbiting cycle.

Besides, the liquid slugging may occur in chamber 3. Hence, the design of current STC in the study can be further improved by using optimum method to determine better bypass holes for varied operating conditions.

4.3 Verification of bypass mechanism

4.3.1 Experimental apparatus

For most of the STC products, the experimental validation to bypass mechanism can be proceeded by calorie-meter which has been constructed by ITRI. But for some refrigerant such as CO₂, the special apparatus needing to accommodate to trans-critical and high pressure process must be constructed. Due to this, ITRI developed an appropriative test rig (Skiple *et al.* [46]). Figure 4-14 shows the apparatus and Fig. 4-15 is the flow chart of the whole working procedure. The apparatus is used to validate the simulation results of a developing high-side CO₂ STC product and feedback the data to modify the simulation model. The details about the test rig and testing process are stated explicitly in [46–48].

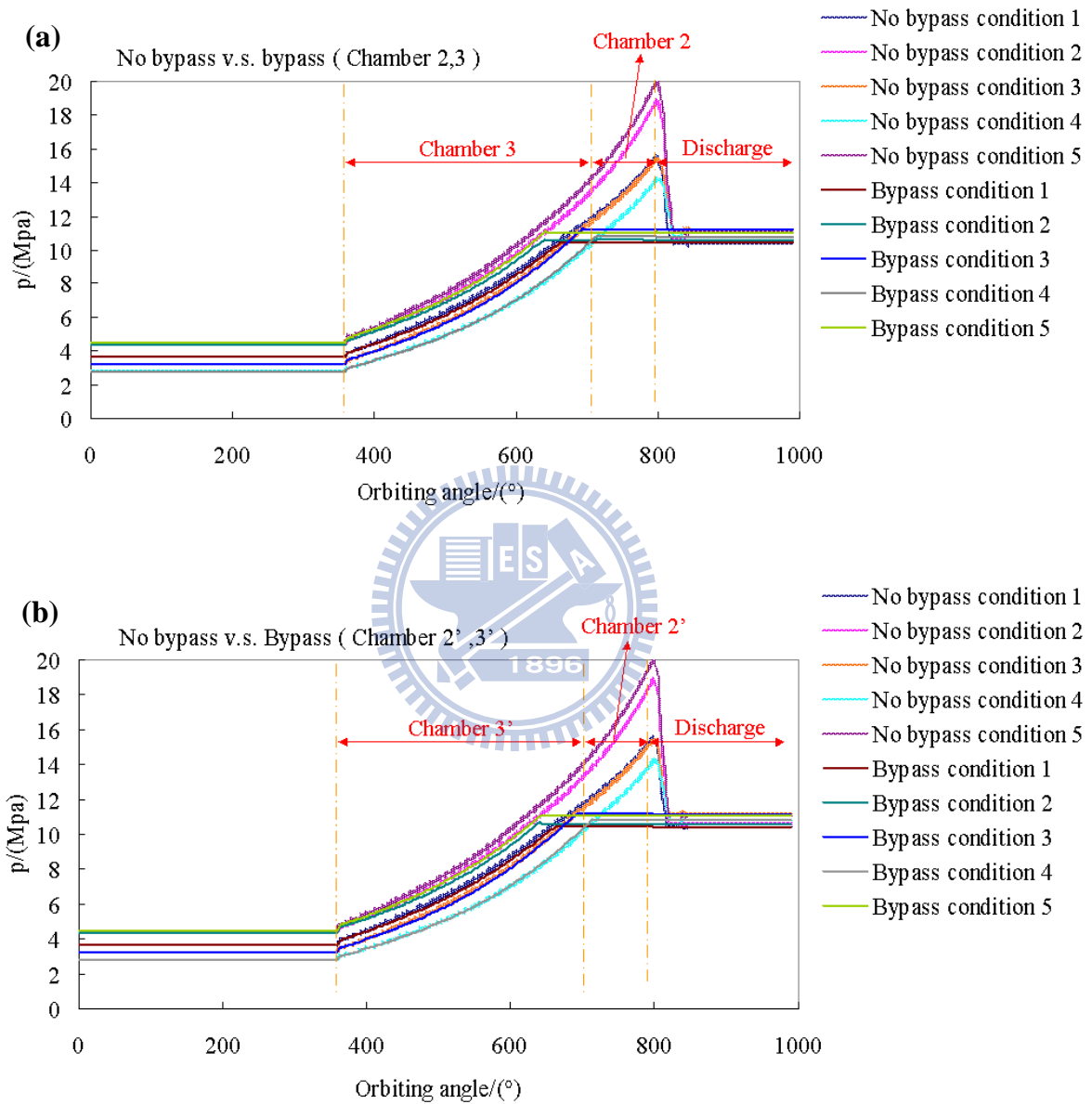


Fig. 4-13 Prediction of pressure variation with and without bypass valves (a) chamber 2, 3 (b) chamber 2', 3'



Fig. 4-14 CO₂ test rig

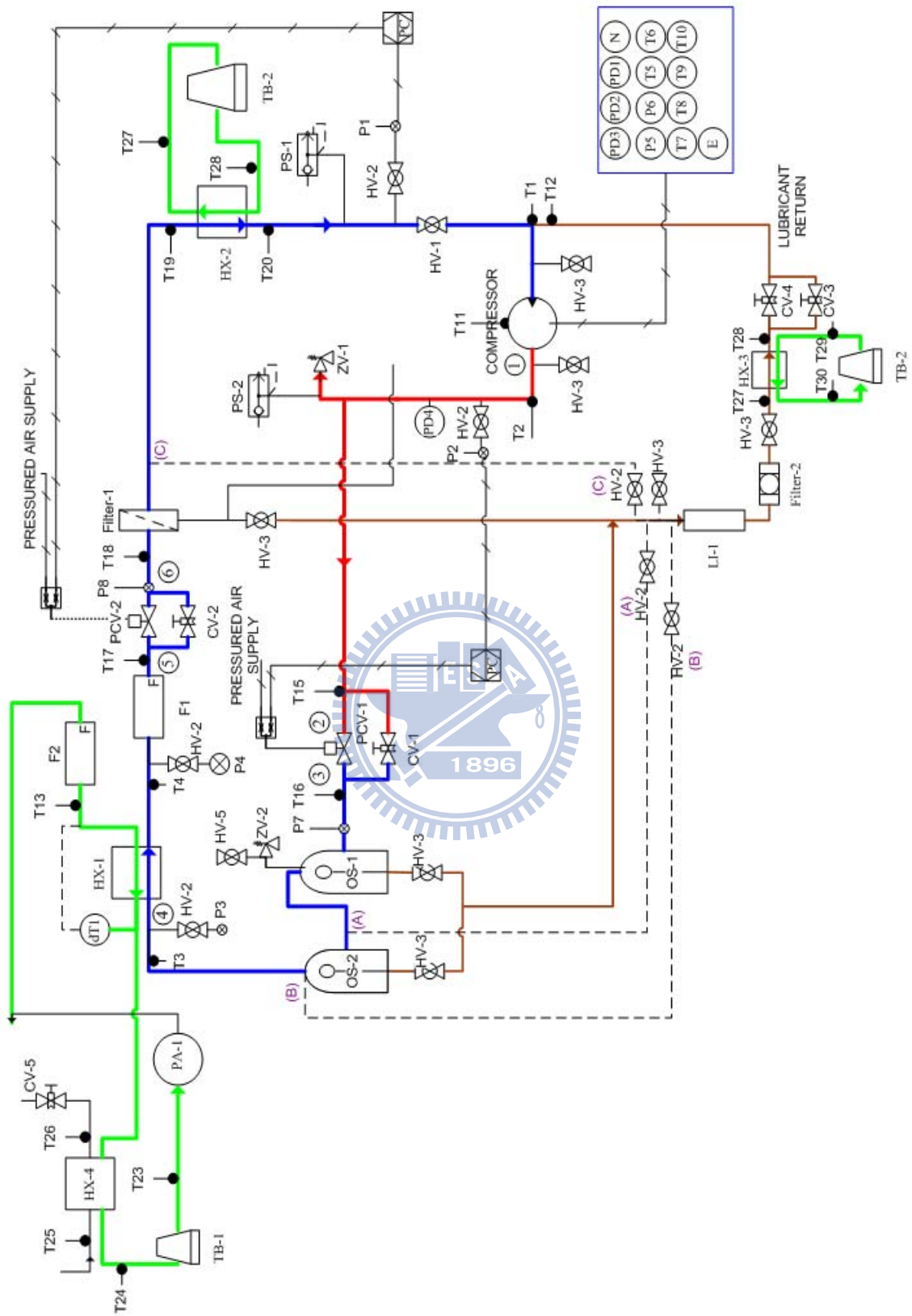


Fig. 4-15 Working procedure of CO₂ test rig

4.3.2 Verification of bypass action

The simulation results were validated through the experimental apparatus described above. A CO₂ STC product for heat pump system was installed in the testing apparatus, as a sample. The compared results between simulation and experiment are shown in Table. 4-8. It was found that the models conform to the experimental results very well and the maximum relative errors for these three results (G, η_v, η_c) are 3.2%, 2.7% and 2% respectively. The models provided in the study can predict the performance with bypass action accurately.

Table. 4-8 Comparisons of sim. & exp. results of \dot{m} , η_v & η_c

| Refrigerant | CO ₂ | | | | | | | | |
|-------------|--------------------|-------|----------|----------|------|----------|----------|------|----------|
| | \dot{m} (kg/min) | | | η_v | | | η_c | | |
| | sim. | exp. | err. (%) | sim. | exp. | err. (%) | sim. | exp. | err. (%) |
| Condition 1 | 0.7 | 0.721 | 2.9% | 0.782 | 0.8 | 2.3% | 0.59 | 0.59 | 0.0% |
| Condition 2 | 1.134 | 1.125 | 0.8% | 0.85 | 0.84 | 1.2% | 0.651 | 0.64 | 1.7% |
| Condition 3 | 0.818 | 0.845 | 3.2% | 0.759 | 0.78 | 2.7% | 0.566 | 0.57 | 0.7% |
| Condition 4 | 0.956 | 0.973 | 1.7% | 0.773 | 0.78 | 0.9% | 0.571 | 0.56 | 2.0% |
| Condition 5 | 1.191 | 1.186 | 0.4% | 0.845 | 0.84 | 0.6% | 0.648 | 0.64 | 1.3% |

4.4 Remarks

The simulation results for several arrangements of the bypass mechanism regarding different STC structures are investigated at first. The change in uncovered areas of bypass holes, the open intervals for corresponding chambers are also be derived.

On the other hand, five specified operating conditions with and without bypass action has been validated by the test rig for a developing CO₂ STC product. It is found that the STC with bypass valves increases 2.5% ~ 10% in compressor efficiency, and volumetric efficiency is scarcely affected. In addition, it is found that the design of the bypass holes for this STC product can avoid over-compression completely inside the compression chambers under the five operating conditions. However, over-compression and liquid slugging probably occur for other operating conditions.

In the next chapter, an optimization module will be developed and linked to the simulation program for aiding with analysis and improving design of STC further.

CHAPTER 5 OPTIMIZATION PROCEDURE APPLIED IN STC MODEL

A design optimization module will be constructed and its procedure will also be illustrated in this chapter. By integrating the verified STC simulation model (as shown in Chapter 2) with an optimum solver, a frictional loss reduced problem of bearing components will be studied. Discussion in regard to design selections and limitations in a R-22 STC product will be investigated. It is expected that various optimum combinations of parameters can be found for different STC design considerations by integrating this optimization procedure into the STC model.

5.1 Researches about optimum design of STC

In viewpoint of papers about optimum design, Etemad and Nieter [49] have provided simple design approach to decide characteristic parameters within manufacturing limitations of STC. The optimum combinations of two characteristic parameters, base circle radius and wrap height in STC for higher efficiency have been investigated by Ishii *et al.* [38, 50, 51]. In addition, Tseng and Chang [52] have used a systematic design procedure to develop a family optimization of STC products with high percentage of share in major components.

For different compressor type, Ooi [53] has presented a study combining the parametric simulation model with iterative optimum algorithm to develop design optimization in rolling piston compressor. However, that kind of application to STC was rarely discussed in literatures.

Therefore, this dissertation proposes to develop a design optimization procedure by integrating the parametric STC model (developed in Chapter 2) with an optimum solver “*MOST*” (Tseng [6]). One case riveted on reduction of the frictional losses for bearing components in STC and investigation of relevant effects, are analyzed and discussed for demonstrating the optimization procedure.

5.2 Verification of simulation results and experiments

One STC model with R-22 refrigerant is used for comparisons between the simulation

and experiment results. The characteristic parameters of the scroll pairs, and the two testing groups, different operating temperatures with constant speed (condition A) and same operating temperature with varying speed (condition B) are showed in Table. 5-1. The STC model has been tested on a R-22 calorimeter (specifications shown in Table. 5-2) and the simulation and experiment results (0.35% expanded uncertainty in measured power and 0.12% expanded uncertainty in measured mass flow rate) are shown in Table. 5-3.

For condition A, Table. 5-3 shows the refrigerant mass flow rate, motor input power, volumetric efficiency (η_V) and compressor efficiency (η_C). The maximum relative error to those values is 3.5%. It is found that the lower temperature in operating conditions, the larger errors produced. Those errors may result from the deviation of the superheat in suction pipe and the evaluation of leakage gaps with linearity simplifications. Fig. 5-1(a) shows the various contributions to frictional losses from simulation at condition A, and it is found that the greatest one is the frictional loss in thrust bearing (42%~48%), followed by the upper bearing (22%~25%), the crank bearing (18%~21%), the lower bearing (6%~8%) and others (3%~5%) in turn. The ratio in various frictional losses is similar at all cases of condition A.

For condition B, the maximum relative error of each index is 5.6%. Fig. 5-1(b) shows the contributions of frictional losses, and it is found that the lower motor speed, the lower amount of frictional losses and the contributive percentages of frictional losses are similar to those in condition A.

Though the simulation results show a little discrepancy with the experiments, the developed STC program with acceptable accuracy can be regarded as the basis for developing optimum design procedure.

Table. 5-1 Parameters and operating conditions of the STC

| Characteristic parameters | | | | | |
|---|---|-------------------------------------|------------------------------------|------------------------------|------------------------------|
| Basic circle radius (r_b) | 2.062 (mm) | | | | |
| Thickness of the scroll (t_h) | 2.65 (mm) | | | | |
| Roll angle of the scroll | 20.25 (rad) | | | | |
| Height of the scroll (h) | 22 (mm) | | | | |
| Discharge angle | 3.79 (rad) | | | | |
| End-plate diameter of the orbiting scroll | 92 (mm) | | | | |
| End-plate height of the orbiting scroll | 7 (mm) | | | | |
| End-plate diameter of the fixed scroll | 112 (mm) | | | | |
| End-plate height of the fixed scroll | 12 (mm) | | | | |
| Suction volume | 3.39×10^{-5} (m ³) | | | | |
| Volume ratio | 3.25 | | | | |
| Condition A | | | | | |
| Motor revolution | 60 rps | | | | |
| Operating conditions | $T_{\text{evap}}(^{\circ}\text{C})$ | $T_{\text{cond}}(^{\circ}\text{C})$ | $T_{\text{suc}}(^{\circ}\text{C})$ | $p_{\text{suc}}(\text{MPa})$ | $p_{\text{dis}}(\text{MPa})$ |
| A1 | 7.2 | 54.4 | 35 | 0.625 | 2.146 |
| A2 | 7.2 | 48.9 | 18.3 | 0.625 | 1.894 |
| A3 | 4.4 | 48.9 | 15.5 | 0.573 | 1.894 |
| A4 | -1.1 | 48.9 | 10 | 0.480 | 1.894 |
| A5 | -6.7 | 48.9 | 4.4 | 0.398 | 1.894 |
| Condition B | | | | | |
| B1 | 30 rps | | | | |
| B2 | 40 rps | | | | |
| B3 | 50 rps | | | | |
| Operating conditions | $T_{\text{evap}}(^{\circ}\text{C})$ | $T_{\text{cond}}(^{\circ}\text{C})$ | $T_{\text{suc}}(^{\circ}\text{C})$ | $p_{\text{suc}}(\text{MPa})$ | $p_{\text{dis}}(\text{MPa})$ |
| | 7.2 | 54.4 | 35 | 0.625 | 2.146 |

Table. 5-2 Specifications of calorimeter for measuring STC performance

| Specifications | | |
|--|---|-----------|
| Refrigerant | R ₂₂ | |
| Capacity range (Watt) | 1500 ~ 12000 | |
| Description of system | According ISO917, design for fully automatic measurements | |
| Measuring method | The secondary refrigerant and liquid flow meter system | |
| Accuracy | | |
| Deviation between the secondary refrigerant and liquid flow system | ≤±4% | |
| Refrigerant flow-measuring instruments | ≤±1% | |
| Speed measuring instruments | ≤±0.75% | |
| Repeatability | ≤±1% | |
| Control items | Range | Stability |
| p_{dis} of Compressor (MPa) | 0.98–2.94 | ± 0.01 |
| p_{suc} of Compressor (MPa) | 0.15–0.91 | ± 0.015 |
| T_{suc} of Compressor (°C) | -25–50 | ± 0.5 |

Table. 5-3 Comparison of sim. & exp. results in different conditions

| | G (kg · s ⁻¹) | | | Motor input (watt) | | | $\eta_v(-)$ | | | $\eta_c(-)$ | | |
|----|-----------------------------|-------|------|--------------------|------|------|-------------|-------|------|-------------|-------|------|
| | sim. | exp. | err. | sim. | exp. | err. | sim. | exp. | err. | sim. | exp. | err. |
| A1 | 2.532 | 2.528 | 0.1% | 2007 | 2014 | 0.3% | 0.943 | 0.946 | 0.3% | 0.749 | 0.754 | 0.7% |
| A2 | 2.715 | 2.707 | 0.3% | 1876 | 1866 | 0.5% | 0.923 | 0.931 | 0.9% | 0.701 | 0.717 | 2.2% |
| A3 | 2.455 | 2.460 | 0.2% | 1852 | 1812 | 2.2% | 0.908 | 0.915 | 0.8% | 0.702 | 0.725 | 3.3% |
| A4 | 2.013 | 2.045 | 1.5% | 1795 | 1737 | 3.3% | 0.882 | 0.877 | 0.6% | 0.683 | 0.706 | 3.2% |
| A5 | 1.643 | 1.665 | 1.3% | 1731 | 1672 | 3.5% | 0.861 | 0.840 | 2.5% | 0.659 | 0.672 | 1.9% |
| B1 | 1.158 | 1.157 | 0.1% | 1034 | 1095 | 5.6% | 0.878 | 0.907 | 3.2% | 0.665 | 0.649 | 2.5% |
| B2 | 1.601 | 1.595 | 0.4% | 1344 | 1374 | 2.2% | 0.908 | 0.883 | 2.9% | 0.706 | 0.672 | 5.1% |
| B3 | 2.075 | 2.083 | 0.4% | 1681 | 1621 | 3.7% | 0.927 | 0.927 | 0.0% | 0.732 | 0.761 | 3.8% |

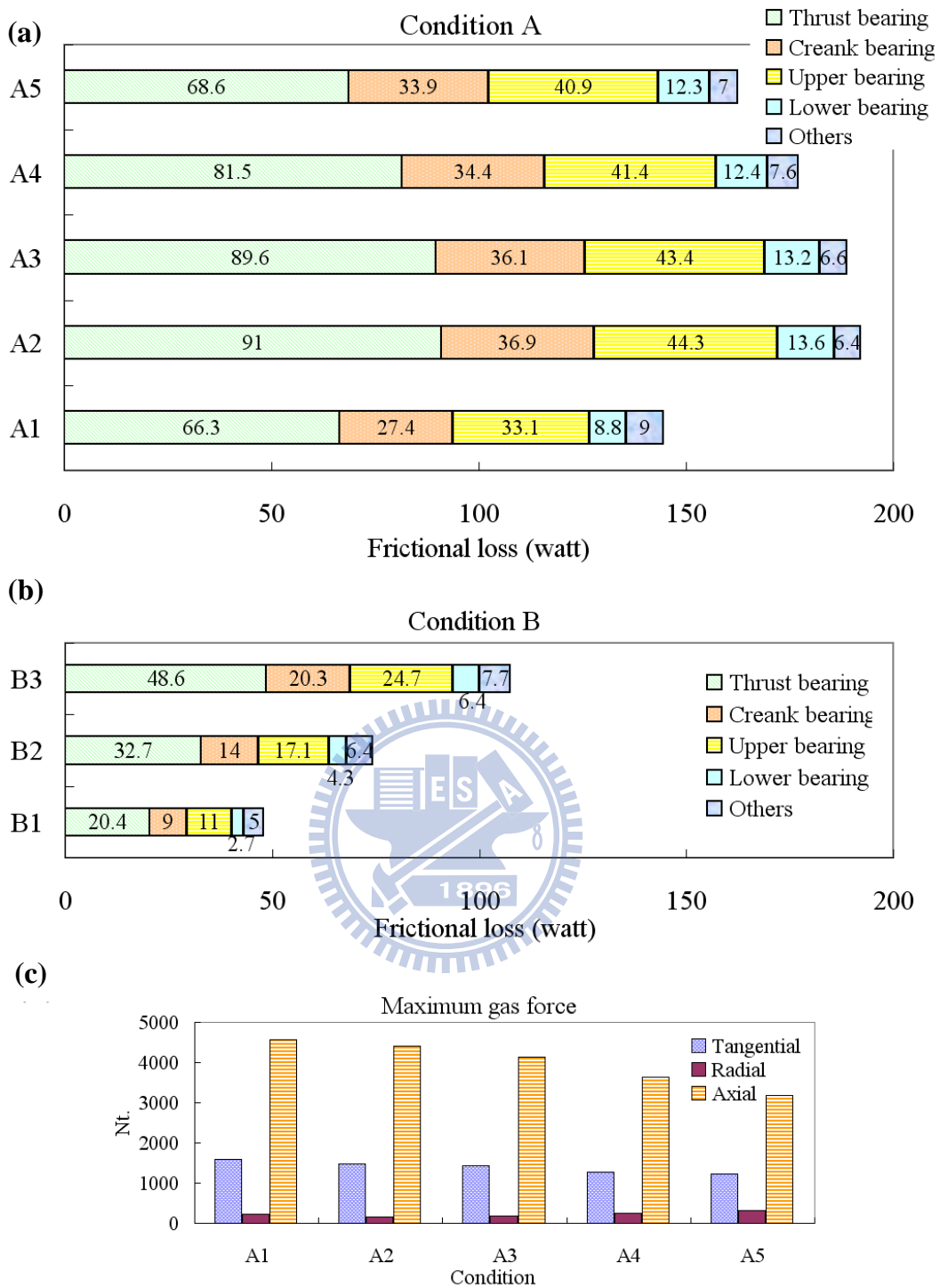


Fig. 5-1 Frictional losses in (a) Condition A (b) Condition B (c) maximum loading in Condition A

5.3 Optimization solver

With advance in computer technology, computerized optimum procedures integrating the simulation program with the optimization algorithm can help designer to determine the

suitable design parameters and get the optimum results within the prescribed constraints. In this study, the solver “*MOST*” [6] is integrated into the STC simulation program to deal with the optimization problem.

5.3.1 Formulation of optimization problem

The solver has been developed by using constrained and gradient methods. The Sequential Quadratic Programming (SQP) method (Arora [54]) has been selected as the kernel for the single objective, minimum type and continuous variables problem in this study. The formulation has been defined as follows:

Find a q-vector $\vec{x} = [x_1, x_2, x_3, \dots, x_q]^T$ of design variables to minimize an objective function

$$F(\vec{x}) = F(x_1, x_2, \dots, x_q) \quad (5.1)$$

which is subject to the constraints

$$h_j(\vec{x}) = 0 ; j = 1, 2, \dots, p \quad (5.2)$$

$$\text{and } g_i(\vec{x}) \leq 0 ; i = 1, 2, \dots, m \quad (5.3)$$

the explicit bounds on design variables

$$x_{\text{low}}(k) \leq x(k) \leq x_{\text{upp}}(k) ; k = 1, 2, \dots, q \quad (5.4)$$

The $F(\vec{x})$ is the objective function and the design variables vector \vec{x} represents the arguments varied in order to generate a better design. The constraints expressed by equations (5.2) and (5.3) define the feasible design space in conjunction with the design variable bounds specified by equation (5.4).

5.3.2 Optimization procedure

The optimization procedure is shown in Fig. 5-2. At the beginning stage, the design variables, objective function and constraint conditions, formulated and set as input data, are passed to the STC simulation program. Secondly, the program is executed and the output data can be obtained. The output data are then analyzed by the optimization solver. If the results do not satisfy the convergent criteria, a new group of design variables is derived by SQP method. This group will be returned to the simulation program as new input data to progress the procedure iteratively, until the convergent conditions are satisfied and finally the optimum result is found.

5.4 Case study: optimization in reducing frictional losses

Owing to the frictional losses are mainly caused from the four bearing components, an optimization case to search the optimum geometrical dimensions of the bearings for minimum frictional losses in STC is investigated.

5.4.1 Selection of objective function and design variables

The mechanical loss P_{mech} is selected as the objective function to be minimized. For the three journal bearings with two parameters, inner diameter (D) and length (L) are specified by design decisions. Hence, there are six design parameters selected for the three journal bearings. For the thrust bearing, the inner and outer diameters ($D_{i,\text{th}}$ and $D_{o,\text{th}}$) are considered as design variables. There are totally eight design variables of the problem and the objective function is mathematically defined as

$$\begin{aligned} & \text{Minimize } P_{\text{mech}} \\ & \text{where } P_{\text{mech}} = F(\vec{x}) = F(L_{b,\text{cr}}, D_{b,\text{cr}}, L_{b,\text{upp}}, D_{b,\text{upp}}, L_{b,\text{low}}, D_{b,\text{low}}, D_{i,\text{th}}, D_{o,\text{th}}) \end{aligned} \quad (5.5)$$

The lower and upper bounds of the design variables are expressed as

$$x_{\text{low}}(i) \leq x(i) \leq x_{\text{upp}}(i) ; i=1,2,\dots,8 \quad (5.6)$$

Those bounds and sizes are decided in consideration of tolerances, fits and space constraints for the developed STC model and values shown in Table. 5-4 are specified to guarantee that the final design is feasible.

Table. 5-4 Bounds of design variables and constraints

| Constraint conditions | | | | | |
|-----------------------|--------------------|-----------------|-----------------|----------------|--|
| No. | Design variables | Lower bound(mm) | Upper bound(mm) | No.Constraints | Descriptions |
| 1 | $L_{b,\text{cr}}$ | 19.0 | 27.0 | 1 | $p_{b,\text{cr}} \leq 10 \text{ Mpa}$ |
| 2 | $D_{b,\text{cr}}$ | 21.5 | 29.5 | 2 | $p_{b,\text{upp}} \leq 10 \text{ Mpa}$ |
| 3 | $L_{b,\text{upp}}$ | 26.5 | 34.5 | 3 | $p_{b,\text{low}} \leq 10 \text{ Mpa}$ |
| 4 | $D_{b,\text{upp}}$ | 21.5 | 29.5 | 4 | $p_{\text{th}} \leq 10 \text{ Mpa}$ |
| 5 | $L_{b,\text{low}}$ | 19.0 | 27.5 | 5 | $h_{b,\text{cr}} \geq 6 \mu\text{m}$ |
| 6 | $D_{b,\text{low}}$ | 16.0 | 22.0 | 6 | $h_{b,\text{upp}} \geq 6 \mu\text{m}$ |
| 7 | $D_{o,\text{th}}$ | 75.0 | 90.0 | 7 | $h_{b,\text{low}} \geq 6 \mu\text{m}$ |
| 8 | $D_{i,\text{th}}$ | 45.0 | 60.0 | 8 | $h_{\text{th}} \geq 6 \mu\text{m}$ |

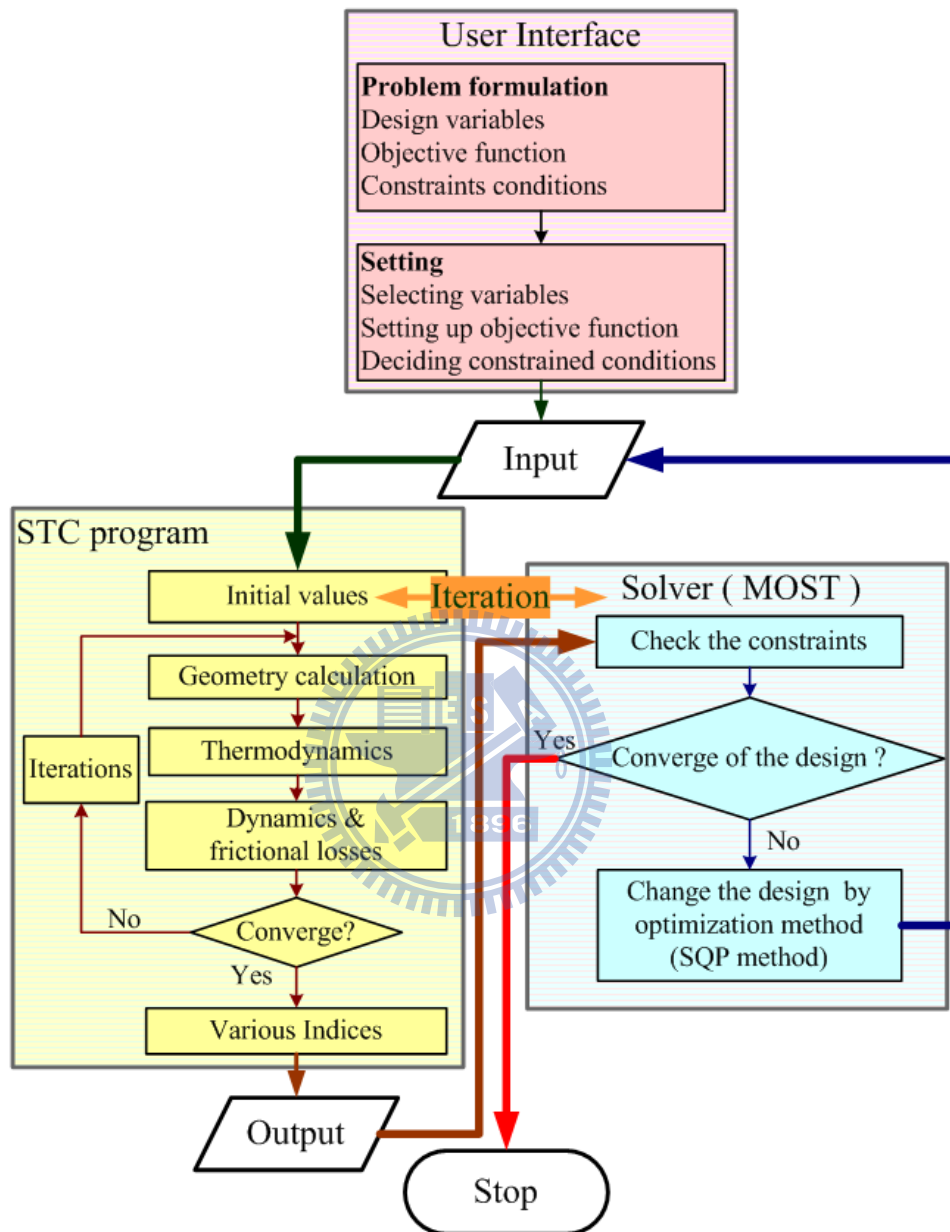


Fig. 5-2 Flow chart of the optimization procedure

5.4.2 Selection of constraint conditions

When considering the behavior of hydrodynamic lubrication, the most important factor is that the full separating oil-film must be retained at running to ensure the mating surfaces are in the ideal operation with minimum wear and friction. So the minimum oil-film thickness should be greater than the roughness of the mating surfaces. The dimensionless film thickness

commonly is defined as

$$\Lambda = \frac{h_{\min}}{\bar{R}} = \frac{h_{\min}}{(\bar{R}_a^2 + \bar{R}_b^2)^{0.5}} \quad (5.7)$$

where \bar{R}_a and \bar{R}_b represented the root-mean-square roughness of mating surfaces. With full-filling hydrodynamic lubrication, $\Lambda \geq 10$ must be satisfied (Khonsari and Booser [55] 2001), so the minimum thickness can be derived once the \bar{R}_a and \bar{R}_b are decided. In this study, both \bar{R}_a and \bar{R}_b are set to $0.4 \mu\text{m}$, then the constraint h_{\min} can be obtained as

$$h_{\min} = \Lambda(\bar{R}_a^2 + \bar{R}_b^2)^{0.5} = 5.66 \mu\text{m} \quad (5.8)$$

Therefore $h_{\min} \geq 6 \mu\text{m}$ was set as the first constraint for the four bearings.

Another consideration is the maximum oil-film pressure on contacted surfaces. For the four bearings, 10 MPa for allowable strength is set as upper limit of the constraint, i.e.

$$P_{\max} \leq 10 \text{ MPa} \quad (5.9)$$

The detailed constraint conditions are summarized in Table. 5-4.

5.5 Case study: optimum results and discussions

5.5.1 Selection of testing conditions

Several testing conditions can be simulated in the optimization procedure. However, the severest condition should be adopted in order to promise that the final design of the STC can sustain well at all conditions. Fig. 5-1(c) shows several maximum gas forces act on the orbiting scroll during the orbiting cycle and it is found that the condition A1 has the greatest loading and is also the most frequent running condition. Hence condition A1 is selected as the testing condition in this optimization problem.

5.5.2 Optimum results

The optimization search has been executed on a PC with 2.6 GHz Pentium C2D processor with 2 GB memory and it takes 2 hours to finish. Fig. 5-3(a) shows that the objective function decreases during the iterations, and the mechanical loss reduces 16% (from 144.6 W to 121.7 W). The history of constrained conditions is shown in Fig. 5-3(b) and Fig. 5-3(c), it is found that all the constraints are satisfied. Moreover, two constraints, 5 and 6, are

active. It reveals that the minimum film thickness of the crank and upper bearing ($h_{b,cr}$ and $h_{b,upp}$) have approached the limitation (6 μm). Table. 5-5 shows the variation of design variables and respective power consumptions before and after the optimization. It is found that the frictional losses of each bearing are reduced in range of 11.4% to 38.1%.

Table. 5-5 Optimized results with design variables

| No | Design variables | Initial(mm) | Optimized(mm) | Variation(%) |
|-------------------------------|------------------|---------------|-----------------|--------------|
| 1 | $L_{b,cr}$ | 23.00 | 27.00 | 17.4% |
| 2 | $D_{b,cr}$ | 25.40 | 22.45 | -11.6% |
| 3 | $L_{b,upp}$ | 31.00 | 31.47 | 1.5% |
| 4 | $D_{b,upp}$ | 25.40 | 22.05 | -13.2% |
| 5 | $L_{b,low}$ | 23.00 | 19.00 | -17.4% |
| 6 | $D_{b,low}$ | 18.95 | 16.00 | -15.6% |
| 7 | $D_{o,th}$ | 85.00 | 75.00 | -11.8% |
| 8 | $D_{i,th}$ | 55.00 | 45.00 | -18.2% |
| Results | | Initial(watt) | Optimized(watt) | Variation(%) |
| Loss of thrust bearing | | 66.54 | 58.95 | 11.4% |
| Loss of crank journal bearing | | 27.48 | 23.28 | 15.3% |
| Loss of upper journal bearing | | 33.21 | 26.23 | 21.0% |
| Loss of lower journal bearing | | 8.82 | 5.46 | 38.1% |
| Others | | 8.55 | 7.78 | 9.0% |
| Summation | | 144.6 | 121.7 | 15.8% |

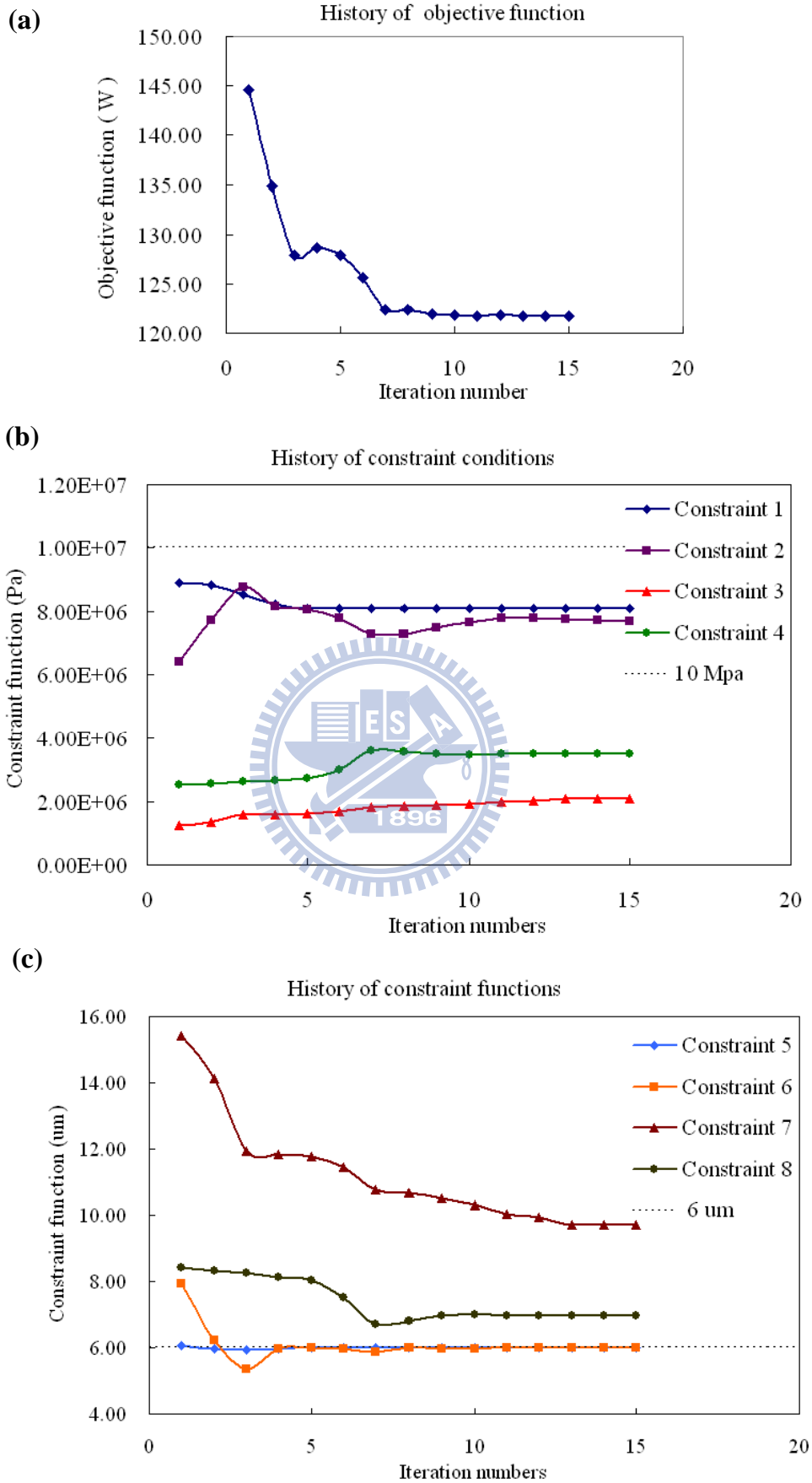


Fig. 5-3 Iteration history (a) Objective function (b) Constraints 1–4 (c) Constraints 5–8

5.5.3 Discussions

The results shown in Fig. 5-3(a), Fig. 5-3(c) and Table. 5-5 imply that the design modifications of crank and upper journal bearings reduce the frictional losses while the constraints of minimum oil-film thickness are met, so the decrease level of the losses is confined. Furthermore, the trend of smaller diameter of the crank and upper bearings can reduce the frictional losses. The design variables related to lower journal bearing ($L_{b,low}$ and $D_{b,low}$) finally locate at the lower bounds, it means that the shorter and narrower one can reduce the frictional losses without violating the specified constraints.

For the thrust bearing that contributed to the maximum power consumption in frictional losses, it is found that the related design variables ($D_{i,th}$ and $D_{o,th}$) are located at the lower bound of the design limitations. It is said that for the specified design bounds and constraint conditions, the smaller inner and outer diameter of the thrust bearing, the larger amount of frictional losses can be reduced. However, Table. 5-5 shows that the variation ratio between initial and optimized reductive frictional losses of the thrust bearing (11.4%) is smaller than those of the three journal bearings (15.3% ~ 38.1%).

In addition, the maximum pressure constraints (constraint 1~4, shown in Fig. 5-3 (b)) are not infringed by the design parameters of the three journal bearings and the thrust bearing during the optimization search. The constraints for the strength consideration do not affect the optimum search in this study, which indicated that the bearing materials may have broader selectivity.

After the optimum search of the STC, the simulated results of the new design in all testing conditions are shown in Fig. 5-4, and it is found that the frictional losses can be reduced in range of 14.1%~18.1%. It demonstrates that this design optimization procedure can help improve STC efficiency effectively.

On the other hand, some values of bearing parameters shown in Table 5-5 are not the ones for standard parts and can not be provided by bearing manufacturers. Therefore, the standard part with approximate values can be used as alternatives in view of practical product design and cost consideration.

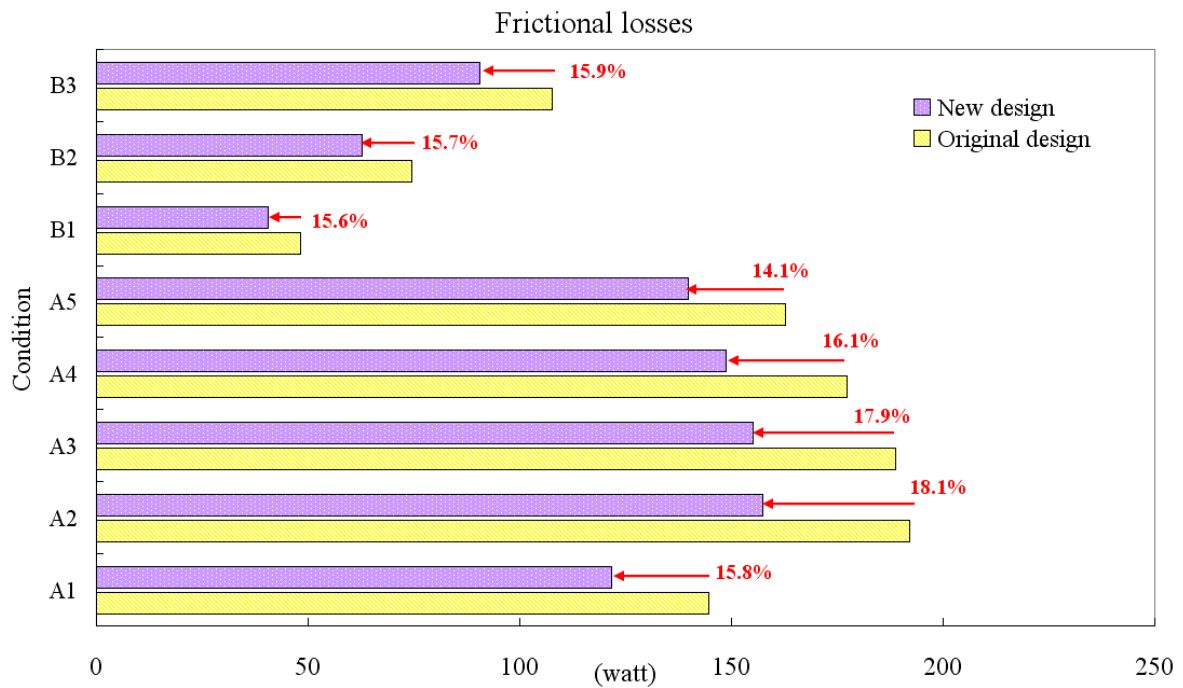


Fig. 5-4 Frictional losses in all testing conditions

5.6 Remarks

An optimum solver has been combined with the model to progress design decision of constrained optimization problems in this Chapter. The optimization results for a selected STC design problem shows that the frictional losses can be reduced in range of 14.1% ~ 18.1% at all testing conditions by new design group which is satisfied at the specified constraint conditions for one thrust and three journal bearings.

For the crank and upper journal bearings, the design modifications can reduce the frictional losses, but the constraints of minimum oil-film thickness for holding hydrodynamic lubrication can block the further decrease of the frictional losses. For the lower journal bearing, the shorter and narrower dimensions can reduce the frictional losses without violating the oil-film constraints. For the thrust bearing, the smaller inner and outer diameter of the thrust surface, the larger reduction in frictional losses with specified design constraints and, the constraints of the maximum pressure that related to the strength consideration of all the bearings are satisfied during all iterations. These results signify wider space for material selection.

Besides, another technique used in STC with variable compression ratio will be illustrated in the subsequent chapters.

CHAPTER 6 INVESTIGATION ON INVOLUTE OF CIRCLE WITH VARIABLE RADII IN A STC

A geometric model of scroll profiles, constructed from an involute of circle with variable radii, has been developed by using the theorem of planar orbiting mechanisms. Parametric studies have also been investigated in this chapter. When compared to the conventional scroll profile with the same suction volume, volume ratio and housing size, this new model demonstrates better reliability and efficiency because of a lower wrap height. Alternatively, a scroll type compressor with a more compact housing size can be achieved by using this new profile but keeping its wrap height the same as the conventional one.

6.1 Various studies for scroll profiles

With regard to the scroll pair (which are the fixed and orbiting scrolls), numerous technical papers and patents have been written and proposed within the last two decades, to improve STC performance. From a geometric viewpoint, many curve profiles that have been used to create the scroll pair (such as the involute of circle, archimedes spirals and segmental arcs) have been investigated continuously in literature [13–16]. In addition, Lee and Wu [9] proved that several theorems related to planar orbiting mechanisms can be used to design a scroll pair.

In the mathematic field of the theoretic study, a planar curve expressed by the intrinsic equation has also been developed to derive a closed analytical expression regarding several scroll profiles [10–12].

Furthermore, several studies using eco-friendly refrigerants (ex. CO₂) in STC have garnered much attention in recent years. But this means that the STC must confront with higher pressure conditions resulted from the specific operating temperatures. Due to this, developing a scroll pair with better rigidity and strength to endure these high pressure conditions has become an issue.

Among the literature about the involute scroll profiles, a new type constructed from an involute of circle with variable radii was proposed for higher efficiency, reliability and wider design freedom (Tojo and Ueda [56, 57]). However, the illustration of this new type of scroll profile lacks specifics. Its advantages and defects have not yet been explained clearly.

Therefore a complete geometric model of the scroll profiles constructed from an involute of circle with variable radii will be formulated and proved by utilizing the theorem of planar orbiting mechanisms in this chapter.

6.2 Geometric model of the scroll profile constructed from an involute of circle with variable radii

The complete mathematic expressions will be delineated in the following paragraphs. However, the theorem of planar orbiting mechanisms [9] must first be reviewed and understood clearly.

6.2.1 Theorem of planar orbiting mechanisms

Theorem 1 [9]: Whenever two curves, one in plane Π_f and the other in plane Π_m , make contact, the contact point must be on the concave side of one curve (called the inner curve) as well as on the convex side of the other curve (called the outer curve). The difference between the radius of curvature (ρ) of the two curves must be equal to the orbiting radius (r_{ob}) at all points of contact.

This theorem can be explained, as shown in Figure 6-1, by considering the origins of the two planes, Π_f and Π_m , as they orbit around each other, and one smooth curve in plane Π_m , which can be expressed as

$$\begin{cases} x_m = x_c(\psi_m) + \rho(\psi_m) \cos \psi_m \\ y_m = y_c(\psi_m) + \rho(\psi_m) \sin \psi_m \end{cases} \quad (6.1)$$

Then a pair of outer and inner conjugate curves can be expressed in plane Π_f as follows

$$\begin{cases} x_{f,ou} = -x_c(\psi_m) - [\rho(\psi_m) + r_{ob}] \cos \psi_m \\ y_{f,ou} = -y_c(\psi_m) - [\rho(\psi_m) + r_{ob}] \sin \psi_m \end{cases} \quad (6.2)$$

$$\begin{cases} x_{f,in} = -x_c(\psi_m) - [\rho(\psi_m) - r_{ob}] \cos \psi_m \\ y_{f,in} = -y_c(\psi_m) - [\rho(\psi_m) - r_{ob}] \sin \psi_m \end{cases} \quad (6.3)$$

when $\rho(\psi_m) - r_{ob} \geq 0$

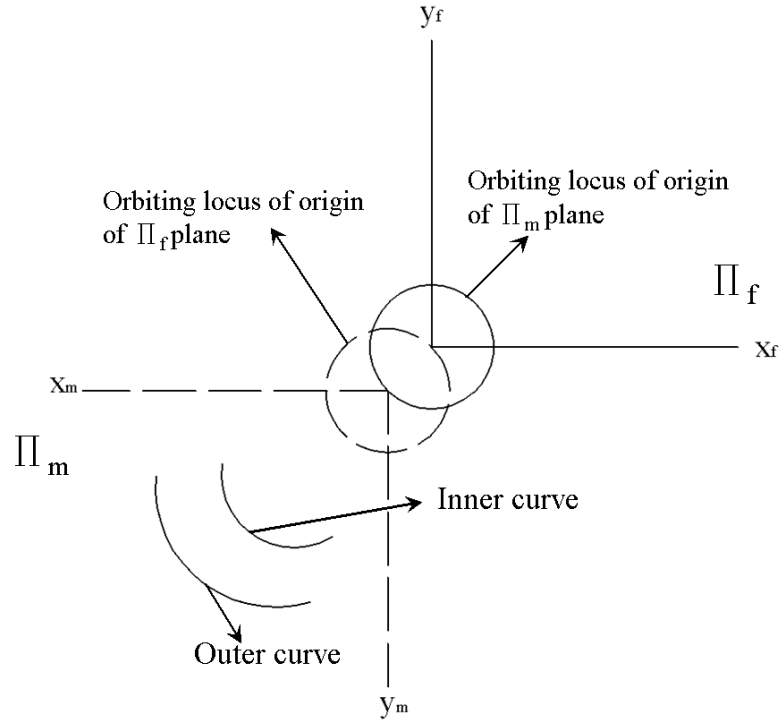


Fig. 6-1 Illustration: theorem of planar orbiting mechanisms

It's also been found that the outer and inner curves expressed by equations (6.2) and (6.3) in plane Π_f respond to the inner and outer conjugate curves that were expressed by the equation (6.1) in plane Π_m . Due to the two planes being rotated 180 degrees ($\psi_f = \psi_m \pm \pi$) toward each other, the equations (6.2) and (6.3) can also be expressed in plane Π_f as follows

$$\begin{cases} x_{f,ou} = -x_c(\psi_f - \pi) - [\rho(\psi_f - \pi) + r_{ob}] \cos(\psi_f - \pi) \\ y_{f,ou} = -y_c(\psi_f - \pi) - [\rho(\psi_f - \pi) + r_{ob}] \sin(\psi_f - \pi) \end{cases} \quad (6.4)$$

$$\begin{cases} x_{f,in} = -x_c(\psi_f + \pi) - [\rho(\psi_f + \pi) - r_{ob}] \cos(\psi_f + \pi) \\ y_{f,in} = -y_c(\psi_f + \pi) - [\rho(\psi_f + \pi) - r_{ob}] \sin(\psi_f + \pi) \end{cases} \quad (6.5)$$

This theorem distinctly shows that the coordinates of the conjugate curves are related to center position (x_c, y_c) , the radius of the curvature (ρ) , the orbiting radius (r_{ob}) and the independent variable (ψ) .

6.2.2 Conceptual illustration and formulations

Conceptual illustration

The basic illustration is shown in Figure 6-2. The conventional scroll curve is constructed from an involute of circle with a fixed radius (a) . This adds to the radius of the

curvature (ρ) at each point of the curve. However, the biggest difference between the conventional scroll curve and the one addressed in this study is that the two parameters (a and ρ) have both been changed by the involute angle (ϕ). By replacing independent variable ψ with the coordinate relation $\psi = \phi - \pi/2$ (as shown in Fig. 6-2), and applying the method of vector projection and trigonometric geometry, the planar coordinates to this involute can be expressed in Cartesian coordinates as:

$$\begin{cases} x = \rho(\phi) \cdot \cos(\psi) - a(\phi) \cdot \sin(\psi) = \rho(\phi) \cdot \cos(\phi - \frac{\pi}{2}) - a(\phi) \cdot \sin(\phi - \frac{\pi}{2}) \\ \quad = a(\phi) \cdot \cos(\phi) + \rho(\phi) \cdot \sin(\phi) \\ y = \rho(\phi) \cdot \sin(\psi) + a(\phi) \cdot \cos(\psi) = \rho(\phi) \cdot \sin(\phi - \frac{\pi}{2}) + a(\phi) \cdot \cos(\phi - \frac{\pi}{2}) \\ \quad = a(\phi) \cdot \sin(\phi) - \rho(\phi) \cdot \cos(\phi) \end{cases} \quad (6.6)$$

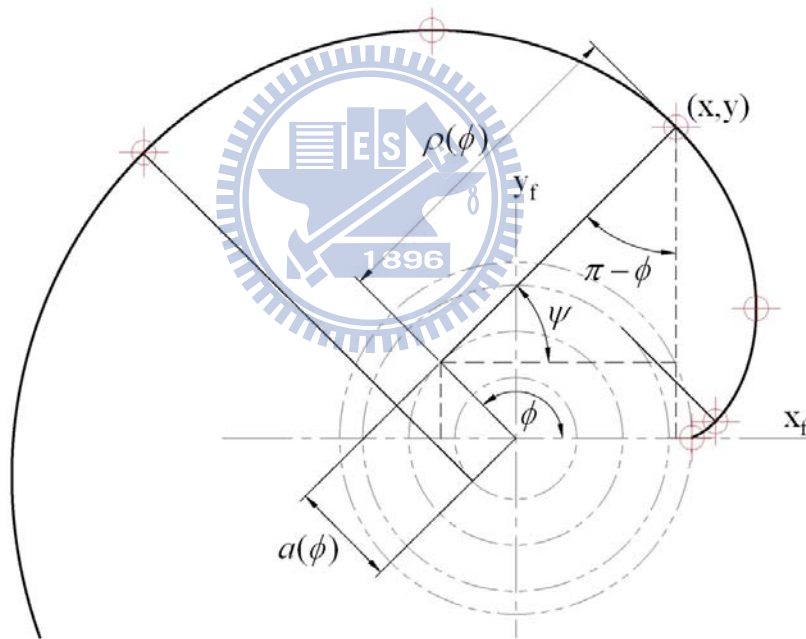


Fig. 6-2 Sketch map and parametric definitions of an involute of circle with variable radii

If a is a constant value, equation (6.6) represents the conventional involute which is used in most of scroll machinery. If both a and ρ are varied with the involute angle ϕ ($a = a(\phi), \rho = \rho(\phi)$), various forms can be further exploited. One of these, the polytropic expression as it relates to the involute angle ϕ , can be devised and expressed as follows:

$$\begin{aligned}
a &= a(\phi) = a_0 + \delta_0 \phi^k, \\
\text{and } \rho &= \rho(\phi) = \int_0^\phi (a_0 + \delta_0 \phi^k) d\phi = a_0 \phi + \frac{\delta_0}{k+1} \phi^{k+1}
\end{aligned} \tag{6.7}$$

k is the polytropic index. a_0 and δ_0 represent the initial radius of the base circle and the corrected increment. One conventional involute can be obtained when $\delta_0 = 0$. If $\delta_0 > 0$ or $\delta_0 < 0$, the distance between the two curves, which correspond to the thickness of the scroll pair, will be increased or decreased toward the peripheral of the scroll wrap.

Formulation

By utilizing equations (6.6) and (6.7) and transforming the parametric relations as shown in Figure 6.3, the outer involute with the involute angle ϕ at the contact point C_0 in plane Π_f can be expressed as

$$\begin{cases} x_{f,ou} = a_{ou} \cos \phi + \rho_{ou} \sin \phi \\ y_{f,ou} = a_{ou} \sin \phi - \rho_{ou} \cos \phi \end{cases} \tag{6.8}$$

where

$$\begin{aligned}
a_{ou} &= a_{ou}(\phi) = a_0 + \delta_0 \phi^k, \\
\text{and } \rho_{ou} &= \rho_{ou}(\phi) = a_0 \phi + \frac{\delta_0}{k+1} \phi^{k+1}
\end{aligned} \tag{6.9}$$

By assuming the starting involute angles α_{in} , α_{ou} for the inner and outer curves respectively, and referring to Fig. 6-3, the contact relation can be derived once the inner curve in plane Π_f expands $\phi' = \phi + \pi - (\alpha_{in} + \alpha_{ou})$ angles. Due to the necessary condition that “a pair of conjugate curves have a common radius of a base circle” must be satisfied, a and ρ for the inner curves at contact point C_1 must be expressed as follows:

$$\begin{aligned}
a_{in} &= a_{ou}(\phi) = a_{in}(\phi') \\
&= a_0 + \delta_0 [\phi' - (\pi - \alpha_{in} - \alpha_{ou})]^k \Big|_{\phi' = \phi + \pi - (\alpha_{in} + \alpha_{ou})} \\
&= a_0 + \delta_0 \phi^k, \\
\text{and } \rho_{in} &= \rho_{in}(\phi') = \int_0^{\phi'} \{a_0 + \delta_0 [\phi' - (\pi - \alpha_{in} - \alpha_{ou})]^k\} d\phi' \\
&= (a_0 \phi') \Big|_0^{\phi + \pi - (\alpha_{in} + \alpha_{ou})} + \left\{ \frac{\delta_0}{k+1} [\phi' - (\pi - \alpha_{in} - \alpha_{ou})]^{k+1} \right\} \Big|_0^{\phi + \pi - (\alpha_{in} + \alpha_{ou})} \\
&= a_0 [\phi + (\pi - \alpha_{in} - \alpha_{ou})] + \frac{\delta_0}{k+1} [\phi^{k+1} + (-1)^{k+2} (\pi - \alpha_{in} - \alpha_{ou})^{k+1}]
\end{aligned} \tag{6.10}$$

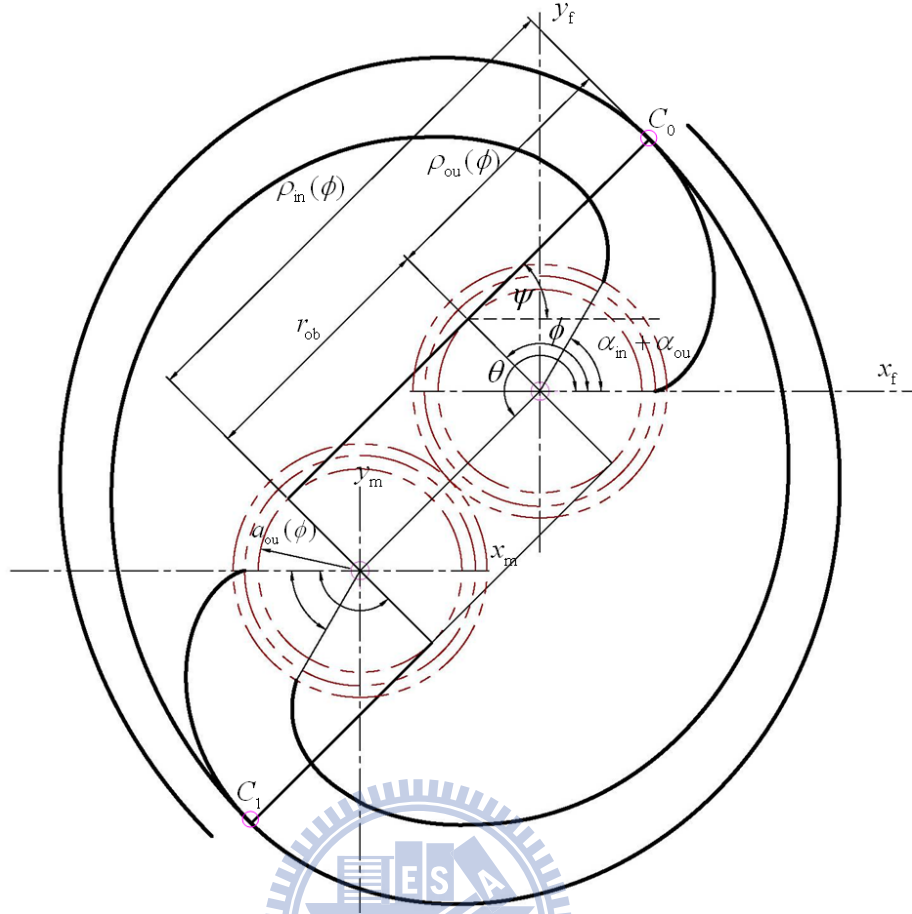


Fig. 6-3 Parametric relations of the scroll profiles constructed from an involute of circle with variable radii

Then the inner curve in plane Π_f can be expressed as:

$$\begin{cases} x_{f,in} = a_m \cos(\phi + \pi) + \rho_{in} \sin(\phi + \pi) \\ y_{f,in} = a_m \sin(\phi + \pi) - \rho_{in} \cos(\phi + \pi) \end{cases} \quad (6.11)$$

From Theorem 1 in Sec.6.2.1 and Fig. 6-3, the conjugate outer curve in plane Π_m can be derived easily from equations (6.3) to (6.6) and stated as follows:

$$\begin{cases} x_{f,ou} = x_{m,in} = -x_{f,in} + r_{ob} \cos \theta \\ y_{f,ou} = y_{m,in} = -y_{f,in} + r_{ob} \sin \theta \end{cases} \quad (6.12)$$

The orbiting angle θ , which defines the orbiting relation for planes Π_f and Π_m and depends on independent variable ψ or involute angle ϕ , can be derived by letting the *Jacobian* of equation (6.12) equal zero, which is shown as follows:

$$\begin{aligned}
Jacobian &= \frac{\partial(x_{m,in}, y_{m,in})}{\partial(\phi, \theta)} = \begin{vmatrix} \frac{\partial x_{m,in}}{\partial \phi} & \frac{\partial y_{m,in}}{\partial \phi} \\ \frac{\partial x_{m,in}}{\partial \theta} & \frac{\partial y_{m,in}}{\partial \theta} \end{vmatrix} \\
&= -(\kappa \delta_0 \phi^{k-1} + \rho_{in})(\cos \phi \cdot \cos \theta + \sin \phi \cdot \sin \theta) = 0
\end{aligned} \tag{6.13}$$

Therefore

$$-\frac{\cos \phi}{\sin \phi} = \frac{\sin(\phi + (m+1/2)\pi)}{\cos(\phi + (m+1/2)\pi)} = \frac{\sin \theta}{\cos \theta}, \text{ where } m = 0, 1, 2, \dots \tag{6.14}$$

The orbiting angle θ can then be derived from equation (6.14) or by referring to Fig. 6-3. It is expressed below:

$$\theta = \psi + \pi = \phi + \pi/2 \tag{6.15}$$

The corresponding outer curve can be expressed as:

$$\begin{cases} x_{f,ou} = x_{m,in} = -x_{f,in} + r_{ob} \cos(\phi + \pi/2) \\ y_{f,ou} = y_{m,in} = -y_{f,in} + r_{ob} \sin(\phi + \pi/2) \end{cases} \tag{6.16}$$

Equations (6.8) and (6.16), which represent the conjugate curves, can be rearranged to compare the coefficients, and then the orbiting radius r_{ob} can be expressed as follows:

$$r_{ob} = a_0(\pi - \alpha_{in} - \alpha_{ou}) + \frac{\delta_0}{k+1} (-1)^{k+2} (\pi - \alpha_{in} - \alpha_{ou})^{k+1} \tag{6.17}$$

6.3 Application for different k values and volume calculations

From the previous description, various curves for different k values can be investigated. By setting the same starting angles to the outer and inner curves, i.e. $\alpha_{ou} = \alpha_{in} = \alpha$, four feasible types of involutes have been constructed in the following statement.

6.3.1 Different k values

1. $k = 0$

Let $k = 0$ and use equations (6.9) and (6.10), equations (6.8) and (6.11) (the outer and inner curves in plane Π_f) can be then expressed as:

$$\begin{cases} x_{f,ou} = (a_0 + \delta_0) \cdot \cos \phi + (a_0 + \delta_0) \cdot \phi \cdot \sin \phi \\ y_{f,ou} = (a_0 + \delta_0) \cdot \sin \phi - (a_0 + \delta_0) \cdot \phi \cdot \cos \phi \end{cases} \tag{6.18}$$

$$\begin{cases} x_{f, \text{in}} = (a_0 + \delta_0) \cdot \cos(\phi + \pi) + (a_0 + \delta_0) \cdot (\phi + \pi - 2\alpha) \cdot \sin(\phi + \pi) \\ y_{f, \text{in}} = (a_0 + \delta_0) \cdot \sin(\phi + \pi) - (a_0 + \delta_0) \cdot (\phi + \pi - 2\alpha) \cdot \cos(\phi + \pi) \end{cases} \quad (6.19)$$

It is easy to find that equations (6.18) and (6.19) are the involutes of circle with a fixed radius ($a = a_0 + \delta_0$), and the orbiting radius is

$$r_{\text{ob}} = a_0(\pi - 2\alpha) + \delta_0(\pi - 2\alpha) = (a_0 + \delta_0)(\pi - 2\alpha) \quad (6.20)$$

2. $k = 1$

Let $k = 1$ and follow the same procedure, and the outer and inner curves become

$$\begin{cases} x_{f, \text{ou}} = (a_0 + \delta_0 \phi) \cdot \cos \phi + (a_0 \phi + \frac{\delta_0}{2} \phi^2) \cdot \sin \phi \\ y_{f, \text{ou}} = (a_0 + \delta_0 \phi) \cdot \sin \phi - (a_0 \phi + \frac{\delta_0}{2} \phi^2) \cdot \cos \phi \end{cases} \quad (6.21)$$

$$\begin{cases} x_{f, \text{in}} = (a_0 + \delta_0 \phi) \cdot \cos(\phi + \pi) \\ \quad + [a_0(\phi + \pi - 2\alpha) + \frac{\delta_0}{2}(\phi^2 - (\pi - 2\alpha)^2)] \cdot \sin(\phi + \pi) \\ y_{f, \text{in}} = (a_0 + \delta_0 \phi) \cdot \sin(\phi + \pi) \\ \quad - [a_0(\phi + \pi - 2\alpha) + \frac{\delta_0}{2}(\phi^2 - (\pi - 2\alpha)^2)] \cdot \cos(\phi + \pi) \end{cases} \quad (6.22)$$

Then the orbiting radius can be expressed as

$$r_{\text{ob}} = a_0(\pi - 2\alpha) - \frac{\delta_0}{2}(\pi - 2\alpha)^2 \quad (6.23)$$

3. $k = 2$

Let $k = 2$ and follow the same procedure, and the outer and inner curves are

$$\begin{cases} x_{f, \text{ou}} = (a_0 + \delta_0 \phi^2) \cdot \cos \phi + (a_0 \phi + \frac{\delta_0}{3} \phi^3) \cdot \sin \phi \\ y_{f, \text{ou}} = (a_0 + \delta_0 \phi^2) \cdot \sin \phi - (a_0 \phi + \frac{\delta_0}{3} \phi^3) \cdot \cos \phi \end{cases} \quad (6.24)$$

$$\begin{cases} x_{f, \text{in}} = (a_0 + \delta_0 \phi^2) \cdot \cos(\phi + \pi) \\ \quad + [a_0(\phi + \pi - 2\alpha) + \frac{\delta_0}{3}(\phi^3 + (\pi - 2\alpha)^3)] \cdot \sin(\phi + \pi) \\ y_{f, \text{in}} = (a_0 + \delta_0 \phi^2) \cdot \sin(\phi + \pi) \\ \quad - [a_0(\phi + \pi - 2\alpha) + \frac{\delta_0}{3}(\phi^3 + (\pi - 2\alpha)^3)] \cdot \cos(\phi + \pi) \end{cases} \quad (6.25)$$

and the orbiting radius is

$$r_{\text{ob}} = a_0(\pi - 2\alpha) + \frac{\delta_0}{3}(\pi - 2\alpha)^3 \quad (6.26)$$

4. $k \neq \text{integer}$

If $k \neq \text{integer}$, the planar coordinates of the conjugate curves and the orbiting radius include complex numbers (because of the term $(-1)^{k+2}$ in equation (6.10)). However, if the real value was adopted only, the conjugate pair can still be created. Let $k = 1.6$, then the outer and inner curves, and the orbiting radius will be as follows:

$$\begin{cases} x_{\text{f,ou}} = (a_0 + \delta_0 \phi^{1.6}) \cdot \cos \phi + (a_0 \phi + \frac{\delta_0}{2.6} \phi^{2.6}) \cdot \sin \phi \\ y_{\text{f,ou}} = (a_0 + \delta_0 \phi^{1.6}) \cdot \sin \phi - (a_0 \phi + \frac{\delta_0}{2.6} \phi^{2.6}) \cdot \cos \phi \end{cases} \quad (6.27)$$

$$\begin{cases} x_{\text{f,in}} = (a_0 + \delta_0 \phi^2) \cdot \cos(\phi + \pi) \\ \quad + \{a_0(\phi + \pi - 2\alpha) + \frac{\delta_0}{2.6}(\phi^{2.6} + \text{Re}[(-1)^{3.6}](\pi - 2\alpha)^{2.6})\} \cdot \sin(\phi + \pi) \\ y_{\text{f,in}} = (a_0 + \delta_0 \phi^2) \cdot \sin(\phi + \pi) \\ \quad - \{a_0(\phi + \pi - 2\alpha) + \frac{\delta_0}{2.6}(\phi^{2.6} + \text{Re}[(-1)^{3.6}](\pi - 2\alpha)^{2.6})\} \cdot \cos(\phi + \pi) \end{cases} \quad (6.28)$$

$$r_{\text{ob}} = a_0(\pi - 2\alpha) + \frac{\delta_0}{2.6} \text{Re}[(-1)^{3.6}](\pi - 2\alpha)^{2.6} \quad (6.29)$$

The involutes for the four cases discussed above are shown in Figure 4. Figure 5 exhibits the structure of the orbiting scroll where $k=1$, $\alpha=50^\circ(5\pi/18)$ and $\delta_0 = -0.05(\text{mm})$.

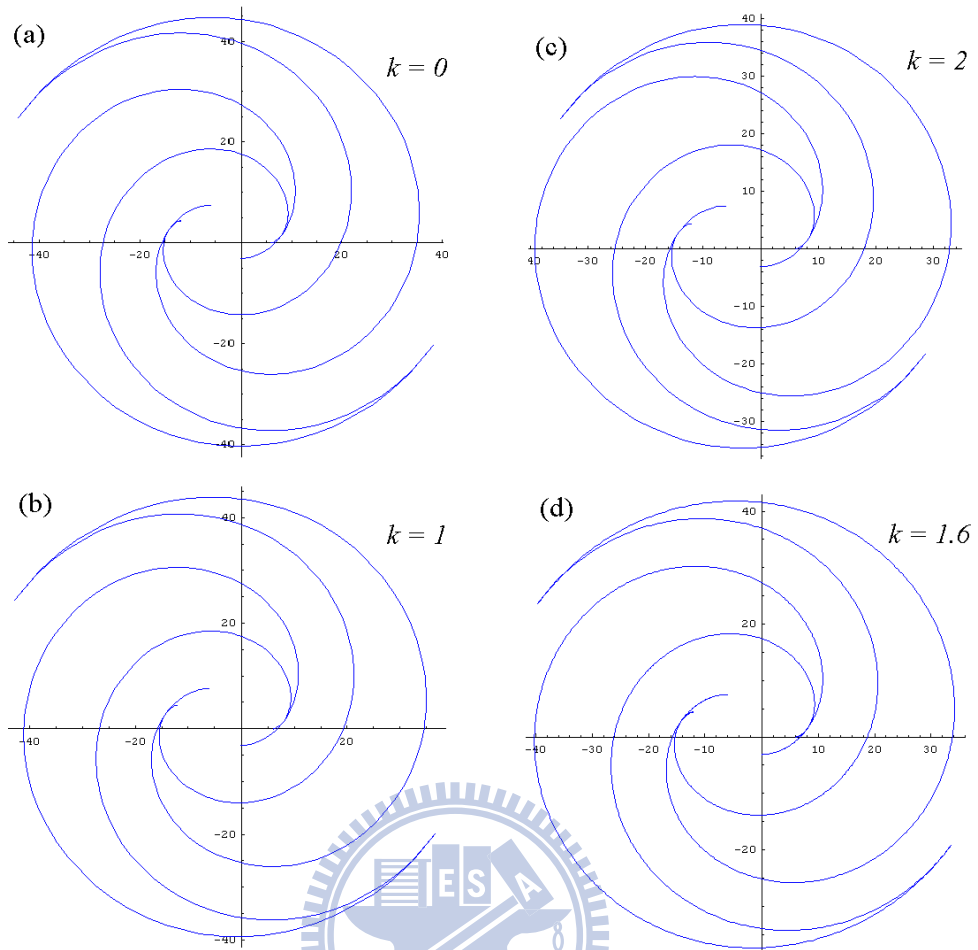


Fig. 6-4 Sketch map of the scroll profiles for different k values

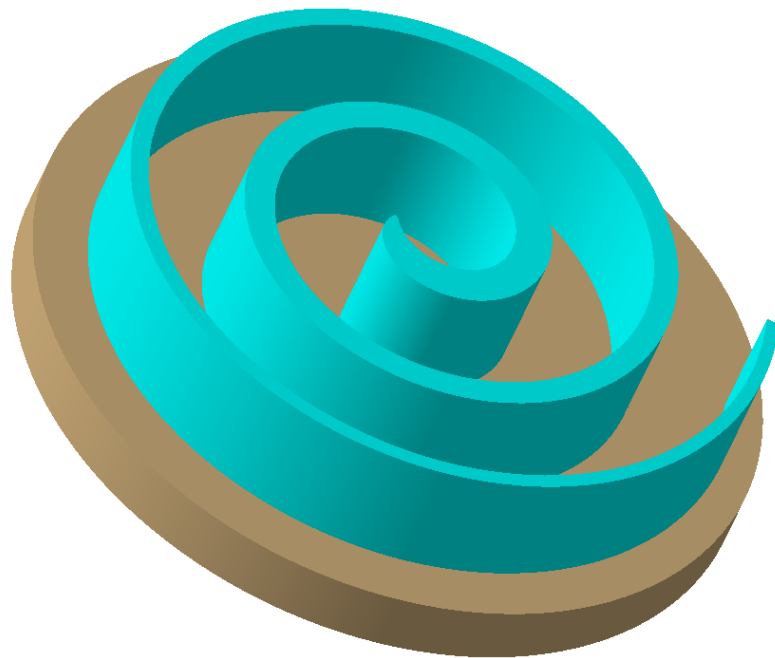


Fig. 6-5 Structure of orbiting scroll ($k=1$, $\alpha=50^\circ$ and $\delta_0 = -0.05\text{mm}$)

6.3.2 Volume calculations

The analytic expression to volume calculation of the case $k=1$ with the same starting angles ($\alpha_{ou} = \alpha_{in} = \alpha$) has been derived. By considering the coordinate expressions of equations (6.11) and (6.13), the enclosed chamber areas formed from the scroll pair can be calculated as follows:

$$\begin{aligned}
 A &= \frac{1}{2} \int_{\phi-2\pi}^{\phi} \left| x_{m,in} \cdot \frac{d(y_{m,in})}{d\phi} - y_{m,in} \cdot \frac{d(x_{m,in})}{d\phi} \right| d\phi \\
 &\quad - \frac{1}{2} \int_{\phi-2\pi}^{\phi} \left| x_{f,ou} \cdot \frac{d(y_{f,ou})}{d\phi} - y_{f,ou} \cdot \frac{d(x_{f,ou})}{d\phi} \right| d\phi \\
 &= -\frac{1}{12} \pi(\pi-2\alpha)[-2a_0 + (\pi-2\alpha)\delta_0] \cdot \\
 &\quad \{-6a_0(\pi+2\alpha-2\phi) + \delta_0[5\pi^2 + 12\pi(\alpha-\phi) + 6(\phi^2 - 2\alpha^2)]\},
 \end{aligned} \tag{6.30}$$

where ϕ represents the involute angle that responds to the contact point of the inner curve. By assuming the symmetrical chambers in a scroll pair, the chamber volume, the variation of it with ϕ and the suction volume V_{SUC} can be expressed as follows:

$$\begin{aligned}
 V(\phi) &= -(h/6)\pi(\pi-2\alpha)[-2a_0 + (\pi-2\alpha)\delta_0] \cdot \\
 &\quad \{-6a_0(\pi+2\alpha-2\phi) + \delta_0[5\pi^2 + 12\pi(\alpha-\phi) + 6(\phi^2 - 2\alpha^2)]\},
 \end{aligned} \tag{6.31}$$

$$\begin{aligned}
 \frac{dV(\phi)}{d\phi} &= -(h/6)\pi(\pi-2\alpha)[-2a_0 + (\pi-2\alpha)\delta_0] \cdot \\
 &\quad [12a_0 + \delta_0(-12\pi + 12\phi)],
 \end{aligned} \tag{6.32}$$

$$\text{and } V_{suc} = V(\phi_e), \tag{6.33}$$

where ϕ_e is the ended involute angle of the scroll pair. It follows that the volume ratio is

$$Vol_r = V(\phi_{suc}) / V(\phi_{dis}), \tag{6.34}$$

where ϕ_{dis} represents the corresponding involute angle at where the discharge step has been designed to arrive. The analytic expression to the volume calculation for the other k values or a different starting angle $\alpha_{ou} \neq \alpha_{in}$ can also be constructed in accordance with the above-mentioned procedure.

6.4 Parametric study and discussion

Several cases of scroll profiles constructed from the involutes of circle with both constant and variable radii are compared. These cases are regarding the condition that the polytropic index $k=1$, and for simplicity, the same starting angles $\alpha_{ou} = \alpha_{in} = \alpha$ are used for the inner and outer involutes.

6.4.1 Fixed suction volume, volume ratio and housing size

The scroll pair with symmetrical chambers has been used with respect to the two different scroll profiles. Important design specifications in STC, such as the suction volume V_{suc} and volume ratio Vol_r are fixed as 4500 mm^3 and 2.3 in this case. These fixed values must be maintained to satisfy the design specifications. Also, the endplate of the orbiting scroll with a suitable diameter D_m must be designed to match up with the limitation of the housing size for STC. This minimum D_m can be calculated approximately as

$$D_m = 2 [\rho_{ou}(\phi_e + \alpha) + r_{ob}] = 2 [a_0 \cdot (\phi_e + \alpha) + 1/2 \cdot \delta_0 \cdot (\phi_e + \alpha)^2 + r_{ob}] \quad (6.35)$$

Therefore, the new type of scroll pair must hold the same D_m as the conventional one.

According to the model of this new type, four design combinations with different a_0 , δ_0 and α values (shown in Table. 6-1) have been calculated. The V_{suc} , Vol_r and D_m were kept the same as the conventional type.

The key design parameters and important results for the conventional scroll profile (A0) and these four combinations (A1 to A4) are all shown in Table. 6-1.

Table. 6-1 Combinations of design parameters and related results

| Design Parameters | unit | A0 | A1 | A2 | A3 | A4 |
|--------------------|---------------|--------|--------|--------|--------|--------|
| ϕ_E | rad | 16.755 | 16.755 | 16.755 | 16.755 | 16.755 |
| α | rad | 0.785 | 0.733 | 0.785 | 0.820 | 0.855 |
| a_0 | mm | 1.9099 | 2 | 2.1 | 2.2 | 2.3 |
| a_0 / δ_0 | - | - | -167 | -89 | -62 | -49 |
| h | mm | 5.19 | 4.56 | 4.525 | 4.428 | 4.357 |
| Results | | | | | | |
| V_{suc} | mm^3 | 4500 | 4500 | 4500 | 4500 | 4500 |
| V_{dis} | mm^3 | 1960 | 1960 | 1960 | 1960 | 1960 |
| Vol_r | - | 2.3 | 2.3 | 2.3 | 2.3 | 2.3 |
| r_{ob} | mm | 3 | 3.3 | 3.3 | 3.3 | 3.3 |
| D_m | mm | 73.00 | 73.02 | 73.09 | 73.05 | 73.02 |
| <i>wrap volume</i> | mm^3 | 4160 | 3123 | 3140 | 3027 | 2951 |

Figure 6-6 displays the derived scroll profiles from A0 to A4. Figure 6-7(a) shows that these four combinations can also lower the wrap height at a ratio from 12.1% to 16.1%. In addition, the wrap volume can also be reduced by -24.9 % to -29.1%. Even though the orbiting radius r_{ob} of the four combinations is bigger than that of the conventional one, the minimum endplate radius D_m can still be approximately the same. Therefore, the limitation of housing size will not be an issue.

Though having the same V_{suc} and Vol_r , a smaller wrap height h in STC is a significant improvement. When the orbiting scroll rotates to compress the refrigerant, the gas forces that are created by the pressure differences between adjacent chambers and exerted on the scroll wrap, will be proportional to the wrap height and give rise to the bending moment on the scroll wrap. Obviously, a bigger bending moment not only generates higher stress on the root part but also causes bigger deformation on the top part of the scroll wrap. Since the higher stress will result in the possibility of fracture and durability issues, and a bigger deformation will lead to severe leakage between adjacent chambers, it will eventually degrade the compressor's efficiency. By changing the wrap height to as low as possible, and using the same design specifications for STC, these two drawbacks can both be reduced.

Increasing attention has been paid to harmless and eco-friendly refrigerants all over the world in recent years due to the threats of ozone depletion and global warming problems. Therefore, some working fluids (as shown in Table. 6-2) like HFC compounds (ex. R407C and R410A) with zero ODP values and some natural refrigerants with lower GWP values (ex. CO₂) have gradually been used to replace the conventional CFC and HCFC refrigerants. However, the needed pressure conditions that correspond to the specified operating temperatures used in the refrigeration and air-conditioning field for these substitutes, such as R410A and CO₂, are 1.5 and 5 times higher compared to the conventional refrigerants (ex. R22). Hence the scroll pair must confront higher pressure differences with these substitutes. In the light of this, the design of the scroll pair to suit these refrigerants must be reconsidered further.

If the conventional design of the scroll profile remains unchanged, higher stress and deformation levels on the scroll wraps could be generated and the durability and efficiency of the scroll pair in STC could be degraded more by adopting these eco-friendly refrigerants. By applying these new types of the scroll profile (for example, $k=1$ and $\alpha_{ou} = \alpha_{in} = \alpha$), once the thickness in the inward portion of the scroll wrap, which bears the higher fluid pressure, can be increased and that in the outward portion, which bears the lower pressure, can be

decreased, the rigidity and strength of the new type of the scroll wrap can be improved. Then the advantages induced by this new scroll profile can be observed more distinctly.

Table. 6-2 ODP/GWP values to several refrigerants

| Name | R12 | R22 | R407C | R410A | CO2 |
|---------------------------------|------|-------|-------|-------|-------------|
| Compositions | CFC | HCFC | HFC | HFC | Natural gas |
| ODP (Ozone depletion potential) | 1 | 0.055 | 0 | 0 | 0 |
| GWP (Global warming potential) | 8100 | 1810 | 1700 | 1975 | 1 |

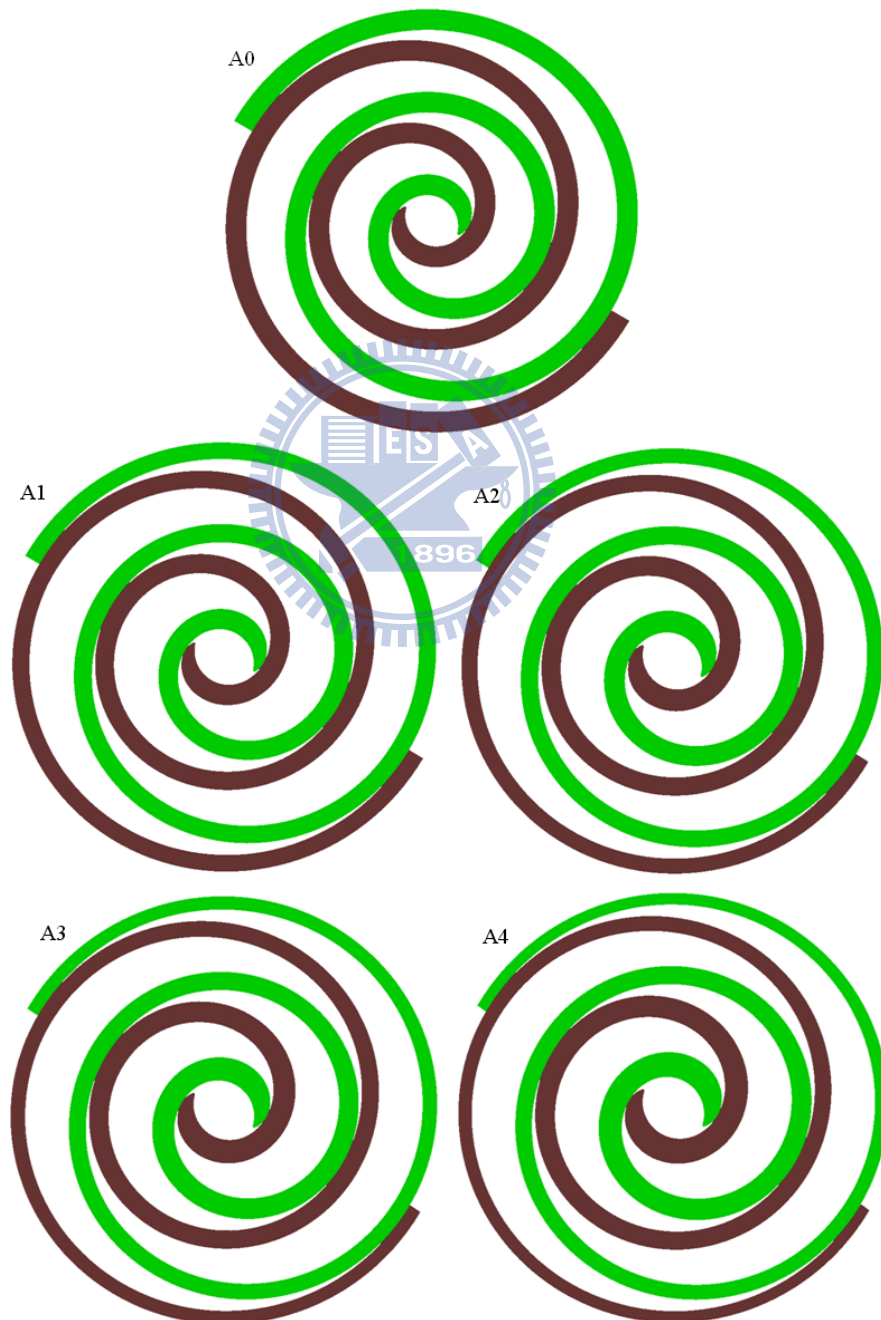


Fig. 6-6 Scroll profiles from A0 to A4

6.4.2 Fixed suction volume, volume ratio and wrap height

If the material used in the scroll pair is properly selected with greater strength and rigidity, then the wrap height h can still hold to the same value as the conventional one. Even so, in order to satisfy the fixed V_{suc} and Vol_r values, other design parameters such as ϕ_E , a_0 , δ_0 and α , need to be adjusted once more. Similarly, four other design combinations (A1' to A4') are also listed in Table. 6-3. Figure 6-7(b) shows that these four combinations can reduce D_m from 4.8% to 7.5%. The wrap volume can be reduced by -12.5% to -27.2%. The orbiting radius r_{ob} to the four combinations is also a little different when compared to the conventional one.

Table. 6-3 Combinations of design parameters and related results

| Design Parameters | unit | A0 | A1' | A2' | A3' | A4' |
|--------------------|-----------------|--------|--------|--------|--------|--------|
| ϕ_E | rad | 16.755 | 16.319 | 16.319 | 16.232 | 16.232 |
| α | rad | 0.785 | 0.794 | 0.845 | 0.895 | 0.935 |
| a_0 | mm | 1.9099 | 2 | 2.1 | 2.2 | 2.3 |
| a_0/δ_0 | - | - | -82 | -58 | -51 | -44 |
| h | mm | 5.19 | 5.19 | 5.19 | 5.19 | 5.19 |
| Results | | | | | | |
| V_{suc} | mm ³ | 4500 | 4500 | 4500 | 4500 | 4500 |
| V_{dis} | mm ³ | 1960 | 1960 | 1960 | 1960 | 1960 |
| Vol_r | - | 2.3 | 2.3 | 2.3 | 2.3 | 2.3 |
| r_{ob} | mm | 3 | 3.1 | 3.1 | 3 | 2.9 |
| D_m | mm | 73 | 67.5 | 67.5 | 68.9 | 69.5 |
| <i>wrap volume</i> | mm ³ | 4160 | 3029 | 3081 | 3392 | 3642 |

The smaller D_m with the same V_{suc} and Vol_r becomes an important factor, even though the rate of the decreasing D_m in this case is smaller than the rate of the decreasing wrap height h in the previous case. The smaller D_m implies that the smaller housing size, which is compared to conventional STC, can accomplish the same V_{suc} and Vol_r . Therefore, a more compact size of STC with the same capacity and volume ratio can provide wider freedom in design consideration by using the involute of circle with variable radii.



Fig. 6-7 Reduction ratio in A1 to A4 and A1' to A4', A0 as standard
 (a) scroll wrap height and wrap volume (A1 to A4)
 (b) diameter of the end-plate and wrap volume (A1' to A4')

6.5 Remarks

The geometric model of the scroll profiles constructed from an involute of circle with variable radii has been built in this chapter, and the analytical expressions to the volume and its variation have been derived as well by designating the polytropic index $k = 1$. Numerical cases show that the smaller stress induced from the bending moment on the root of the scroll wrap and smaller deformation on the top of the scroll wrap will result if the scroll wrap height is lowered while keeping the suction volume, volume ratio and housing size the same as the conventional one. This profile suits STCs with operating pressures several times higher than the conventional ones. In addition, more compact housing sizes of the STC can be devised by this new type of profile when holding the suction volume, volume ratio and wrap height the same as the conventional profile.

CHAPTER 7 PERFECTLY MESHING MODIFICATION FOR INVOLUTE OF CIRCLE WITH VARIABLE RADII

Similar to the conventional scroll profiles, the perfectly meshing modifications for avoiding interference at the center portion of the scroll profile still needs to be addressed. Both arc and line modifications will be built in this chapter to provide wider design varieties. In addition to avoid interference at the center of the scroll pair, these modifications are also used to boost the volume ratio of this new scroll profile.

7.1 Introduction of modifications at the center of the scroll pair

When the orbiting scroll rotates around the fixed scroll, the center portion of their profiles must confront interference mutually providing that this portion maintains the original involute profiles (involute of circle, archimedes spirals...and so on). This interference will reduce the durability of the scroll pair, result in vibration problem and eventually degrade the performance of STC.

To overcome this deficiency, some methods and modifications have also been presented for reaching the perfectly meshing engagement at the center of the scroll pair, thus avoiding the mutual interference and improving its efficiency [17–19].

Based on the references [58–60], it is found that the arc and line modifications are both easy to understand and convenient to be translated into CAM (computer-aided manufacturing) procedures. However, the mathematical expression to these two modifications is just for the conventional scroll profile, means the scroll profile constructed from an involute of circle with a fixed radius. By refining them, the arc and line shapes to the center portion of the scroll profile constructed from an involute of circle with variable radii will be formulated investigated and in the following paragraphs.

7.2 Arc modification of involutes of circle with variable radii

Two respective arc curves can be used to join the inner and outer involutes when modifying them. In order to guarantee the meshing engagement (with the same tangential slope or holding first-order continuous at the joint of two curves), the following three necessary conditions must be satisfied (Fu *et al.* [59] and Feng [60]):

1. The joining of one arc curve with the outer involute must be first-order continuous.
2. The joining of the other arc curve with the inner involute must be first-order continuous.
3. The joining of these two arc curves must be first-order continuous.

7.2.1 Formulation

For the involute of circle with variable radii, the contact relation between the two arc curves and the involutes must be illustrated in order to formulate their mathematic relations. As shown in Fig. 7-2, let β be a modified angle that corresponds to the center curve between the outer and inner involutes and C_{ou} represent the joint point of the arc and the outer involute. Similarly, let angle $\beta + \pi$ be another corresponding angle and let C_{in} represent the joint point of the arc and the inner involute. By leading those two arc curves to the center portion and applying the theorem of planar orbiting mechanisms [19] and trigonometry [59], the relations can be expressed as follows:

$$(R_{in} + R_{ou})^2 - (2a_{ou})^2 = (2d)^2 \quad (7.1)$$

$$d = \rho_{ou} - R_{ou} \quad (7.2)$$

$$R_{in} - R_{ou} = r_{ob} \quad (7.3)$$

where R_{ou} and R_{in} represent the radius of the two arc curves that connect to the outer and inner involute curves. a_{ou} and ρ_{ou} represent the radius of the base circle and the radius of curvature at contact point C_{ou} . The formulation can be expressed as:

$$\begin{aligned} a_{ou} &= [a_0 + \delta_0(\beta + \alpha)^k] \\ \rho_{ou} &= [a_0(\beta + \alpha) + (-1)^{k+2} \frac{\delta_0}{k+1} (\beta + \alpha)^{k+1}] \end{aligned} \quad (7.4)$$

Using equation (7.4) and solving equations (7.1) to (7.3), important relations can be obtained as follows:

$$R_{ou} = [a_0(\beta + \alpha) + (-1)^{k+2} \frac{\delta_0}{k+1} (\beta + \alpha)^{k+1}] - d \quad (7.5)$$

$$R_{in} = R_{ou} + r_{ob} \quad (7.6)$$

$$d = \frac{[a_0(\beta + \alpha) + (-1)^{k+2} \frac{\delta_0}{k+1} (\beta + \alpha)^{k+1} + \frac{r_{ob}}{2}]^2 - [a_0 + \delta_0(\beta + \alpha)^k]^2}{2[a_0(\beta + \alpha) + (-1)^{k+2} \frac{\delta_0}{k+1} (\beta + \alpha)^{k+1} + \frac{r_{ob}}{2}]} \quad (7.7)$$

The corresponding parameters, the derivative angle γ and the orbiting angle at the discharge moment θ_{dis} (as shown in Fig. 7-2) can then be expressed as

$$\gamma = \beta - \tan^{-1} \left(\frac{d}{a_{\text{ou}}} \right), \quad (7.8)$$

$$\text{and } \theta_{\text{dis}} = 2\pi - \gamma$$

Finally, the parametric expressions of the two arc curves (R_{ou} and R_{in}) are

$$\begin{cases} x_{R_{\text{ou}}} = R_{\text{ou}} \cdot \cos \theta + \sqrt{a_{\text{ou}}^2 + d^2} \cdot \cos \gamma \\ y_{R_{\text{ou}}} = R_{\text{ou}} \cdot \sin \theta + \sqrt{a_{\text{ou}}^2 + d^2} \cdot \sin \gamma \end{cases}, \text{ where } \theta \in [\gamma - \pi, \beta - \frac{\pi}{2}] \quad (7.9)$$

$$\begin{cases} x_{R_{\text{in}}} = R_{\text{in}} \cdot \cos \theta + \sqrt{a_{\text{ou}}^2 + d^2} \cdot \cos(\gamma + \pi) \\ y_{R_{\text{in}}} = R_{\text{in}} \cdot \sin \theta + \sqrt{a_{\text{ou}}^2 + d^2} \cdot \sin(\gamma + \pi) \end{cases}, \text{ where } \theta \in [\gamma, \beta + \frac{\pi}{2}] \quad (7.10)$$

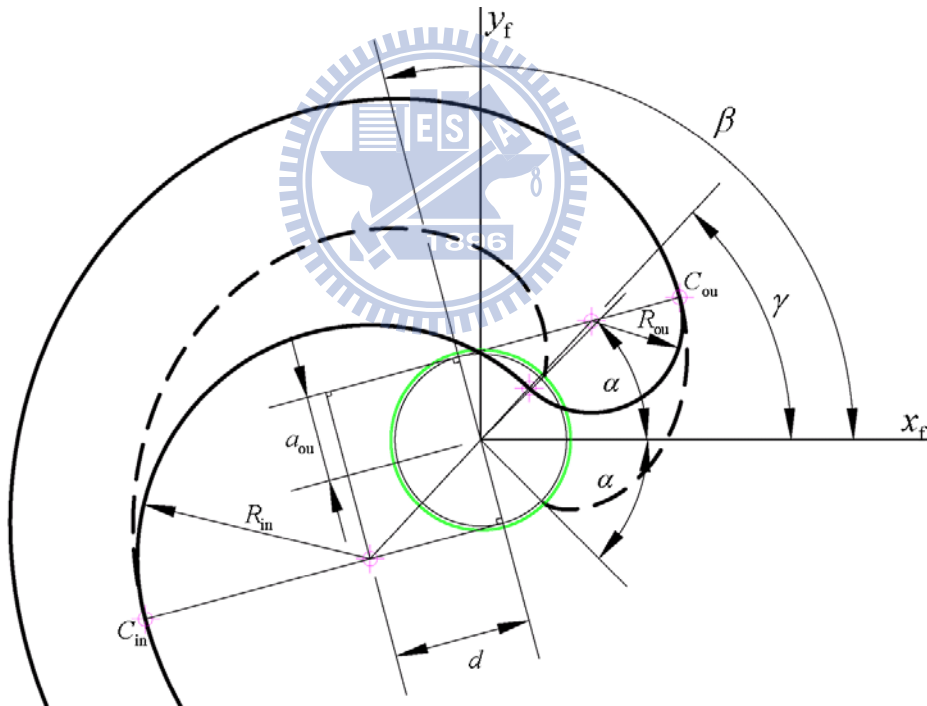


Fig. 7-1 Parametric definitions of the arc modification

7.2.2 Discussion

Several related constraint conditions from these parameters must be considered once the arc modification has been applied. These include:

1. $R_{\text{ou}} > 0$: the outer arc curve exists if $R_{\text{ou}} > 0$, otherwise the tip point could happen

(if $R_{ou} \leq 0$) at the joint of the outer involute and the inner arc curve, so the stress concentration could arise in the tip of the scroll wraps.

2. $\beta > -\alpha$ guarantees an intersection between the outer arc and the outer involute curve.
3. Larger β value means larger R_{ou} and R_{in} values, which represents a thicker wrap profile at the center portion.

Several arc curves with corresponding R_{ou} and R_{in} can be derived to assist this modification by choosing a different modified angle β . Figure 7-2 shows the modifications when β is set as $65^\circ(13\pi/36)$, $85^\circ(17\pi/36)$, $105^\circ(21\pi/36)$, $125^\circ(25\pi/36)$, $145^\circ(29\pi/36)$ and $165^\circ(33\pi/36)$. From equation (43) and Figure 9, it is found that when a lower β angle is used, a larger orbiting angle at the discharge moment (θ_D) can be obtained while still keeping the same values of the other parameters, which means the planar orbiting motion can reach the discharge step much later. Hence the volume ratio (V_{SUC}/V_{DIS}) can be raised substantially and if possible, surpass the needed design requirements for the designated operating conditions (pressure ratio or compression ratio) of STC. Owing to this, some defects (e.g. over-compression) may occur during the compression step and consume unnecessary work.

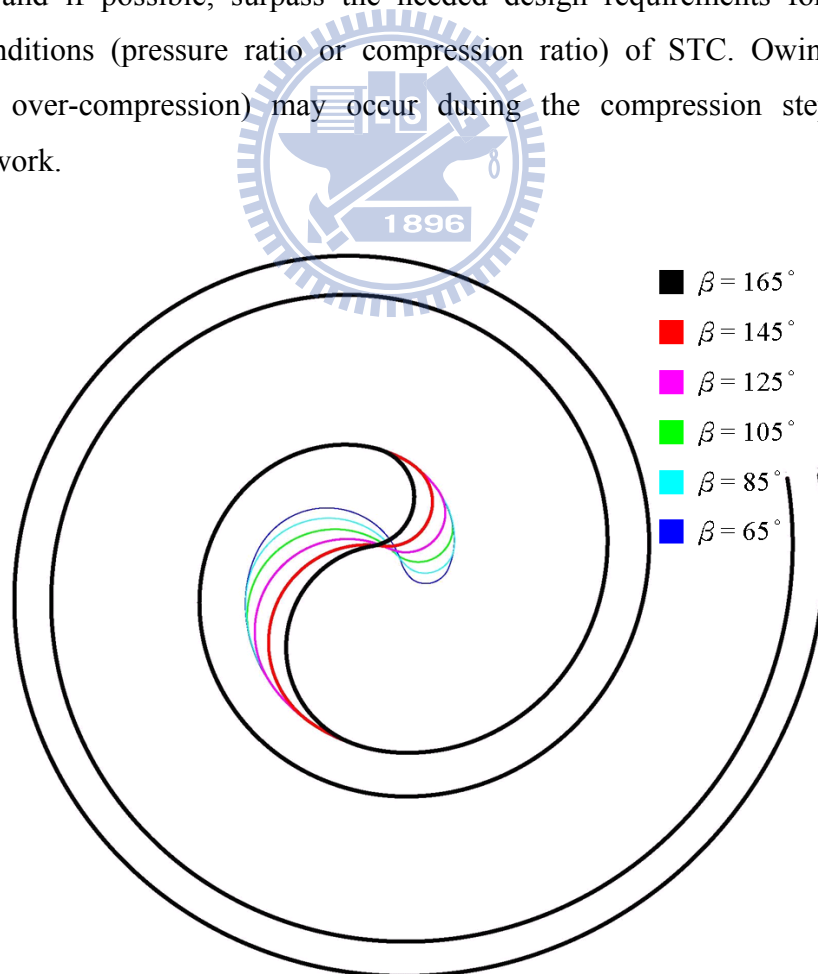


Fig. 7-2 Comparison of different β values to the scroll profile with arc modification

7.3 Line modification of involutes of circle with variable radii

This modification uses two conjugate straight lines to collocate with two arc curves to achieve a perfect mesh. By doing this, the increased level of the volume ratio ($V_{\text{suc}}/V_{\text{dis}}$) can be lowered when compared with the arc modification.

7.3.1 Formulation

In addition to the modified angle β , another parameter Δr (as shown in Fig. 7-3), called the modified distance, must be introduced into this modification. From equation (7.3), it is known that the difference between the radii of the inner and outer arcs must be equal to the orbiting radius ($R_{\text{in}} - R_{\text{ou}} = r_{\text{ob}}$). This equation can also be rewritten as follows [59]

$$(R_{\text{in}} - \Delta r) - (R_{\text{ou}} - \Delta r) = R_{\text{in}}' - R_{\text{ou}}' = r_{\text{ob}} \quad (7.11)$$

The planar orbiting motion and perfect conjugate mesh are still maintained because of the unchanged r_{ob} value. As shown in Fig. 7-3, the modified parameters are expressed below

$$\begin{aligned} R_{\text{in}}' &= R_{\text{in}} - \Delta r \\ R_{\text{ou}}' &= R_{\text{ou}} - \Delta r \end{aligned} \quad (7.12)$$

and $d' = d + \Delta r$

Therefore, the derivative angle γ is

$$\gamma = \beta - \tan^{-1}\left(\frac{d'}{a_{\text{ou}}}\right) \quad (7.13)$$

Another derivative angle $\Delta\theta$, defined by the included angle between the modified line and the connecting line between the center of the two arc curves, can be expressed as

$$\Delta\theta = \sin^{-1}\left(\frac{R_{\text{in}}' + R_{\text{ou}}'}{2\sqrt{a_{\text{ou}}^2 + d'^2}}\right) \quad (7.14)$$

In addition, another derivative angle σ , defined by the included angle between the modified line and the coordinate x_f axis (shown in Fig. 7-3) is

$$\sigma = \gamma - \Delta\theta \quad (7.15)$$

Then the orbiting angle at the moment of discharge can be expressed as

$$\theta_{\text{dis}} = 2\pi - \left(\sigma + \frac{\pi}{2}\right) \quad (7.16)$$

Finally, the parametric expressions of the two arc curves (R_{ou}' and R_{in}') are

$$\begin{cases} x_{R_{\text{ou}}'} = R_{\text{ou}}' \cdot \cos \theta + \sqrt{a_{\text{ou}}^2 + d'^2} \cdot \cos \gamma \\ y_{R_{\text{ou}}'} = R_{\text{ou}}' \cdot \sin \theta + \sqrt{a_{\text{ou}}^2 + d'^2} \cdot \sin \gamma \end{cases}, \text{ where } \theta \in \left[\sigma - \pi, \beta - \frac{\pi}{2}\right] \quad (7.17)$$

$$\begin{cases} x_{R_{in}'} = R_{in}' \cdot \cos \theta + \sqrt{a_{ou}^2 + d'^2} \cdot \cos(\gamma + \pi) \\ y_{R_{in}'} = R_{in}' \cdot \sin \theta + \sqrt{a_{ou}^2 + d'^2} \cdot \sin(\gamma + \pi) \end{cases}, \text{ where } \theta \in [\sigma, \beta + \frac{\pi}{2}] \quad (7.18)$$

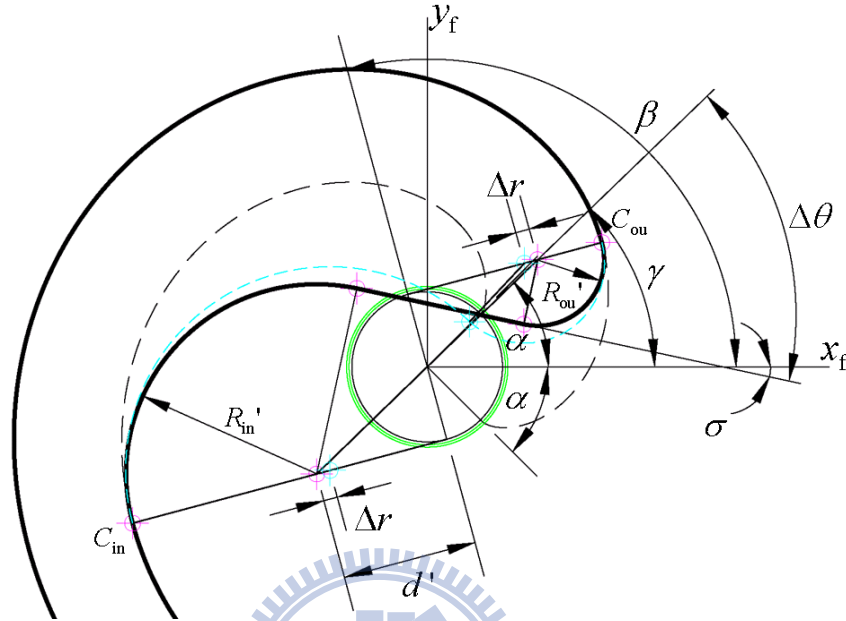


Fig. 7-3 Parametric definitions of the line modification

7.3.2 Discussion

Several related constraint conditions from these parameters must be considered once the arc modification has been applied. These include:

1. $R_{ou} > 0$: the outer arc curve exists if $R_{ou} > 0$, otherwise the tip point could happen (if $R_{ou} \leq 0$) at the joint of the outer involute and the inner arc curve, so the stress concentration could arise in the tip of the scroll wraps.
2. $\beta > -\alpha$ guarantees the existence of an intersection between the outer arc and the outer involute curve.
3. Larger β value means larger R_{ou} and R_{in} values, which represents a thicker wrap profile at the center portion.

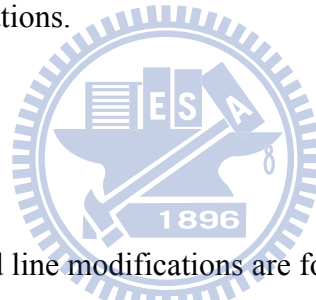
Several arc curves with corresponding R_{ou} and R_{in} can be derived to assist this modification by choosing a different modified angle β . Fig. 7-4(a) shows the modifications when β is set as $65^\circ(13\pi/36)$, $85^\circ(17\pi/36)$, $105^\circ(21\pi/36)$, $125^\circ(25\pi/36)$, $145^\circ(29\pi/36)$ and $165^\circ(33\pi/36)$. From equation (43) and Figure 9, it is found that when a lower β angle

is used, a bigger orbiting angle at the discharge moment (θ_{dis}) can be obtained while still keeping the same values of the other parameters, which means the planar orbiting motion can reach the discharge step much later. Hence the volume ratio (V_{suc}/V_{dis}) can be raised substantially and if possible, surpass the needed design requirements for the designated operating conditions (pressure ratio or compression ratio) of STC. Owing to this, some defects (e.g. over-compression) may occur during the compression step and consume unnecessary work.

It is found that once $\Delta r > 0$, then θ_{dis} is smaller than that by using arc modification. Moreover, the bigger Δr used, the earlier the discharge step will be reached (because of smaller θ_{dis}). Therefore the corresponding volume ratio can be designed according to specified requirements. On the other hand, the result of constant Δr (0.5 mm) and variable β values ($65^\circ \sim 165^\circ (13\pi/36 \sim 33\pi/36)$) is shown in Fig. 7-4(b). Hence various parameter combinations and design varieties can be put in use to reform and improve the center portion of the scroll profile with these two modifications.

7.4 Remarks

Two measures, the arc and line modifications are formulated in order to achieve perfectly meshing engagement at the center portion of the scroll profiles constructed from an involute of circle with variable radii. This chapter demonstrates that those two modifications which used in the conventional scroll profile can still be applied to this new scroll profile. The two most important purposes, avoiding interference at the center of the scroll pair and boosting the volume ratio to match the specified operating conditions, are both achieved by suitably choosing one of these two modifications, depending on design requirements.



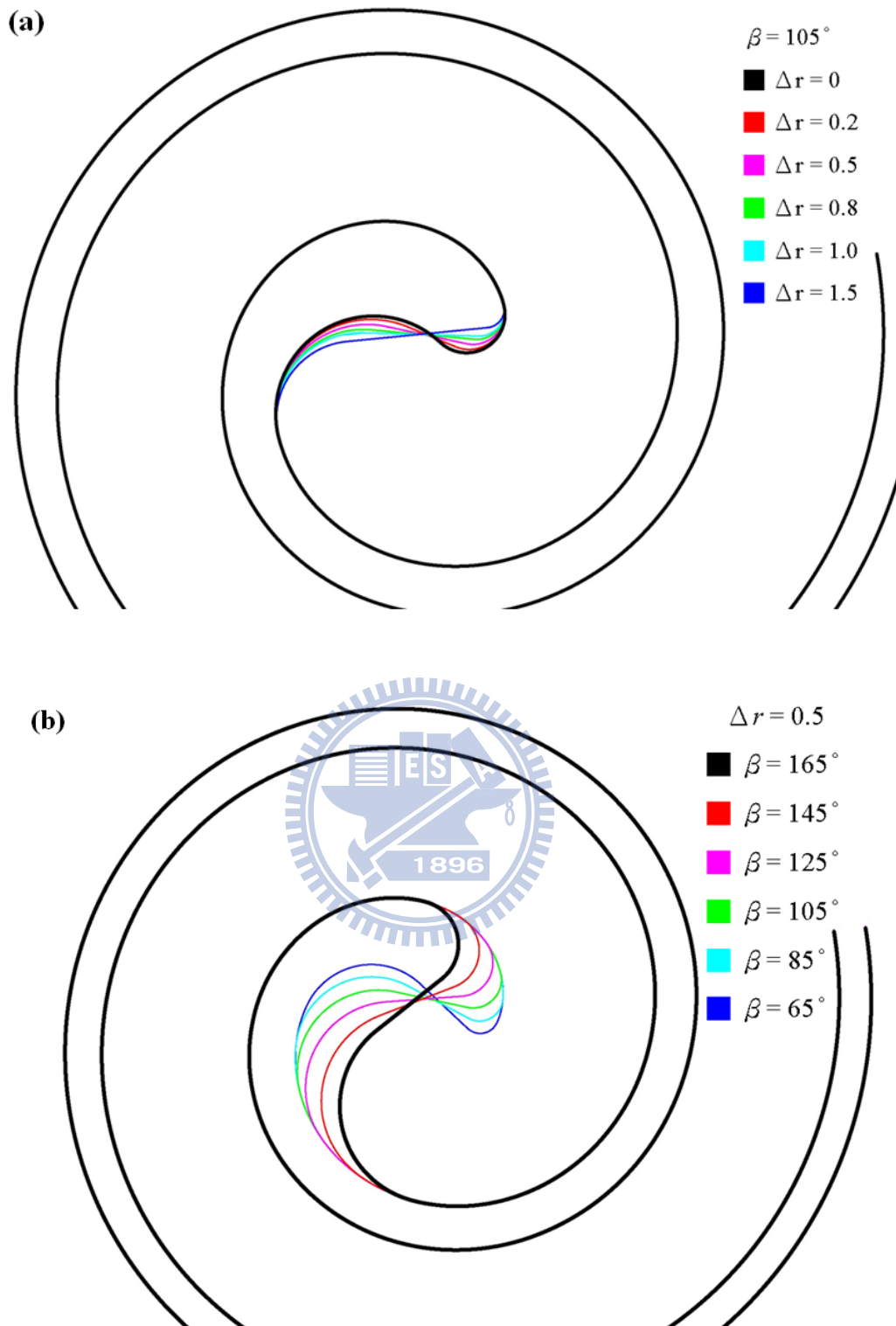


Fig. 7-4 (a) Comparison of different Δr values ($\beta=105^\circ$ ($21\pi/36$ rad)) (b) Comparison of different β values ($\Delta r=0.5$ mm)

CHAPTER 8 CONCLUSIONS AND FUTURE WORKS

8.1 Conclusions

Several critical techniques for accomplishing the function of variable compression ratio in a STC are developed. By taking the well-developed STC mathematical model and computer simulation package as the foundation, three of these techniques for improving STC performance and providing wider operating capacities while running STC with variable compression ratio are developed in this dissertation.

At first, the mathematical model of bypass valves has been constructed, and the advantages of this model are confirmed by means of cases discussion with experimental validations. Secondly, a design optimization module has been built up and integrated into the STC simulation package. Case studies demonstrate its usefulness, such as aiding in designing STC products with power-saving and durability considerations. Furthermore, a mathematical model regarding the scroll profiles created by an involute of circle with variable radii in a STC has also been formulated. Parametric studies are also implemented to evaluate its merits and defects.

The important aspects of this research are summarized as follows.

For bypass mechanism mathematical model used in STC:

- (1) The change of uncovered areas of bypass holes can be derived through the whole orbiting cycle of the developing STC by using coordinate transformation and some numerical schemes. Then the open and closed interval and corresponding chambers are also determined.
- (2) The model is integrated into the compression and discharge processes of a comprehensive STC simulation package that can predict general efficiencies and performance.
- (3) The model has been simulated under five specified operating conditions with and without bypass action and its accuracy has been validated by the experimental testing apparatus for a developing CO₂ STC product. It was found that the STC in this study with bypass valves increases 2.5% ~ 10% in compressor efficiency and volumetric efficiency is scarcely affected.
- (4) Pressure variations inside the chambers can also be viewed from the simulation results. It

was found that the design of the bypass holes in the study can avoid over-compression completely inside the compression chambers under the five operating conditions. However, for other different conditions, over-compression may occur because an interval (540° to 620°) with covered bypass hole in chamber 3' exists during the orbiting cycle. In addition, liquid slugging probably occurs at the initial stage (360° to 426°) in chamber 3.

- (5) When exploiting a STC product for varied pressure ratio, the bypass valves model presented in the research is a useful tool that can determine whether the design is suitable or not for specific operating conditions. In addition, it can be further combined to an optimization tool to obtain new designs for particular conditions.

For design optimization module combining with the STC simulation procedure:

- (1) A mathematical model of STC has been developed and verified by the experiments with different testing conditions. An optimum solver has been combined with the model to progress design decision of constrained optimization problems.
- (2) The optimization results for a selected STC design problem shows that the frictional losses can be reduced in range of 14.1% ~ 18.1% at all testing conditions by new design group which is satisfied at the specified constraint conditions for one thrust and three journal bearings.
- (3) For the crank and upper journal bearings, the design modifications can reduce the frictional losses, but the constraints of minimum oil-film thickness for holding hydrodynamic lubrication can block the further decrease of the frictional losses. For the lower journal bearing, the shorter and narrower dimensions can reduce the frictional losses without violating the oil-film constraints. For the thrust bearing, the smaller inner and outer diameter of the thrust surface, the larger reduction in frictional losses with specified design constraints. Furthermore, the constraints of the maximum pressure that related to the strength consideration of all the bearings are satisfied in all iterations during optimization and these results signify wider space for material selection.
- (4) The integration between the parametric simulation model of STC and optimum solver in this study can be a useful procedure and as the basis to progress various STC design optimization problems.

For scroll profiles which is constructed from an involute of circle with variable radii:

- (1) A geometric model of the scroll profiles constructed from an involute of circle with variable radii has been built and the analytical expressions to the volume and its variation

have been derived by designating the polytropic index $k = 1$.

- (2) Smaller stress induced from the bending moment on the root of the scroll wrap and smaller deformation on the top of the scroll wrap will result if the scroll wrap height is lowered while keeping the suction volume, volume ratio and housing size the same as the conventional one. Therefore, the reliability and efficiency of STC can be improved.
- (3) One kind of these profiles with greater wrap thickness at the center and decreasing thickness from the inside outwards can provide better strength and rigidity. This profile suits STCs with operating pressures several times higher than that of the conventional ones.
- (4) More compact housing sizes of the STC can be achieved by this new type of profile when holding the suction volume, volume ratio and wrap height are the same as the conventional profile. This provides wider design varieties in STC product development.

For the arc and line modifications (in order to achieve perfectly meshing engagement at the center portion of the scroll profiles from an involute of circle with variable radii):

- (1) The arc and line modifications used in the conventional scroll profile can still be applied to this new scroll profile. Mathematic derivations and discussions regarding those modifications have been delivered in this study.
- (2) The two most important purposes, avoiding interference at the center of the scroll pair and boosting the volume ratio to match the specified operating conditions, are both achieved by suitably choosing one of these two modifications, depending on design requirements.

8.2 Future works

Though the design towards a high-efficiency STC with variable compression ratio can be addressed by the STC mathematical model and simulation package constructed in this study, there exist researches and issues must be done in the future.

- (1) For bypass mechanism, the high-side STC product has been initially verified, but only five operating conditions were experimented. The tests for other operating conditions will be carried out to provide more data for modifying and correcting the models. Besides, the low-side structure of STC has not been demonstrated. So the experiments for the bypass mechanism in low-side STC will be carried out to validate the correctness of the developed models.
- (2) The design of bypass mechanism with different arrangements may not be the optimum

one because of the open delay of valve and insufficient bypass rate of refrigerant. Those effects may lower the compression efficiency. Therefore, optimum arrangements and parametric design of bypass valves for different design requirements will be considered by using the optimization module.

- (3) The optimum design regarding the frictional losses for bearing components is just a case discussed in this dissertation, many different optimization problems can also be investigated consecutively, such as deriving the optimization thermal efficiency for characteristic parameters of the scroll pair with stiffness, strength and manufacture constraints,...and so on.
- (4) The scroll profiles created by involute of circle with variable radii can be developed much extensively. For example, to derive the complete analytical expressions for different initial angle or different polytropic index, or to specify design parameters to form different scroll pairs, and followed by using the finite element method to estimate the structure characteristics. Furthermore, optimum parametric design of the scroll profiles can be investigated with the help of the developed optimization procedure.
- (5) The mathematical model of bypass mechanism can also be used to another technique, refrigerant injection. Because the injection holes are also added on the fixed scroll, so the same mathematical models of geometry can be used. The obvious differences between bypass and injection mechanism are the simulation process in thermodynamics. So in the future, the research can be focused on modifying the bypass model into an injection model and integrating it into the developed package. Then the simulations and experimental verifications can be conducted to estimate the effects of injection model for STC.

REFERENCES

- [1] Chang, Y.C., “Family Design of Scroll Compressors with Optimization”, National Chiao Tung University, Ph.D. dissertation, 2007.
- [2] Sarma, M.S., Electric Machines 2nd, West publishing company, 1994.
- [3] Engelmann, R.H., Middendorf, W.H., Handbook of Electric Motor, Marcel Dekker Inc, 1995.
- [4] Igata, M., *et al.*, “High Efficiency Hermetic Compressor Operated by IPM Motor and Inverter System”, In: Proceedings of International Compressor Engineering Conference at Purdue, pp.385–390, 1998.
- [5] Schein, C., Radermacher, R., “Scroll Compressor Simulation Model”, Journal of engineering for gas turbines and power, Transactions of the ASME, Vol.123, pp.217–225, 2001.
- [6] Tseng, C.H., MOST 1.1, Department of Mechanical Engineering of National Chiao Tung University, Taiwan, 1996.
- [7] Morishita, E. *et al.*, “Scroll Compressor Analytical Model”, In: Proceedings of International Compressor Engineering Conference at Purdue, pp.487–495, 1984.
- [8] Morishita, E. *et al.*, “Scroll Compressor Dynamics (1st Report, The Model for the Fixed Radius Crank)”, Bulletin of JSME 29 (248), pp.476–482, 1986.
- [9] Lee, Y.R., Wu, W.F., “A Study of Planar Orbiting Mechanism and Its Applications to Scroll Fluid Machinery”, Mechanism and Machine Theory, 31, pp.705–716, 1996.
- [10] Gravesen, J., Henriksen, C., “The Geometry of the Scroll Compressor”, Society for industrial and applied mathematics, 43, pp.113–126, 2001.
- [11] Bukac, H., “The Theory of Scroll Profile”, In: Proceedings of International Compressor Engineering Conference at Purdue, C080, 2006.
- [12] Qiang, J., “Study on Basic Parameters of Scroll Fluid Machine Based on General Profile”, Mechanism and machine theory, 45, pp.212–223, 2010.
- [13] Gagne, D.P., Nieter, J.J., “Simulating Scroll Compressors Using a Generalized Conjugate Surface Approach”, In: Proceedings of International Compressor Engineering Conference at Purdue, pp.553–557, 1996.
- [14] Mahfouz, H., *et al.*, “Theoretical Study on Scroll Compressor of New Hexagonal Involute”, In: Proceedings of International Compressor Engineering Conference at Purdue, C073, 2004.
- [15] Liu, T., Liu, Z.Q., “Study on Geometry of Trigonometric-curve Modification of Scroll

- Profile for Scroll Compressor”, In: Proceedings of International Compressor Engineering Conference at Purdue, C043, 2004.
- [16] Wang, B., Li, X., Shi, W., “A General Geometrical Model of Scroll Compressors Based on Discretional Initial Angles of Involute”, Int J. Refrig., 28, pp.958–966, 2005.
- [17] Terauchi, K., Hiraga, M., “Scroll type fluid compressor with thickened spiral elements”, U.S. Patent Number: 4,547,137, Date of Patent: October 20, 1985.
- [18] Hirano, T., Hagimoto, K., “Scroll-type fluid machine with specific inner curve segments”, U.S. Patent Number: 4,856,973, Date of Patent: August 15, 1989.
- [19] Lee, Y.R., Wu, W. F., “On the Profile Design of a Scroll Compressor”, Int J. Refrig. 18, pp.308–317, 1995.
- [20] Li, L.S., *et al.*, “The Effect of Scroll Wraps on the Performance of Scroll Compressors”, Int J. Refrig., 20, pp.326–331, 1997.
- [21] Yanagisawa, T., *et al.*, “A Study on Suction Gas Heating in a Rolling Piston Type Rotatory Compressor”, Bulletin of JSME, 27, no.226, 1984.
- [22] Yanagisawa, T., Shimizu, T., “Leakage Losses with a Rolling Piston Type Rotary Computer II: Leakage Losses through Clearances on Rolling Piston Faces”, Int J. Refrig., 8 (3), pp. 152–158, 1985.
- [23] Nieter, J.J., Gagne, D.P., Analytical Modeling of Discharge flow Dynamics in Scroll Compressors”, In: Proceedings of International Compressor Engineering Conference at Purdue, pp.85–94, 1992.
- [24] Morimoto, T., *et al.*, “Development of a High SEER Scroll Compressor”, in: Purdue International Compressor Engineering Conference Proceedings, pp.317-322, 1996.
- [25] Chen, Y., *et al.*, “Mathematical Modeling of Scroll Compressors—Part I: Compression Process Modeling”, Int J. Refrig., 25, pp.731–750, 2002.
- [26] Chen, Y., *et al.*, “Mathematical Modeling of Scroll Compressors—Part II: Overall Scroll Compressor Modeling”, Int J. Refrig., 25, pp.751–764, 2002.
- [27] Kulkarni, S.S., “Scroll Compressor: Thrust Bearing Design under Laminar Conditions”, In: Proceedings of International Compressor Engineering Conference at Purdue, pp.327–332. 1990.
- [28] Kulkarni, S.S., “Scroll Compressor: Thrust Bearing Design with Rigid Body Dynamics of the Runner Plate”, In: Proceedings of International Compressor Engineering Conference at Purdue, pp.333–344. 1990.
- [29] Sato, H., *et al.*, “Frictional Characteristics of Thrust Bearing in Scroll Compressor”, In:

- Proceedings of International Compressor Engineering Conference at Purdue, C027, 2004.
- [30] Booker J.F., “Dynamically Loaded Journal Bearings: Mobility Method of Solution”, ASME Journal of Basic Engineering, pp.537-546, 1965.
- [31] Booker J.F., “Dynamically Loaded Journal Bearings: Maximum Film Pressure”, ASME Journal of Lubrication Technology, Vol.91, pp534-543, 1969.
- [32] Booker, J.F., “Dynamically-loaded Journal Bearings: Numerical Application of the Mobility Method”, Journal of Lubrication Technology, Transaction of the ASME, pp.168–176, 1971.
- [33] Geonka, P.K., “Analytical Curve Fits for Solution Parameters of Fynamically Loaded Journal Bearings”, Journal of Tribology, 106, pp.421–428, 1984.
- [34] Lemmon, E.W., *et al.*, “Refprop 7.0”, NIST, MD, USA, 2002.
- [35] Winandy, E., *et al.*, “Experimental Analysis and Simplified Modeling of a Hermetic Scroll Refrigeration Compressor”, Applied Thermal Engineering, 22, pp. 107–120, 2002.
- [36] Fukuta, M., *et al.*, “Compression Characteristics of Refrigerant-oil Mixture in Refrigerant Compressors”, Trans. Jpn. Soc. Mech. Eng., 61 (582) pp.542–548 [in Japanese], 1995.
- [37] DeBlois, R.L., Stoeffler, R.C., “Instrumentation and Data Analysis Techniques for Scroll Compressors”, in: Purdue International Compressor Engineering Conference Proceedings, pp.182-188, 1988.
- [38] Ishii, N., *et al.*, “A Study on High Mechanical Efficiency of a Scroll Compressor with Fixed Cylinder Diameter”, In: Proceedings of International Compressor Engineering Conference at Purdue, pp.677–682, 1994.
- [39] Akei, M., *et al.*, “Analysis of Scroll Thrust Bearing”, In: Proceedings of International Compressor Engineering Conference at Purdue, C136, 2006.
- [40] Oku, T., *et al.*, “Theoretical Model of Lubrication Mechanism in the Thrust Slide Bearing of Scroll Compressors”, HVAC&R Research, 14(2), 2008.
- [41] Murayama, A., *et al.*, “Scroll Compressor with Valid Port for each Compressor Chamber”, U.S. Patent Number: 4,818,195, Date of Patent: April 4, 1989.
- [42] Fuji, K., *et al.*, “Scroll Compressor Having Bypass Valves”, U.S. Patent Number: 5,855,475, Date of Patent: January 5, 1999.
- [43] Tsubono, I., *et al.*, “Scroll Compressor Having a Valved Back Pressure Chamber and a

- Bypass for Overcompression”, U.S. Patent Number: 6,769,888, Date of Patent: August 3, 2004.
- [44] Wang, B., *et al.*, “Numerical Research on the Scroll Compressor with Refrigeration Injection”, Applied Thermal Engineering, 28, pp. 440–449, 2007.
- [45] Yamada, T., *et al.*, “Scroll Gas Compressor Having Asymmetric Bypass Holes”, U.S. Patent Number: 6,273,691, Date of Patent: August 14, 2001.
- [46] Skiple, T., *et al.*, “CO₂ Technology Transfer”, Technical Report No. 061206151146, SINTEF Energy Research. 2007.
- [47] Rekstad, H., 2007. “Technical Specifications of CO₂-compressor Test Rig”, Technical Report No. 03082192212, SINTEF Energy Research, 2007.
- [48] 劉陽光, CO₂ 壓縮機測試平台標準操作流程操作手冊, 技術報告, EEL. ITRI, 2007.
- [49] Etemad, S., Nieter, J.J., “Design Optimization of the Scroll Compressor”, Int J. Refrig., 12, pp.146–150, 1989.
- [50] Ishii, N., *et al.*, ”Optimum Combination of Parameters for High Mechanical Efficiency of a Scroll Compressor”, In: Proceedings of International Compressor Engineering Conference at Purdue, pp.118a1–118a8, 1992.
- [51] Ishii, N., *et al.*, “A Fundamental Optimum Design for High Mechanical and Volumetric Efficiency of Compact Scroll Compressor”, In: Proceedings of International Compressor Engineering Conference at Purdue, pp.639–644, 1996.
- [52] Tseng, C.H., Chang, Y.C., “Family Design of Scroll Compressors with Optimization”, Applied Thermal Engineering, 26, pp.1074–1086, 2006.
- [53] Ooi, K.T., "Design Optimization of a Rolling Piston Compressor for Refrigerators”, Applied Thermal Engineering, 25, pp.813–829, 2005.
- [54] Arora, J.S., Introduction to Optimum Design. McGraw-Hill, 2004.
- [55] Khonsari, M.M., Booser, E.R., Applied Tribology—Bearing Design and Lubrication, John-Wiley, 2001.
- [56] Tojo, K., Ueda, H., “New Wrap Profile for Scroll Type Machines”, International Congress of refrigeration Proceedings 19, pp.515–521, 1995.
- [57] Tojo, K., Ueda, H., 1995, “Scroll Type Fluid Compressor with an Involute Spiral Based on a Circle Having a Varying Radius”, U.S. Patent Number: 5,425,626, Date of Patent: June 20, 1995.
- [58] Hirano, T., Hagimoto, K., “Rotary Type Fluid Machine”, U.S. Patent Number: 4,678,415, Date of Patent: July 7, 1987.

- [59] Fu, Z.L., *et al.*, Scroll Compressor and Other Scroll Machine, Xi'an Jiaotong University, book [in Chinese] , 1998.
- [60] Feng, S.Y., “Modification and Investigation in Scroll Curves of Scroll Compressor for Vehicle Conditioning”, Xi'an Jiaotong University, master thesis [in Chinese], 1998.
- [61] Chang, Y.C., *et al.*, Chang, L.T., “Computer Simulation and Experimental Validation of Scroll Compressor”, In: Proceedings of International Compressor Engineering Conference at Purdue, C016, 2004.
- [62] Park Y.C., *et al.*, “Thermodynamic Analysis on the Performance of a Variable Speed Scroll Compressor with Refrigerant Injection”, Int J. Refrig., 25, pp.1072–1082, 2002.

